A Voltage Instability Predictor Using Local Area Measurements

VIP++

Leif Warland

A dissertation submitted to

The Norwegian University of Science and Technology
Faculty of Electrical Engineering and Telecommunications
Department of Electric Power Systems

in partial fulfilment of the requirements for the degree of
Doktor Ingeniør
Trondheim

February 12, 2002

URN:NBN:no-2337

URN:NBN:no-2337

Acknowledgements

I would like to express my sincere gratitude for assistance and support in connection with this dissertation to a number of people including:

My supervisor Professor Arne T. Holen for his guidance and support during all these years. His careful reading of the manuscript and papers submitted to conferences has been of great importance.

Kjetil Uhlen at SINTEF Energy Research, as it was through discussion with him that the main idea of this dissertation was born.

Harald Musum, with whom I have shared office with for the last four years. He has been listening to all my complaints and thoughts on the matters of voltage stability, and has contributed with constructive comments. He has also been my main computer support, as he seem to know everything within that field.

Stewart Clark, Student and Academic Division, NTNU for his assistance with the English edition of the final version of this dissertation.

My friend Lars Imsland for answering all kinds of questions, it is just to much to mentioned them all here.

My brother Geir who I have had many arguments with in preparation for his final dissertation, has also contributed to my dissertation.

Both my father Asgaut and my mother-in-law Liv Olaug Dahl have helped me with the English edition of this dissertation.

And last but not least, my wife Inger Aase who has supported me throughout my work, not to mention the inspiration of our daughter Andrea.

This work has been carried out at the Norwegian University of Science and Technology (NTNU), Faculty of Electrical Engineering and Telecommunications. The work started in July 1997 and has received financial support from the Research Council of Norway through a dr.ing scholarship in the “EFFEKT” program.

Trondheim, February 12, 2002

Leif Warland

URN:NBN:no-2337

Abstract

There has been a pressure to operate power systems closer to their security limits. This has partially been due to financial imperatives following the deregulating of markets. Other practical difficulties have been obtaining authorization from regulatory bodies to build power plants and transmission lines.

In this situation it is essential to monitor the system and to have tools that can predict the distance to the point of collapse (PoC). Much effort has been put into research of the phenomenon *voltage collapse*, and many approaches have been explored. Both dynamic and steady-state behavior have been studied thoroughly, though very few protection and control schemes have been implemented. In this dissertation the possibility of an index based on local area measurements have been explored. Voltage stability can be classified as either a transient or a long-term stability problem, and the index proposed in this dissertation is based on long-term dynamics.

VIP algorithm

This is a method that uses the maximum loadability of a transmission network as the PoC, thus by estimating a Thevenin equivalent the method can track the distance to the PoC as this occurs when the two impedances are equal in absolute value.

The problem of the VIP algorithm is that it is based on a system with two equations and four unknowns, thus it is not observable. In order to make it observable the assumption of constant Thevenin equivalent between two sets of measurements is made. When this is not the case the method will estimate a Thevenin impedance of the same size as the measured load impedance, but with a negative sign.

Changes in the Thevenin equivalent can be traced to both angle variation in a remote generator area or to variations in load impedances on nearby buses. The problem of angle variations can be mitigated by the selection of an appropriate reference bus. A method to solve the second problem, of variation in load admittances, has been proposed in this dissertation and given the acronym VIP++, using additional measurements on the surrounding load buses.

URN:NBN:no-2337

VIP++

The distance to the PoC does not only depend on the present state of the system but also on future changes. Therefore, an algorithm that tries to track the system trajectory is based on an assumption or hypothesis about how the system will move. Two such hypotheses, called "Distance to the PoC along the gradient" and "Shifting the gradient in the y_1 direction", have been explored in this dissertation.

"Distance to the PoC along the gradient" assumes that the two loads $\mathbf{y}_1$ and $\mathbf{y}_2$ increase according to a constant gradient. "Shifting the gradient in the y_1 direction" estimates at each time step the sudden load increase at bus no. 1 that would immediately bring the system to the PoC. When the system is far from the PoC the VIP++ method gives an approximate distance to the PoC and indicates that the distance is quite large. As the system trajectory moves closer to the actual PoC the method will become more accurate, and it will be more or less exact at PoC. This is true for both alternatives verified by the time domain simulations as shown in the dissertation.

The VIP++ method has been tested with promising results on a simple four bus system and on a simplified 313 bus model of the Norwegian grid. As measurements from a real system have not been available, simulations have been performed, including both generator dynamics and load dynamics according to the exponential load recovery model. The results from the simulations have been used as input to the VIP++ algorithms, and it has been demonstrated that VIP++ is able to track voltage collapse scenarios.

Both proposed methods could be extended to include more "known" load buses. This extension results in a few more equations being solved, but that can be handled quite easily. On the other hand the improvement in robustness and accuracy in the estimation of the PoC by including more measurements is not quite clear. A few tests have shown that the benefit may be marginal, but more thorough investigations are needed. One should also keep in mind that the basic idea is to estimate the PoC based on local measurements, and including too many buses brings us away from this idea.

Main conclusions

It has been shown that voltage stability assessment can be performed using local area measurements. Important issues are:

- Using phasor measurements of voltage and current on a load bus it is possible to track the distance to the PoC by the estimation of a Thevenin Equivalent.
- Under certain conditions the estimation might fail, though by including additional measurements of voltages and currents from surrounding buses the robustness of the estimation can be improved.

URN:NBN:no-2337

- VIP++ makes a prediction of the trajectory to PoC, therefore a hypothesis on "future" changes in load on the measured buses is required.
- Two hypotheses are explored and both are able to track the distance to the PoC.

Contents

Chapter 1

Introduction

This chapter gives a brief description of background, motivation and the major contributions of this dissertation. Finally there is an outline of the dissertation.

1.1 Background

During the last couple of decades, the complexity of transmission systems has increased. There are an increasing amount of interconnections in power systems, and at the same time they are being operated closer to their capability limits, due to economic and environmental considerations. As a result of this there have been many power disruptions [9, 36], typically these are characterized by a progressive fall of voltages and shortage of reactive power supply. As opposed to the much studied angular stability, this is an event that can take place over a long period of time from minutes to hours. Eventually it can lead to voltages going under acceptable levels, tripping of different equipment and islanding of the system or total blackout. The phenomenon characterizing these catastrophic events is often referred to as a *voltage collapse* and a comprehensive body of literature exists on this subject.

Although the problems associated with voltage stability are not new, there have not been set any universally accepted criteria, study methods or procedures to cope with them. Work is currently being done on both the dynamic and steady-state aspects of voltage collapse, to establish universal methods that are similar to those established for angular stability.

1.1.1 Incidents

There have been several incidents[6] of *voltage collapse* over the past decades. Tables 1.1 list some of these incidents grouped by time frame.

Table 1.1: Voltage collapse incidents.

Date	Location	Time Frame
1986-11-30	SE Brazil, Paraguay	2 seconds
1985-05-17	South Florida	4 seconds
1987-08-22	Western Tennessee	10 seconds
1983-12-27	***Sweden***	***50 seconds***
1977-09-22	Jacksonville, Florida	few minutes
1982-09-02	Florida	1 – 3 minutes
1982-11-26	Florida	1 – 3 minutes
1982-12-28	Florida	1 – 3 minutes
1982-12-30	Florida	2 minutes
1965-12-09	Brittany, France	?
1976-11-10	Brittany, France	?
1982-08-04	Belgium	4.5 minutes
1987-01-12	Western France	4 – 6 minutes
1987-07-23	***Tokyo***	***20 minutes***
1978-12-19	France	26 minutes
1970-08-22	Japan	30 minutes

The Power Failure in Sweden – Desember 27, 1983

Before the disturbance the transmission system was highly loaded. In an important section north to south of the Swedish network the transfer was 5600 MW. This was 200 MW below the recommended maximum.

In a major 400 kV switch yard in eastern Sweden one bus bar section was subjected to an earth fault. Normally, the faulty section should have been isolated, but because of special breaker arrangements this possibility was not at hand, and the whole station tripped. As a result of this two out of seven 400 kV lines, going from north to south, tripped. The rest of the network remained intact during the first few seconds. The only remaining eastern line, a 220 kV line through Stockholm, became heavily loaded. After 8 seconds this line tripped because of overload by a special function in the protection. Still the frequency in the system remained fairly constant.

After another 42 seconds, in which the transfer on the central northern-southern lines increased and the voltage decreased, one more 400 kV line tripped. The other lines became overloaded and cascade tripping took place. The connections towards Norway and Denmark tripped too, which islanded the southern part of Sweden. The frequency and the voltage dropped rapidly, more than 50 %, due to a large power deficit.

Because of the large and rapid frequency and voltage decay all generators in the south tripped. The load shedding could not save the system, and the blackout was a fact. An hour after the blackout large part of the system was restored.

Probable explanations for the collapse were:

- Load characteristics at low voltage
- Operation of on-load tap changers
- Current limiters of generators
- Relay protection

The Power Failure in Tokyo – July 23, 1987

The event occurred on a hot summer afternoon and resulted in the loss of most of the 500 kV system of the Tokyo Electric Power Company as well as 8000 MW of load to almost three million customers for about three hours.

The event was initiated by a sharp increase in the demand that was estimated to reach about 38000 MW with a 33 °C ambient temperature. It was assumed that a 3.8 % margin was adequate. By afternoon the temperature had risen to 39 °C and the load correspondingly so that the margin was wiped out. The 500 kV voltages were reduced to 460 kV, or 0.92 pu, and eventually lines were tripped on over current, and seven substations were without supply.

The only indication that something out of the ordinary was happening was that the rate of the load was 400 MW/minute, which was twice as much as ever recorded before.

The use of modern air conditioner motor controls results in very high reactive requirements under conditions of low voltage. It is believed that the fairly extensive use of these air conditioners could be an important factor in explaining the voltage collapse in Japan.

1.2 Scope of the dissertation

Much effort has been put into research of the phenomenon *voltage collapse*, and many approaches have been explored. Both dynamic and steady-state behavior have been studied thoroughly, though very few protection and control schemes have been implemented. As seen from the two incidents just presented, there is a need for an online indicator capable of predicting or tracking a voltage collapse scenario. In the “Tokyo” incident the system operator was given enough time to counteract the collapse, though there was no indication of any actions necessary. The voltage levels were all within limits.

After contingencies in heavily loaded systems, there have been experience with relatively low voltage profile, which has been within acceptable limits that without any further

warning experienced voltage collapse. As the voltage profile has not indicated the collapse some other measure should be used to predict the collapse. The main goal of this work has been to study the dynamic aspects of voltage collapse, with the aim of finding a voltage stability index for online use. The index or indicator must be able to tell a system operator if the system is stable or if it is so close to the "edge" that the there is a great chance the system will collapse.

Calculating a stability index based on wide area measurements requires far too much CPU time for it to be used in an online mode. Thus, emphasis has been put on using local area measurements to calculate the index.

1.3 Contributions

The main contribution of this work is a "smart relay", given the acronym VIP++, which detects voltage stability problems using local area measurements. The VIP++ algorithm is an expansion of the VIP method proposed by Khoi Vu [18, 29–32]. Aspects of the VIP algorithm are explored in this dissertation, though it must be noted that all conclusions are based on the simple algorithm of the VIP presented in papers.

The VIP is based on the steady-state assumption that voltage instability is closely related to the maximum loadability of a transmission network. The maximum loadability point or the point of collapse (PoC) is given by the maximum point on the nose curve. The VIP++ is based on the VIP methods, thus it is based on the same assumptions as the VIP, but both should be able to track a dynamic system trajectory in an online mode. They are both proposed as relays, which are placed in the system together with a Phasor Measurement Unit (PMU). In fact the VIP/VIP++ methods will be incorporated into what has been called a "black box", consisting of the necessary measuring, communication and computational devices to perform a phasor measurement. The VIP/VIP++ is simply code implemented in the computer installed at site.

The distance to the PoC does not only depend on the present state of the system but also on future changes. Therefore, an algorithm such as the VIP++ that tries to track the system trajectory is based on an assumption or hypotheses about how the system will move. Four such hypothesis have been proposed, where two, called "Distance to the PoC along the gradient" and "Shifting the gradient in the y_1 direction", have been studied thoroughly. The two other methods are just mentioned, as one failed to track the Thevenin equivalent, and the other has been considered too complex for further exploration.

1.4 Outline of the dissertation

The dissertation is organized as follows:

Chapter 2 This chapter gives a general description of voltage stability phenomena. Some proposed definitions of *voltage stability*, *voltage collapse* and *voltage security* are presented. Major components contributing to voltage instability will also be presented, together with the established methods to analyze and counteract voltage collapse.

Chapter 3 This chapter gives an introduction to the Voltage Instability Predictor (VIP), a smart relay based on local area measurements. The principle of the method is presented, together with several algorithms.

Chapter 4 This chapter presents the VIP++, which is an extension to the VIP, presented in Chapter 3. The VIP++ seeks to improve the robustness of the estimation of distance voltage collapse by including measurements on one or more surrounding buses. The distance to the PoC does not only depend on the present state of the system but also on future changes. Therefore, an algorithm that tries to track the system trajectory is based on an assumption or hypothesis about how the system will move. In this chapter several such hypotheses (methods) are illustrated and discussed

Chapter 5 Simulations of voltage collapse scenarios have been performed on a four bus test system and a 313 bus simplified model of the Norwegian grid. The simulated data is used as measured input data for the proposed algorithms to test the ability of the VIP and VIP++ methods to track the system trajectory towards PoC. In a real case these data would be measured using a PMU on site.

Chapter 6 This chapter gives a brief discussion of the objective of this dissertation. It also include the main conclusions that can be drawn from this work, and some proposals for further work are presented.

Appendix A This appendix gives a detailed mathematical description of the VIP++ algorithms. For the specific case with measurement on two load buses equations for both methods are derived. For the general case with n "known" load buses it can be difficult to find a general expression, at least for the method "Distance to the PoC along the gradient". Thus, this is only done for "Shifting the gradient in the y_1 direction", while the maximum size of the polynomial to be solved is found for the method "Distance to the PoC along the gradient".

Appendix B This appendix shows five configurations of the VIP++ method used in Section 5.1.

Appendix C This appendix contains some general theory and notations used in the dissertation.

Appendix D In order to calculated the distance to the PoC at any given point, a set of parameters has to be calculated for each measurement. Finding the expression for these parameters can be rather difficult if not impossible for large systems without the use of symbolic calculation programs such as Maple. In this appendix the maple functions to calculate the parameters for both methods are shown. A description of how they are used is also presented.

Chapter 2

Voltage Stability - Overview

This chapter gives a description of voltage stability. Important definitions of voltage stability are introduced, together with factors causing voltage instability such as mechanisms for load restoration. An overview of some commonly used voltage stability indices is also included. These indices are used to predict the proximity to voltage collapse. Many different methods for voltage stability analysis have been implemented and these are briefly described. Finally, a particular implementation of the continuation power flow and a load factor are described in some detail.

2.1 Introduction

Power system voltage stability is a dynamic phenomenon involving power generation, transmission and distribution. Voltage stability is closely associated with other aspects of power system steady-state and dynamic performance. Voltage control, reactive power compensation and management, rotor angle (synchronous) stability, protective relaying, and control center operations all influence voltage stability.

Voltage stability covers a wide range of phenomena. Induction motors, air conditioning or HVDC links can lead to fast acting system responses that within seconds can lead to system collapse. For on-load tap changers the process is slow, where a possible system collapse due to voltage instability may take several minutes to evolve. Thus, voltage stability might mean different things to different engineers.

Voltage problems are expected when developing power systems, and likewise in the case of major system breakups. Also in mature power systems, voltage stability may be a matter of concern. Two possible reasons are the pressure to operate existing generation and transmission systems closer to their capability limits and the increased use of shunt capacitors for reactive compensation. Excessive use of shunt capacitors will extend the transfer limits, but at the same time make the system more prone to voltage collapse.

The time frame of a voltage collapse can vary from a few seconds to several minutes. For some of these events this might be enough time for operators to act. Thus, there is a need for reliable indices for the detection of proximity to voltage collapse.

Voltage stability is a dynamic phenomenon, thus there should be an obvious need for dynamic voltage stability analysis. For the faster transient phenomena, dynamic simulations are necessary, but for slower, longer term phenomena, steady-state based methods might suffice. A brief overview of some commonly used methods for voltage stability analysis is provided in Section 2.4. Neither the list of methods, nor the depth of description is exhaustive.

The part of the chapter describing the general voltage stability theory is mainly based on [1, 2, 9, 15–17, 25, 28, 37, 38], while the part describing voltage stability analysis is based on [3–5, 7, 19, 21–23, 41].

2.1.1 Definitions

In this section some definitions for *voltage stability*[1], *voltage collapse* and *voltage security* will be presented. They are proposed by: CIGRE working group 38[2] and Mansour [9].

Definition 1 (Voltage stability)

CIGRE: *A power system at a given operating state is* small-disturbance voltage stable *if, following any small disturbance, voltages near loads are identical or close to the pre-disturbance values. (Small-disturbance voltage stability corresponds to a related linearized dynamic model with eigenvalues having negative real parts. For analysis, discontinuous models for tap changers may have to be replaced with equivalent continuous models.)*

A power system at a given operating state and subject to a given disturbance is voltage stable *if voltages near loads approach post-disturbance equilibrium values. The disturbed state is within the region of attraction of the stable post-disturbance equilibrium.*

Mansour: *voltage stability is the ability of a system to maintain voltage so that when load admittance is increased, load power will increase, and so that both power and voltage are controllable.*

Definition 2 (Voltage collapse)

CIGRE: *A power system at a given operating state and subject to a given disturbance undergoes* voltage collapse *if post-disturbance equilibrium voltages are below acceptable limits. Voltage collapse may be total (blackout) or partial.*

[1] voltage stability is sometimes referred to as *load stability*

Mansour: *is the process by which* voltage instability *leads to very low voltage profile in a significant part of the system (voltage may collapse due to* angular instability *as well, and sometimes only a careful post-incident analysis can discover the primary cause).*

Definition 3 (Voltage Security)
CIGRE: *means the ability of a system, not only to operate stably, but also to remain stable following credible contingencies or load increase. It often means the existence of considerable margin from an operating point to the voltage instability point (or the maximum power transfer point) following credible contingencies.*

Mansour: *The ability of a system to remain stable (voltage wise) following first and/or second contingencies as might be specified in voltage criteria.*

The CIGRE group 38 has also made a proposal for the definition of *Voltage instability*

Definition 4 (Voltage instability)
CIGRE: *is the lack of voltage stability, and results in progressive voltage decrease (or increase).*

2.1.2 Time frames for voltage instability

Voltage instability and collapse dynamics span a range from a few milliseconds to tens of minutes. Voltage stability is often classified as either [1, 28]:

- transient voltage stability,
- longer-term voltage stability.

There is usually a clear separation between the two time frames. Figure 2.1 shows many power system components and controls that play a role in voltage stability. However, only some will significantly participate in a particular incident or scenario. The system characteristics and the disturbance will determine which phenomena are important.

The time frame of *transient voltage stability* is zero to about 10 seconds. A voltage collapse is often caused by unfavorable fast-acting load dynamics of components such as induction motors or DC converters. The scenarios will often involve large disturbances like temporary short circuits. The unfavorable fast-acting load dynamics will also often be the *final cause* of any longer term voltage collapse.

Introduction of high voltage direct current (HVDC) transmission has also been known to cause transient voltage stability problems, the HVDC inverter presenting the more unfavorable “load” characteristic.

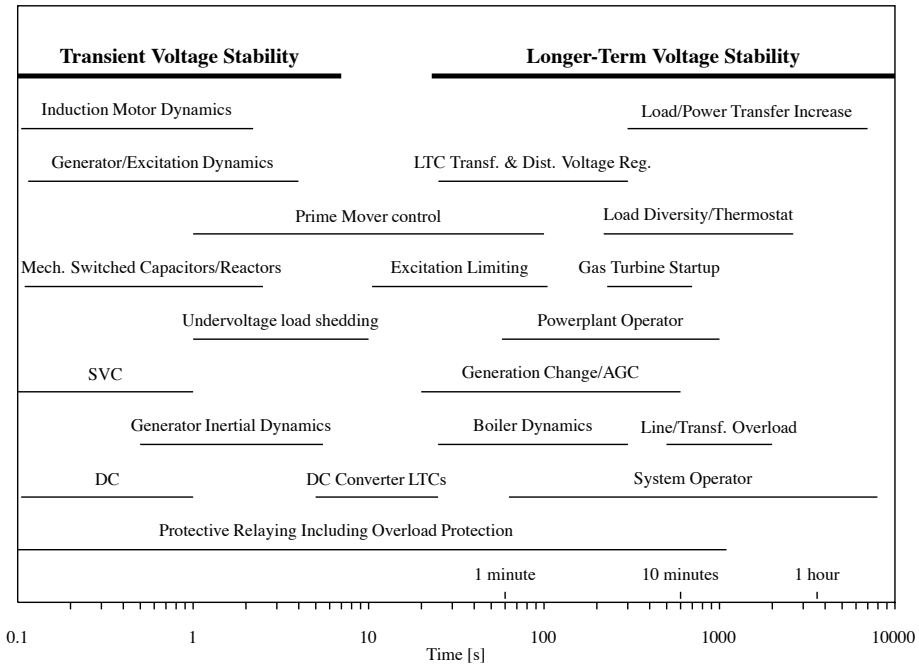

Figure 2.1: Voltage stability phenomena and time responses [28]

For *longer-term voltage stability* the time frame is from 10 seconds to 10 – 20 minutes. Such scenarios often involve high loads, high power imports and sudden large disturbances. The disturbance causes high reactive power losses and voltage sags in load areas. Load can be restored by different mechanisms like the action of on-load tap changers or thermostatic controls. Load restoration in load areas causes further sags of transmission voltages. Local reactive support can be lost when the field current of nearby, overloaded and overexcited generators, is reduced by over–excitation limiters. Thus, load voltages will sag even more.

The longer-term instability can also be driven by a very large load buildup or large rapid power transfer increase.

For this time frame, the overall response time is quite slow, the mechanisms causing the voltage instability to act slowly compared to the speed of response of the voltage controlled equipment, such as generator excitation controls and SVC controls. Voltages at controlled buses are therefore restored much faster than the overall load dynamics could managed this.

2.2 Factors affecting voltage stability

Voltage instability and collapse are dynamic and normally large disturbance phenomena, involving load, transmission and generation subsystems of large power systems. Three key aspects of voltage stability are:

1. The reactive power support either through power transfer, or at loading point.
2. The load characteristics as seen from the bulk power network.
3. The available means for voltage control at generators and in the network.

2.2.1 Reactive power support [25]

In the main grid there is a strong connection between voltage magnitude U and the reactive power Q, and similar between voltage angle δ and active power P. Using the two-bus

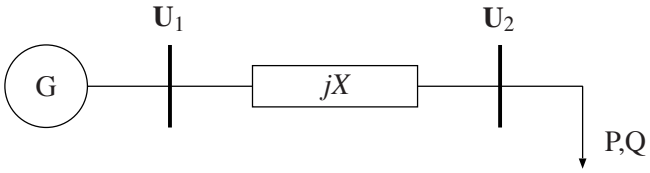

Figure 2.2: Two-bus system

system in Figure 2.2 the characteristics of voltage stability can be studied. The generator is represented by an infinite bus supplying both reactive and active load, keeping the voltage at $1.0pu$. The transmission line is represented by a reactance jX, and the load is constant power, both reactive Q and real P.

Generally, voltages are solved using the Newton-Raphson algorithm in a load-flow program, but the load voltage can be calculated analytically in this simple example. The solution of Equation (2.1) is the load voltage for the load-flow equations of the example, when the voltage angle is eliminated.

$$U_2 = \sqrt{\frac{(U_1^2 - 2QX) \pm \sqrt{V_1^4 - 4QXV_1^2 - 4P^2X^2}}{2}} \tag{2.1}$$

The solutions of load voltages are often presented as a PV-curve (see Figure 2.3). The PV-curve presents load voltages as a function of load or sum of loads. Equation (2.1) yields two solutions of voltages to any set of load flow, represented by the upper and lower parts of the PV-curve. Power systems are operated in the upper part of the PV-curve. This part of the PV-curve is statically and dynamically stable. The tip of the “nose curve” is called

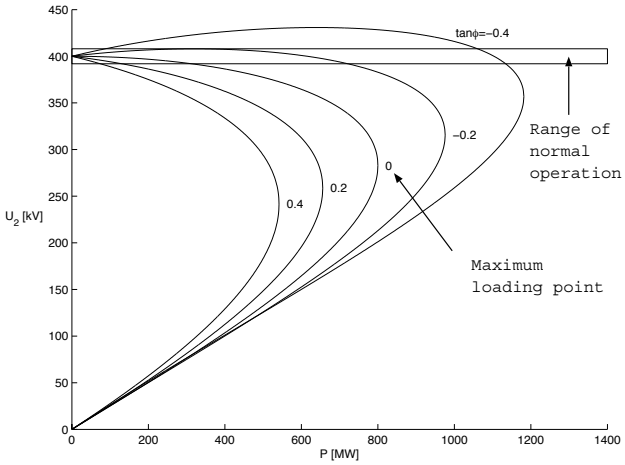

Figure 2.3: PV-curve

the maximum loading point. The critical point where the solutions unite is the voltage collapse point. The maximum loading point is more interesting from the practical point of view than the true voltage collapse point, because the maximum of power system loading is achieved at this point. The maximum loading point is the voltage collapse point when constant power loads are considered, but are different for the general case. The voltage dependence of loads affects the point of voltage collapse point. A constant controllable impedance supplied by an infinite bus over a single transmission line can be operated on any part of the PV-curve, thus even the lower part of the curve is statically stable[2]. However, when dynamic impedances are considered, the system is unstable on the lower part of the PV-curve, as a decrease in load impedances would result in a decrease in load. The power system can only operate in stable equilibrium so that the system dynamics act to restore the state to equilibrium when it is perturbed.

Figure 2.3 presents five PV-curves for the system given in Figure 2.2 with $X = 100\ \Omega$ and $V_1 = 400$ kV. Since inductive line losses make it inefficient to supply a large amount of reactive power over long transmission lines, the reactive power loads must be supported locally. According to Figure 2.3, the addition of load compensation (decrement of the value $\tan\phi$) is beneficial for the power system. The load compensation makes it possible to increase the loading of the power system according to voltage stability. Thus, the monitoring of power system security becomes more complicated because the critical voltage might be close to voltages in the normal operation range.

The opportunity to increase power system loading by load and line compensation is

[2]This contradicts the definition of voltage stability given by Mansour, but this definition accounts for the dynamic behavior of load so that the lower part of the *nose curve* is considered unstable.

valuable nowadays. Compensation investments are usually much less expensive and more environmentally friendly than line investments. Furthermore, the construction of new lines has become time-consuming and even impossible in some cases. At the same time new generation plants are being constructed further away from load centers, fossil-fired power plants are being shut down in the cities and more electricity is being exported and imported. This trend inevitably requires addition of transmission capacity in the long run.

The description of the voltage stability phenomenon has been limited to a radial system because it presents a simple and clear picture of the problem. In practical power systems, many factors affect the progress of voltage collapse due to voltage instability.

2.2.2 Load restoration

Voltage stability is closely related to load characteristics. The load is the aggregate load seen at the transmission system high voltage buses, and includes the effect of subtransmission and distribution systems. After sudden disturbances causing changes in voltage magnitudes these aggregate loads can be restored to near pre-disturbance values by three mechanisms. This load restoration is an important aspect of voltage stability. The mechanisms of (active) load restoration are [28]:

1. After a sudden change in voltage, induction motors will respond rapidly and within seconds match their mechanical load. Immediately after a sudden change in the source system, induction motors will act as impedance loads, since the motor slip cannot change instantaneously because of motor inertia. For slow-moving decay, fast-responding motors track the slow dynamics of other equipment, acting as constant active power loads.

2. Automatic tap changing on bulk power delivery transformers and distribution voltage regulators operate over tens of seconds to several minutes to restore load-side voltage, and thus voltage sensitive loads. Reactive power load and reactive power output of shunt compensators are also restored.

3. Constant energy loads are restored by thermostatic or manual control.

The dynamics of all three load restoration mechanisms can, at first, be approximated by a first order model using a single time constant. Important insight into the mechanisms can be obtained using such simplified models, incorporating only the elements that are dominant.

Induction motor

The induction motor [12, 38] is one of the loads that play an important part of a voltage collapse. The induction motor in Figure 2.4 is a simple model of an induction motor. The

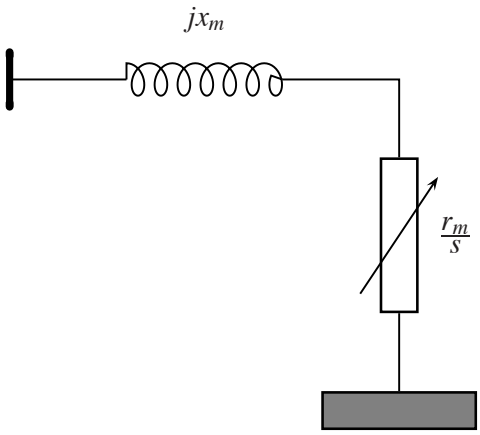

Figure 2.4: Induction motor

equations for the motor are given in Equations (2.2 - 2.4),

$$s = \frac{\omega_0 - \omega_r}{\omega_0} \tag{2.2}$$

$$\frac{ds}{dt} = \frac{1}{M{\omega_0}^2}(T_m - P_e) \tag{2.3}$$

$$P_e = V^2 \frac{\frac{r_m}{s}}{(\frac{r_m}{s})^2 + x_m^2} \tag{2.4}$$

where

- s - slip of the motor
- ω_r - rotor speed
- ω_0 - network synchronous speed
- T_m - mechanical torque [pu]
- P_e - electrical power delivered to the motor [pu].

Thermostatically controlled loads

Thermostatically controlled loads are operated in on/off states, where there is a control of the on/off times. This response can be approximated with a first order model as given in

Equation (2.5) assuming the load is combined of many such loads [28].

$$\frac{dG}{dt} = \frac{1}{T_L}(P_0 - V_L^2 G) \tag{2.5}$$

where

G - load conductance

T_L - load time constant

P_0 - reference active power

V_L - actual load bus voltage.

On load tap changers

The role of on-load tap changers (OLTC) in the voltage collapse has been studied in [9, 33–35]. The literature proposes a stability region, called the *leaf*, based on the characteristics of the OLTC, the generator and the load. Inside this region the voltage increases with increasing tap ratio n, while outside the region it drops.

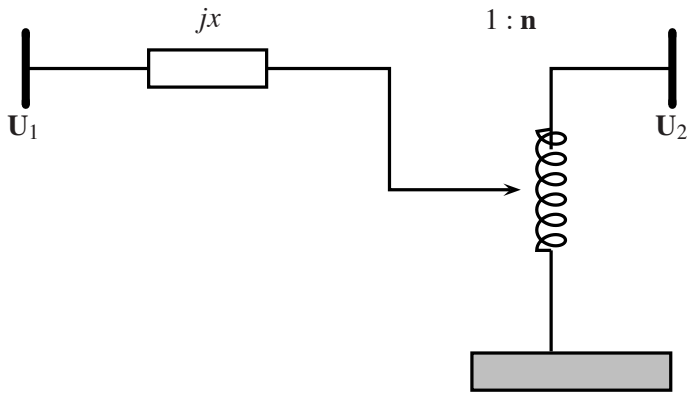

Figure 2.5: On-load tap changer

$$\mathbf{U}_1 = \frac{\mathbf{U}_2}{n} + Z \cdot \mathbf{I} \tag{2.6}$$

The tap movements on the OLTC in Figure 2.5 are discrete and are modeled by Equation (2.7).

$$n_{k+1} = n_k - d \cdot f(U_{2ref} - U_2) \tag{2.7}$$

$$f(x) = \begin{cases} -1 & \text{if} \quad x < -\Delta v \\ 0 & \text{if} \quad |x| < \Delta v \\ 1 & \text{if} \quad x > \Delta v \end{cases} \tag{2.8}$$

The discrete equation is often approximated to the continuous model when doing system analysis:

$$\frac{dn}{dt} = \frac{1}{T_t}(V_{2ref} - V_2) \tag{2.9}$$

where

n - tap changer turns ratio

T_t - tap changing time constant

V_{2ref} - reference voltage at the regulated side

V_2 - actual voltage at the regulated side.

When running simulations on computer-based simulation tools there is no need for this approximation, the discrete steps can easily be incorporated in the programs.

For tap changers, the formulation could be changed so that Equation (2.5) applies, where G is the conductance reflected to the high voltage side by tap changing. For tap changing involving deadbands, voltage and timer relays, and discrete taps, a continuous first order model is a quite crude approximation.

Stability of loads [28]

As each state variable increases from zero, load power increases, reaches a maximum, and then decreases. For all three mechanisms, the active power versus state variable will be as in Figure 2.6. For stability following a large disturbance, the state variable at the moment of the final source system configuration must be within the *region of attraction* of the stable equilibrium point, x^s. The region of attraction extends to the unstable equilibrium point, x^u. For state variables less than x^s and greater than x^u, the right-hand side of Equations (2.3), (2.5) and (2.9) are positive, causing an increase in state variable. For the remaining region the right-hand side of the equations is negative, and there is a reduction in the state variables.

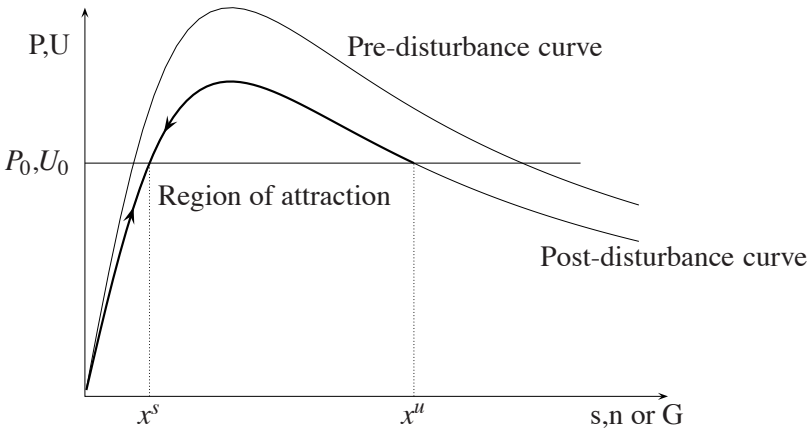

Figure 2.6: Active power versus state variable at the moment of the final source

Exponential load recovery model

Instead of using physical models as in the three previous paragraphs a generic model or black box approach can be adopted. In [16] Karlsson and Hill propose the exponential load recovery model in Equations (2.10) and (2.11).

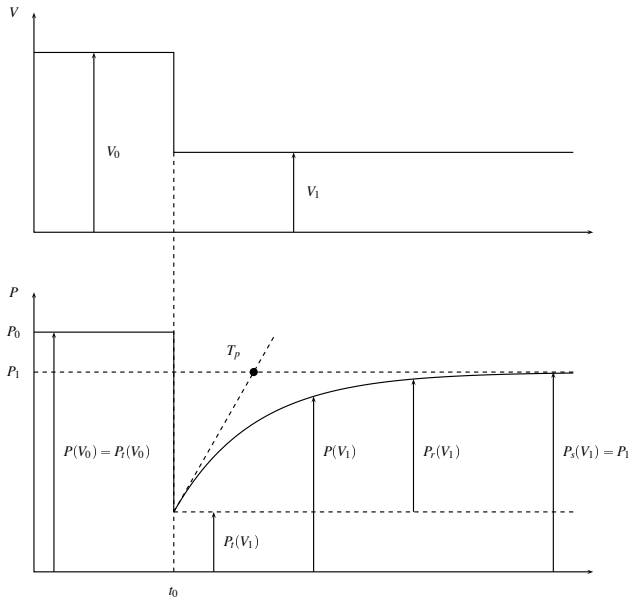

Figure 2.7: Exponential load recovery

$$P = P_r + P_0 \left(\frac{V}{V_0}\right)^{\alpha_t} \tag{2.10}$$

$$Q = Q_r + Q_0 \left(\frac{V}{V_0}\right)^{\beta_t} \tag{2.11}$$

where P_r and Q_r are given by the dynamic Equations (2.12) and (2.13).

$$T_{pr}\frac{dP_r}{dt} + P_r = P_0 \left[\left(\frac{V}{V_0}\right)^{\alpha_s} - \left(\frac{V}{V_0}\right)^{\alpha_t}\right] \tag{2.12}$$

$$T_{qr}\frac{dQ_r}{dt} + Q_r = Q_0 \left[\left(\frac{V}{V_0}\right)^{\beta_s} - \left(\frac{V}{V_0}\right)^{\beta_t}\right] \tag{2.13}$$

where α_r and β_r are the transient exponents, and α_s and β_s are the stationary exponents. Figure 2.7 show the general exponential response to a voltage drop. The figure shows the response of the active load, but the reactive is similar only with different parameters. Initially the dynamic equations are at a stable equilibrium point given by $V = V_0$ and $P_r = Q_r = 0$. When there is a voltage drop from V_0 to V_1 the active load drops with the fraction $(V_1/V_0)^{\alpha_r}$. There is an exponential load recovery from this drop to a new stable equilibrium point given by the fraction $P_0(V_1/V_0)^{\alpha_s}$, or P_1 as given in the figure. This can be the same as pre-contingency, in case $\alpha_s = 1$, or it can be lower $\alpha_s < 1$, as is the case in the figure.

The exponents are dependent on the load area, whether it is domestic or industrial load, and will also change with different times of day, week or year.

2.2.3 Combination of dynamic factors

Thermostatically controlled loads are dynamical loads with large time constants. In this section some fundamental aspects of the dynamics of a voltage collapse will be presented using a simple model, with an OLTC regulating the voltage on a thermostatically controlled load [17], see Figure 2.8.

Model

In this system there are *two* dynamic mechanisms, which both have influence on the voltage stability. The dynamics of the OLTC and the thermostatically controlled load is given by Equations (2.5) and (2.9), where V_L in Equation (2.5) is replaced by U_2. Ohm's law and

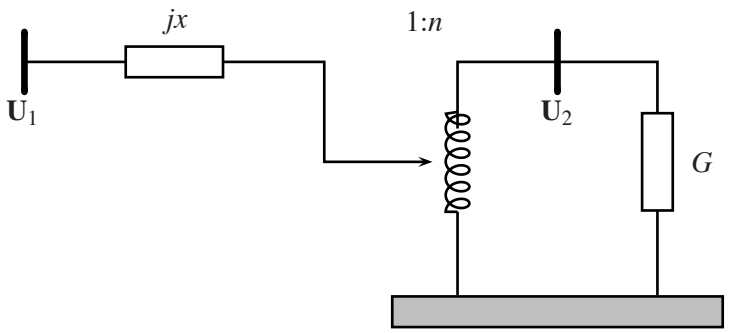

Figure 2.8: On-load tap changer and thermostatically controlled load

Table 2.1: System values

Description	variable	value (pu)
Line reactance	x	0.1
Voltage reference OLTC	V_{2ref}	0.9
Load reference	P_{ref}	4.0

ratio on the transformer is given by Equations (2.14) and (2.15) respectively.

$$\mathbf{I_1} = \frac{\left(\mathbf{U_1} - \frac{\mathbf{U_2}}{n}\right)}{jx} \tag{2.14}$$

$$\mathbf{I_1} = n\mathbf{I_2} = n\mathbf{U_2}G \tag{2.15}$$

By substituting Equation (2.15) into Equation (2.14) the absolute value of the voltage on regulated bus can be found as

$$V_2 = V_1 \frac{n}{\sqrt{1+(Gx)^2 n^4}} \tag{2.16}$$

In steady-state

$$U_2 = U_{ref} \quad \text{and} \quad G = G_{ref} = \frac{P_{ref}}{U_{2ref}^2}$$

Solving Equation (2.16) for step n in steady-state

$$n = \frac{\sqrt{U_1^2 \pm \sqrt{U_1^4 - 4x^2 P_{ref}^2}}}{\sqrt{2}\frac{P_{ref}}{U_{2ref}}x} \tag{2.17}$$

For any given value of the voltage $\mathbf{U_1}$, the steady-state step n value can be calculated using Equation (2.17). The equation yields two solutions, but as will be shown, only one is stable.

Case study

The following cases have been explored:

1. The conductance G is locked to its original steady-state value $G = G_0 = G_{ref}$, while the step changer act according to Equation (2.9).
2. The step changer is locked to its original steady-state value $n = n_0$, while the conductance act according to the Equation (2.5).
3. Both state variables act according to dynamic equations.

There is a step change in voltage U_1 from $U_1 = 1.0$ pu to $U_1 = 0.9$ pu for all the cases.

Fixed conductance The conductance is given by $G_0 = G_{ref} = \frac{P_{ref}}{U_{2ref}^2}$, which substituted into Equation (2.16) gives a voltage U_2 on the load conductance given by Equation (2.18).

$$U_2(n) = \frac{nU_1U_{2ref}^2}{\sqrt{U_{2ref}^4 + P_{ref}^2x^2n^4}} \tag{2.18}$$

Figure 2.9 plots two curves of U_2, using $U_1 = 1.0$ pu and $U_1 = 0.9$ pu respectively. Where both the curves intersect the straight line given by the voltage reference $U_{2ref} = 0.9$ pu, there will be both stable and unstable equilibrium points.

Steady-state stability is analyzed by using the eigenvalues of the linearized system. The dynamical equation is given by

$$\frac{dn}{dt} = f(U_2) = \frac{1}{T_t}(U_{2ref} - U_2) \tag{2.19}$$

Linearizing Equation (2.9) gives:

$$\Delta\frac{dn}{dt} = \frac{\partial f}{\partial n}\Delta n = -\frac{1}{T_t}\frac{\partial U_2}{\partial n}\Delta n = \lambda\Delta n \tag{2.20}$$

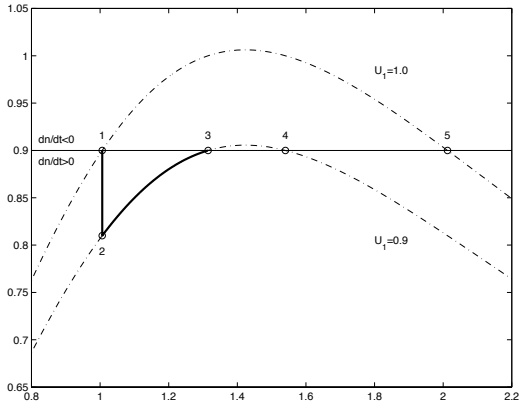

Figure 2.9: Tap changer motion, fixed conductance

The criteria for steady-state stability is given by $\lambda < 0$, thus the eigenvalues must be in the left half plane. This leads to a criteria for stability as given in Equation (2.21).

$$\frac{\partial U_2}{\partial n} > 0 \tag{2.21}$$

From Figure 2.9 it is clear that this condition is met by both equilibrium points 1 and 3 on the curves for $U_1 = 1.0$ pu and $U_1 = 0.9$ pu respectively, while both points 4 and 5 do not meet this condition, and are thus unstable equilibrium points.

As indicated in the figure any system trajectory above the straight line will have a reduction in the tap changer, while it is increasing below. For the curve given by $U_l = 1.0$ pu we see that "region of attraction" for point 1 is from $n = 0$ and up to point 5. Similar for the case $U_1 = 0.9$ pu where the "region of attraction" for point 3 is from zero and up to point 4.

Given a system in point 1 with a drop in the voltage U_l from 1.0 pu to 0.9 pu, the system will immediately jump to point 2, which is in the "region of attraction" of point 3, thus the system will move to this new stable equilibrium point.

Locked tap changer The load is given by

$$P = U_2^2 G \tag{2.22}$$

Using Equation (2.18) the load can be rewritten as

$$P = \frac{n^2 U_1^2 G}{1 + G^2 x^2 n^4} \tag{2.23}$$

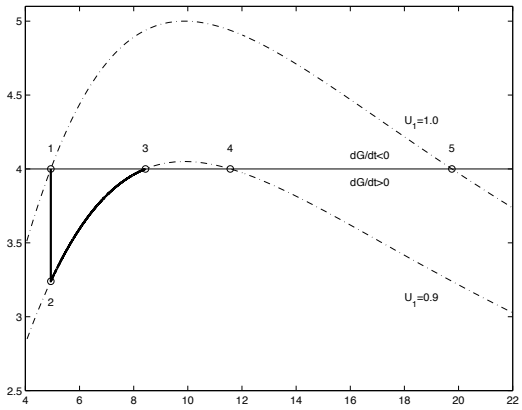

Figure 2.10: Motion of conductance with locked tap changer

The two curves for $U_1 = 1.0$ pu and $U_1 = 0.9$ pu are shown in Figure 2.10. The equilibrium points, the intersections of the two lines with the straight line given by the load reference $P = P_{ref}$, can be found by solving Equation (2.23) for G.

$$G = \frac{U_1^2 \pm \sqrt{U_1^4 - 4P_{ref}^2 x^2}}{2x^2 n^2 P_r ef} \tag{2.24}$$

The equation gives two equilibrium points for both cases of U_1, one stable and the other unstable. As in previous section the steady-state stability can be analyzed using the eigenvalues of the linearized system. The dynamical equation is given by

$$\frac{dG}{dt} = f(P) = \frac{1}{T_L}(P_{ref} - P) \tag{2.25}$$

which can be linearized as

$$\Delta\frac{dG}{dt} = -\frac{1}{T_L}\frac{\partial P}{\partial G}\Delta G = \lambda\Delta G \tag{2.26}$$

The steady-state stability is given by $\lambda < 0$, thus

$$\frac{\partial P}{\partial G} > 0 \tag{2.27}$$

From the figure it is clear that points 1 and 3 are stable while points 4 and 5 are unstable. The "region of attraction" can be found in a similar way as in the previous section.

Free state variables The system will after a step change in voltage U_1 seek a new steady state equilibrium given by setting both Equations (2.5) and (2.9) to zero, thus $P = P_{ref}$ and $U_2 = U_{ref}$. This is the same steady-state equilibrium found in Section 2.2.3, see Figure 2.11. There will be a difference in the system trajectory, moving from the old steady state to the new, since the conductance G also is "free" and will follow the given dynamic equation.

Whether the system trajectory will end in a steady-state equilibrium or will become unstable depends on the system dynamics. More precisely, will the two time constants T_L and T_t for the thermostatically controlled load and OLTC respectively, have great impact on the stability of the system.

Substituting Equations (2.16) and (2.23) into the dynamic Equations (2.5) and (2.9), the dynamic equations can be written as given in Equations (2.28) and (2.29).

$$\frac{dG}{dt} = f_1(G,n) = \frac{1}{T_L}\left(P_0 - {V_1}^2 \frac{Gn^2}{1+(Gx)^2n^4}\right) \tag{2.28}$$

$$\frac{dn}{dt} = f_2(G,n) = \frac{1}{T_t}\left(V_{2ref} - V_1 \frac{n}{\sqrt{1+(Gx)^2n^4}}\right) \tag{2.29}$$

Setting both these two equations to zero and solving for *G(n)* results in the isoclines given by Equations (2.30) and (2.31). The isoclines are plotted in Figure 2.11

$$G(n) = \frac{1}{2n^2P_0x^2}\left({V_1}^2 \pm \sqrt{{V_1}^4 - 4x^2{P_0}^2}\right) \qquad (\dot{g}=0) \tag{2.30}$$

$$G(n) = \frac{1}{xn^2}\sqrt{\left(\frac{V_1}{V_{2ref}}\right)^2 \cdot n^2 - 1} \qquad (\dot{n}=0) \tag{2.31}$$

There are two isoclines given by Equation (2.30), and only one for Equation (2.31). The equilibrium points can be found in the intersections of the isoclines given by the two equations.

$$G_0 = \frac{P_0}{V_{2ref}^2} \tag{2.32}$$

$$n_{(0,1,2)} = \frac{V_{2ref}}{2xP_0}\sqrt{V_1^2 \pm \sqrt{V_1^4 - 4x^2P_0^2}} \tag{2.33}$$

In Figure 2.11 (n_0,G_0) is calculated using $V_1 = 1.0$ pu, while (n_1,G_0) and (n_2,G_0) are the solution to Equations (2.32) and (2.33) using $V_1 = 0.9$ pu. In the gray area in Figure 2.11 the derivative $\dot{G}$ is negative, thus any system trajectory in that area will move downwards

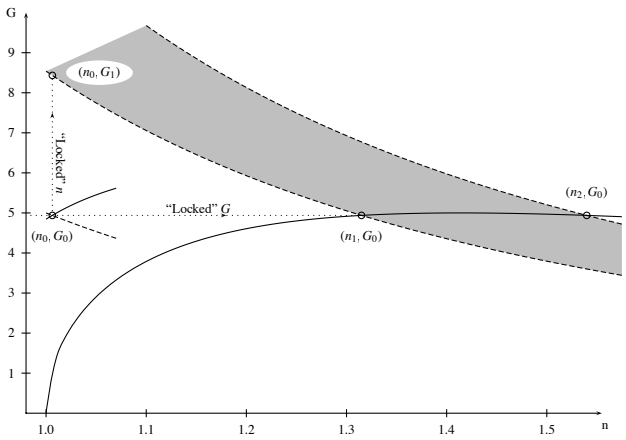

Figure 2.11: Isoclines in *G*-*n* space

in the figure, while outside the gray area, $\dot{G}$ is positive and the system is moving upwards. On the dotted line the derivative is zero and any trajectory crossing this line will do it horizontally. Similarly any trajectory above the solid line will have a positive derivative $\dot{n}$, and a negative below, with the system trajectory moving either to the right or the left respectively. Any crossing of the solid line will happen vertically. The two cases with locked conductance or locked tap changer, presented in the two previous sections are also plotted in the figure with the system trajectory moving from point (n_0, G_0) to (n_1, G_0) or (n_0, G_1).

Steady-state stability can be analyzed using the eigenvalues of the linearized system.

$$\frac{d}{dt}\begin{bmatrix} \Delta G \\ \Delta n \end{bmatrix} = \begin{bmatrix} \frac{\partial f_1}{\partial G} & \frac{\partial f_1}{\partial n} \\ \frac{\partial f_2}{\partial G} & \frac{\partial f_2}{\partial n} \end{bmatrix} \cdot \begin{bmatrix} \Delta G \\ \Delta n \end{bmatrix} = A \cdot \begin{bmatrix} \Delta G \\ \Delta n \end{bmatrix} \tag{2.34}$$

Due to the complexity of the matrix A, the eigenvalues will be analyzed for each equilibrium point numerically. For all the cases the values of T_L and T_t are assumed positive.

Point (n_0, G_0):

$$A = \begin{bmatrix} \frac{-0.48}{T_L} & \frac{-4.77}{T_L} \\ \frac{0.04}{T_t} & \frac{-0.54}{T_t} \end{bmatrix} \tag{2.35}$$

The eigenvalues are given by

$$\lambda = 0.32(-\sqrt{0.58T_t^2 + 1.27T_tT_L + 0.70T_L^2} \pm \sqrt{0.58T_t^2 - 2.97T_tT_L + 0.70T_L^2}) \tag{2.36}$$

Since the two time constants T_L and T_t are assumed positive, the eigenvalues will have negative real parts, thus the equilibrium point is a *stable node*.

Point (n_1, G_0):

$$A = \begin{bmatrix} \frac{-1.13}{T_L} & \frac{-0.95}{T_L} \\ \frac{0.08}{T_t} & \frac{-0.11}{T_t} \end{bmatrix} \tag{2.37}$$

The eigenvalues are given by

$$\lambda = 0.15(-\sqrt{0.18T_t^2 + 0.30T_tT_L + 0.13T_L^2} \pm \sqrt{0.18T_t^2 - 3.53T_tT_L + 0.13T_L^2}) \tag{2.38}$$

The point is a *stable node* since the eigenvalues have negative real parts.

Point (n_2, G_0):

$$A = \begin{bmatrix} \frac{0.13}{T_L} & \frac{0.82}{T_L} \\ \frac{0.11}{T_t} & \frac{0.09}{T_t} \end{bmatrix} \tag{2.39}$$

The eigenvalues are given by

$$\lambda = 0.08(\sqrt{0.63T_t^2 + 0.91T_tT_L + 0.33T_L^2} \pm \sqrt{0.63T_t^2 + 12.49T_tT_L + 0.33T_L^2}) \tag{2.40}$$

The point has eigenvalues with one positive real part and one negative real part, thus it is an *unstable saddle* point.

Two simulations were permformed to test the stability of the system. In both cases teh time constant for the tap changer is $T_t = 1$ seconds.

Case: $T_L = 10$ seconds If the ratio in the time constants between the thermostatically controlled conductance and the tap changer is 10 to 1, the system will converge to a new steady-state stable equilibrium point as shown in Figure 2.12, which is the same as Figure 2.11 but with a different axis and with a system trajectory plotted as a solid line. Since the time constant of the conductance is so large, the value of G as it crosses the dotted line isocline $\dot{G} = 0$ is low enough for the system to reach down past the dotted isocline $\dot{n} = 0$ and into the region of reducing n. This saves the system as it converges to equilibrium point (n_1, G_0). In Figure 2.13 both the values of P_{load} and U_2 are over compensated, before they are reduced to their reference values. This over-compensation is shown for both system variables in Figure 2.13 and the state variables in Figure 2.12.

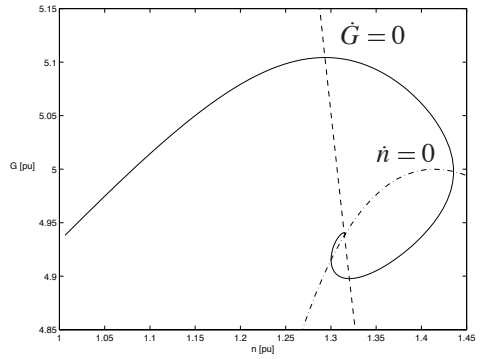

Figure 2.12: System trajectory in *G*-*n* plan for simulation using $T_L = 10$ sec

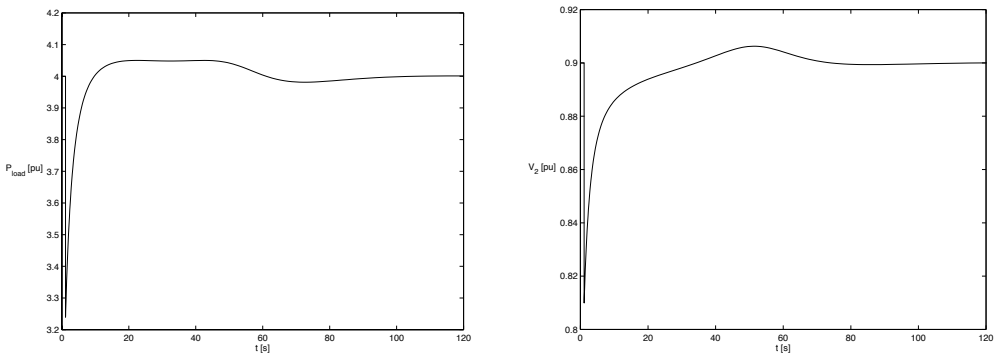

(a) Load

(b) Voltage

Figure 2.13: Thermostatically controlled load and voltage

Case: $T_L = 5$ **seconds** By reducing the ratio between the two time constants T_L and T_t the system becomes unstable, as shown in Figure 2.14. After the initial voltage drop, G is increased to a level such that when it passes the first isocline $\dot{G} = 0$, it is not able to reach down below the isocline $\dot{n} = 0$, but passes the second isocline $\dot{G} = 0$ and into a region where both state variables are increasing towards infinity. Throughout the simulation the value of n is increasing since the voltage on the secondary side of the OLTC never reaches its reference value. Since the load reference is reached, there is a temporary reduction in the conductance, but the combination of increasing n and reducing G is not enough for the voltage to reach its reference value. When the system trajectory passes the second isocline

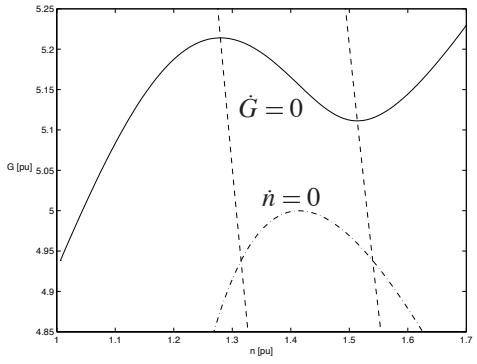

Figure 2.14: System trajectory in *G*-*n* plan for simulation using $T_L = 5$ sec

there is an immediate increase in both G and n, at the same time as both the voltage and load are reduced dramatically. In the period from 10 to 25 seconds both voltage and load are kept at almost a constant level, which would be satisfactory from an operator's point of view. At the same time there are changes in both the load conductance and the tap changer,

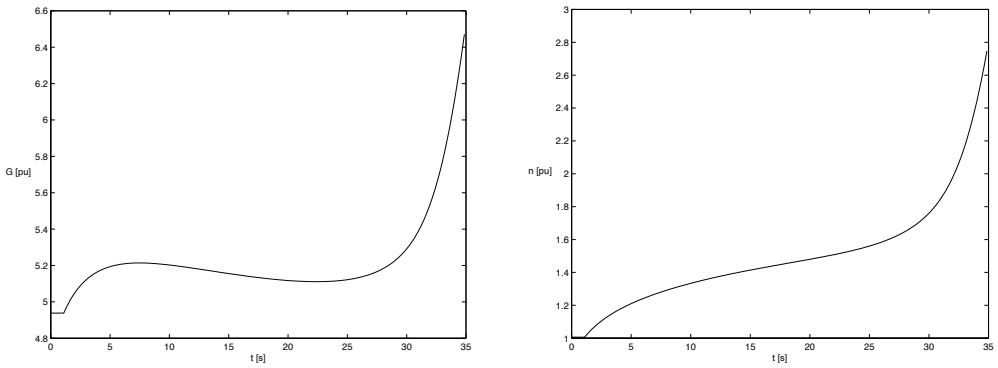

(a) Admittance G (b) Step change n

Figure 2.15: Thermostatically controlled load and voltage

as shown in Figure 2.15. It is clear from the measurements of load or voltage that an oncoming voltage collapse would be hard to detect as both seem to stabilize. The system is in reality lost as the trajectory passes the second isocline, blocking the tap changer cannot save the system as the conductance keeps on increasing. Any action on the tap

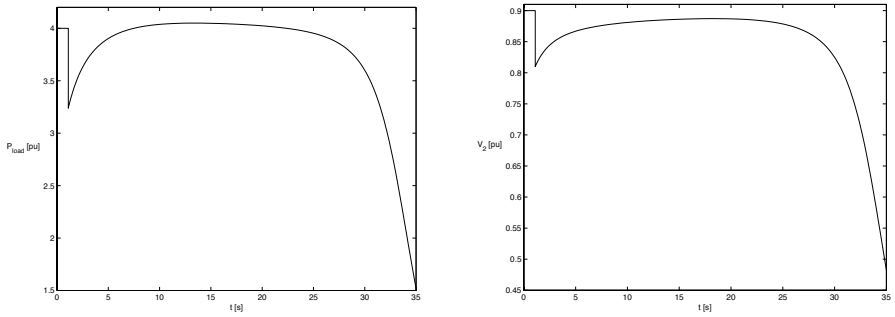

(a) Load (b) Voltage

Figure 2.16: Thermostatically controlled load and voltage

changer before this crossing would save the system, as the conductance would be reduced down to reference value. In such a case, the secondary steady state value of the voltage would be below the reference value U_{2ref}, but a voltage collapse would have been avoided.

Conclusion

The final conclusion is that a system might become unstable although steady-state equilibrium points exist. In the cases presented here the time constants have been crucial about whether the system becomes unstable or converges to a stable equilibrium point after a contingency.

2.3 Countermeasures for voltage collapse

Only a short description of the different countermeasures will be given [2], and they are divided into two sub-categories given by transient and long-term voltage stability.

2.3.1 Transient voltage instability

Generation control

Generators operate in the same time frame as the destabilizing mechanisms of transient voltage stability. Therefore, generator reactive output is very important in preventing transient voltage collapse. The generator has substantial overload capability, and it is vital that the excitation limiter takes advantage of this capability.

Network reactive power compensation

Due to the strong connection between reactive power and voltage magnitude, voltage stability can be improved by increasing the reactive power production at load centers. Some shunt compensations that can be applied are:

- Shunt capacitor banks
- Static var compensators
- Synchronous condensers
- GTO-thyristor-based static var compensators (advanced SVC or STATCON)

Undervoltage load shedding

Undervoltage load shedding is a low-cost, powerful countermeasure to maintain transient voltage stability for severe contingencies. For transient voltage stability, the time delays applied are critical and cannot be much longer than one second.

2.3.2 Long-term voltage instability

Generation design characteristics

By using generators with higher nominal power factor, $\cos\phi_N$, at rated active power, a higher reactive power reserve is available. The power factor at normal operation should be maintained close to 1.0, using other components for reactive power compensation. Thus, providing a fast continuous reactive power reserve.

Effective reactive power compensation

The most robust transmission network-based countermeasure for voltage collapse is new transmission. However, new transmission is very costly and, unless justified by other benefits, is unlikely to be a practical solution to voltage collapse. The more practical transmission network-based solutions are series and shunt reactive power compensation. There are five sources of reactive power for improving voltage stability:

- Series capacitors
- Switched shunt capacitor banks
- Generators
- SVCs

- Synchronous condensers

Such compensation as the passive components mentioned above are valuable when preventing voltage collapse, but at the same time they allow the system to be operated closer to the critical point.

Tap changer control

For voltage collapse scenarios, the bulk system voltages slowly decrease while the OLTCs restore the distribution system voltages. Therefore, the process takes a long time before a new steady-state situation is reached (or voltage collapse occurs). In this situation, the OLTCs may be working for several minutes before the load is fully restored, or the voltage collapses.

A delay of the load restoration gives time for other corrective actions. The load restoration may be delayed and/or limited by certain measures, such as blocking of OLTCs, limiting number of steps, or lengthening the time delay between steps.

Load shedding

Undervoltage load shedding (UVLS) is a very effective solution to voltage stability problems, providing a good protection against system blackout for emergency operating conditions following unusual disturbances outside normal planning and operating criteria.

2.4 Methods for voltage stability analysis

This section gives an overview of methods to analyze voltage instability scenarios and correspondingly assess system security. These methods are used at the various decision stages from planning to real-time.

2.4.1 Contingency analysis

Contingency analysis [7] aims at analyzing the system response to large disturbances that may lead to instability and collapse. The system is considered secure if it can withstand each set of credible incidents, referred to as contingencies. For long-term voltage stability analysis, the credible contingencies are outages of transmission and generation facilities; the sequence of events leading to such outages does not really matter. A well known criterion is the N-1 security according to which a system must be able to withstand any single transmission or generation outage.

2.4.2 Loadability limit determination

While contingency analysis focuses on a particular operating point, it may be desirable to determine how far a system can move away from this operating point and still remain in a stable state. This type of analysis involves large but smooth deviations of parameters p, which we refer to as the system stress.

A case of practical interest is when the stress is distributed over a set of buses, according to participation factors. This leads to parameter changes of the type [7]

$$p = p_0 + \mu\lambda \tag{2.41}$$

where

- p_0 is the initial parameter vector
- μ is a scaling factor
- λ is the direction of system stress.

The load flow equations are given by

$$f(x, p) = 0 \tag{2.42}$$

where

$$x = \begin{bmatrix} V \\ \delta \end{bmatrix} \quad \text{and} \quad p = \begin{bmatrix} P \\ Q \end{bmatrix} \tag{2.43}$$

P-V curves

P-V curves [21, 28] are useful for a conceptual analysis of voltage stability. A disadvantage is that the power flow simulation will diverge near the nose or maximum power point on the curve. Another disadvantage is that generation must be realistically rescheduled as the area load is increased.

Figure 2.3 shows the family of P-V curves for different power factors. At more leading power factors the maximum power is higher (leading power factor is obtained by shunt compensation). The critical voltage is also higher, which is a very important aspect of voltage stability.

V-Q curves

For large systems, the curves are obtained by a series of power flow simulations. V-Q curves [21, 28] plot voltage at a test or critical bus versus reactive power on the same bus. A fictitious synchronous condenser is represented at the test bus. In computer program

parlance, the bus is converted to a *PV bus* without reactive power limits. Power flow is simulated for a series of synchronous condenser voltage schedules, and the condenser reactive output is plotted versus scheduled voltage. Voltage is the independent variable and is the abscissa variable.

Advantages of V-Q curves:

- voltage security is closely related to reactive power, and a V-Q curve gives reactive power margin at the test bus. The reactive power margin is the MVAr distance from the operating point to either the bottom of the curve, or to a point where the voltage squared characteristic of an applied capacitor is tangent to the V-Q curve. The test bus could be representative of all buses in a "voltage control area"
- V-Q curves can be computed at points along a P-V curve to test system robustness.
- The characteristics of the test bus shunt reactive compensation (capacitor, SVC, or synchronous condenser) can be plotted directly on the V-Q curve. The operating point is the intersection of the V-Q system characteristic and the reactive compensation characteristic. This is useful since reactive compensation is often a solution to voltage stability problems.
- The slope of the V-Q curve indicates the stiffness of the test bus (the ΔV for a ΔQ).
- For more insight, the reactive power of generators can be plotted on the same graph. When nearby generators reach their VAr limits, the slope of the V-Q curve becomes less steep and the bottom of the curve is approached.

Point of collapse

The point of collapse method [5] solves the conditions for the bifurcation point. The bifurcation point is characterized by the steady-state Jacobian, denoted by $D_z f(z,\lambda)$ having a single and unique zero eigenvalue, with non-zero left and right eigenvectors. These conditions can be summarized by:

$$\begin{array}{rcr} f(x,\lambda)=0 & & f(x,\lambda)=0 \\ D_x f(x,\lambda)=0 & \text{or} & D_x^T f(x,\lambda)=0 \\ \|v\| \neq 0 & & \|w\| \neq 0 \end{array} \tag{2.44}$$

where

- $D_x f(x,\lambda)$ is the system Jacobian
- w and v are the left and right eigenvectors

The point of collapse method has the advantage of producing left and right eigenvector information. The left eigenvector can be used to compute an optimal control strategy to avoid saddle-node bifurcations, whereas the right eigenvector can be used to detect variables (areas) in the network prone to voltage collapse.

Optimization based methods

Loadability limits can be computed as corresponding to the maximum value of μ such that Equations (2.41) and (2.42) have a solution. Hence, the following optimization problem has to be solved [7]:

$$\begin{aligned} \max \quad & \mu \\ \text{subject to} \quad & f(x, p_0 + \mu\lambda) = 0 \end{aligned} \tag{2.45}$$

Defining the Lagrangian L relative to (2.45), and setting its derivatives with respect to x, μ and Lagrangian multipliers w to zero, we obtain the first-order optimality conditions:

$$f_x^T w = 0 \tag{2.46}$$

$$f(x, p_0 + \mu\lambda) = 0 \tag{2.47}$$

$$1 + w^T f_{p_0}\lambda = 0 \tag{2.48}$$

The nonlinear Equations (2.46)-(2.48) are solved using the Newton method. The limit is computed directly, without determining the solution path between the base case and limit points. The optimization method is thus expected to be computationally more efficient than the continuation method. On the other hand, the latter is more attractive when the effect of controls acting along the solution path must be incorporated, or when it is of interest to obtain the solution path explicitly.

Continuation power flow

The Jacobian matrix of the power flow equations becomes singular at the voltage stability limit. Consequently, conventional power-flow algorithms are prone to convergence problems at operating points near the stability limit. The continuation power-flow [3, 21] analysis overcomes this problem by reformulating the power-flow equations so that they remain well conditioned at all possible loading conditions. This allows the solution of the power-flow problem for stable as well as unstable equilibrium points.

The continuation power-flow analysis uses an iterative process involving predictor and corrector steps as depicted in Figure 2.17. From a known initial solution (A), a tangent predictor is used to estimate the solution (B) for a specified pattern of load increase. The corrector step then determines the exact solution (C) using a conventional power-flow analysis with the system load assumed to be fixed. The voltages for a further increase

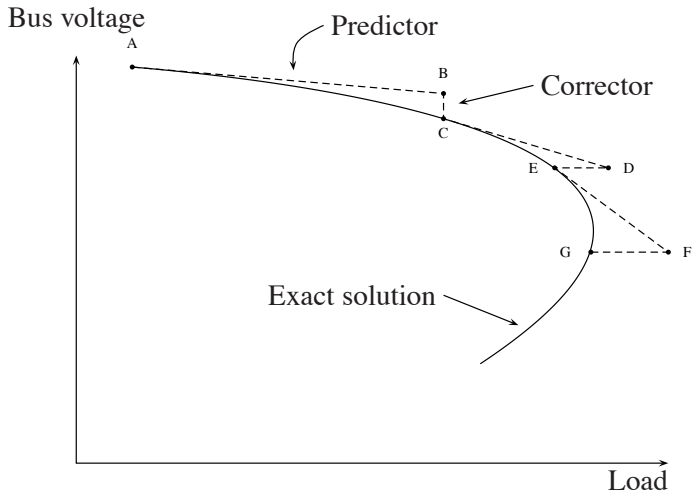

Figure 2.17: A typical sequence of calculations in a continuation power-flow analysis

in load are then predicted based on a new tangent predictor. If the new estimate load (*D*) is now beyond the maximum load on the exact solution, a corrector step with fixed loads would not converge; therefore, a corrector step with a fixed voltage at the monitored bus is applied to find the exact solution (*E*). As the voltage stability limit is reached, the size of load increase has to be reduced gradually during the successive predictor steps to determine the exact maximum load.

Shortest distance to instability

The distance to voltage instability is normally determined by increasing the system load in a predefined manner, representing the most probable stressing scenario based on historical and forecast data. However, we are also interested in knowing the loading pattern that results in the smallest stability margin [4, 21]. What we want is to find the set of load MW and MVAr increments whose vector sum is minimum, and when imposed on the initial operating condition, cause the power-flow Jacobian to be singular.

Let J_x and J_p be the Jacobian matrices of the vector function f with respect to x and p respectively. The system reaches its voltage stability critical point if the parameter vector $p_\star$ are such that the power-flow Jacobian matrix J_x is singular. Let S denote the hypersurface in the N-dimensional parameter space such that $J_x(x_\star, p_\star)$ is singular if $p_\star$ is a point on S.

Given an initial system operating point (x_0, p_0), we wish to find the parameter vector $p_\star$ on S such that the distance between p_0 and $p_\star$, $\mu = |p_\star - p_0|$, is a local minimum for the distance between p_0 and S. The following procedure determines the vector $\eta_\star$ along which

the distance between the initial equilibrium point (x_0, p_0) and the singular point $(x_\star, p_\star)$ is the shortest:

1. Let λ_0 be an initial guess for the direction $\lambda_\star$, $|\lambda_0| = 1$.
2. Stress the system by incrementally increasing p along the direction of λ_i until J_x becomes singular; that is, determine μ_i, p_i and x_i so that $p_i = p_0 + \mu_i \lambda_i$ is on the surface S.
3. set $\lambda_{i+1} = w_i J_p$, and $|\lambda_{i+1}| = 1$, where w_i is the left eigenvector of J_x.
4. Iterate steps 1,2,3 until λ_i converges to a value $\lambda_\star$. Then, $p_\star = p_0 + \mu_\star \lambda_\star$ is the corresponding equilibrium condition.

Load factor L

The load index [19, 23] is a state-based index that measures "how close" a load bus is to the maximum loadability limit, often denoted as the steady-state voltage stability limit, or the bifurcation point. This load index can be used to measure the risk of a possible voltage collapse, as the system loading is increased.

Line model The fundamental theory for this load index is described and proved for the simplest of power systems. Such a power system is represented in Figure 2.18 and consists of a single load bus supplied by a single generator bus across a transmission line. The

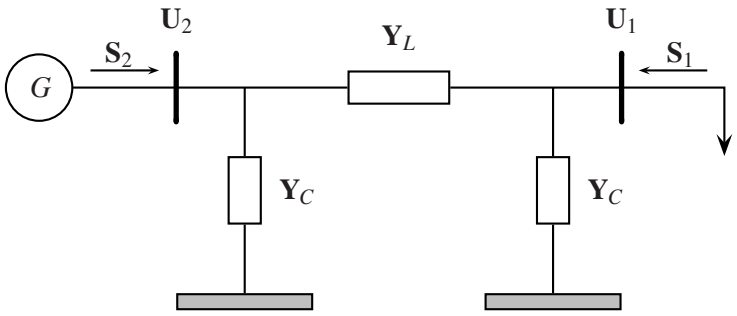

Figure 2.18: A single load supplied from a single generator across a transmission line

voltage at bus no. 1 can be expressed as given in Equation (2.49).

$$V_1 = \sqrt{\frac{|\mathbf{S}_1|}{|\mathbf{Y}_{11}|} \cdot (r \pm \sqrt{r^2 - 1})} \tag{2.49}$$

where:

$$r = \frac{V_0^2 \cdot |\mathbf{Y}_{11}|}{2 \cdot |\mathbf{S}_1|} + \cos(\phi_{S_1} + \theta_{11}) \tag{2.50}$$

ϕ_{S_1} is the phase angle of the complex power and θ_{11} is the phase angle of the admittance element $\mathbf{Y}_{11}$.

Stability criterion The region of feasible (practical solutions) voltage solutions lies on the upper part of the PV curve. The voltage solutions on the bottom part of the curve may also be found analytically, but they are (most likely) unstable in terms of voltage. The limit for this region, also called the steady-state voltage stability limit or bifurcation point, is determined by:

$$\pm\sqrt{\frac{V_0^4}{4} + a \cdot V_0^2 - b^2} = \pm\frac{|\mathbf{S}_1|}{|\mathbf{Y}_{11}|}\sqrt{r^2 - 1} = 0 \tag{2.51}$$

At this point the multiple solutions of the power flow coalesce into one solution, and power-system Jacobian becomes singular. Using $r = 1$, which is necessary to satisfy Equation (2.51), Equation (2.49) can be transformed to:

$$\frac{|\mathbf{S}_1|}{|\mathbf{Y}_{11}| \cdot V_1^2} = |1 + \frac{\mathbf{U}_0}{\mathbf{U}_1}| = 1 \tag{2.52}$$

This last relation is then used to define an index or indicator L for the assessment of the voltage stability. The index or indicator is defined by:

$$L = |1 + \frac{\mathbf{U}_0}{\mathbf{U}_1}| = \frac{|\mathbf{S}_1|}{|\mathbf{Y}_{11}| \cdot V_1^2} = \frac{1}{r \pm \sqrt{r^2 - 1}} \tag{2.53}$$

In the stable region, Equation (2.53) can be written as (note that the plus sign is used):

$$\sqrt{r^2 - 1} = \frac{1}{L} - r > 0 \tag{2.54}$$

Which leads to ($r > 1$):

$$0 < L < \frac{1}{r} < 1 \tag{2.55}$$

The range of L for the feasible (voltage stable) solutions (the larger solution of V_1) is: $R = \{L : 0 \leq L < 1\}$. For the unstable region, the negative sign in Equation (2.53) is used, and it can be transformed to:

$$\frac{1}{L}(r + \sqrt{r^2 - 1}) = (r - \sqrt{r^2 - 1}) \cdot (r + \sqrt{r^2 - 1}) = 1 \tag{2.56}$$

$$\sqrt{r^2 - 1} = L - r > 0 \tag{2.57}$$

The range of L for the voltage unstable solution is : $R = \{L : L > r > 1\}$.

2.4.3 Modal analysis

By linearizing the nonlinear differential equations in an operating point, valuable information can be extracted from the eigenvalues and eigenvectors of the system [21]. Stable and unstable states can be identified depending on the real value of the eigenvalue. A negative real eigenvalue indicates positive damping, which gives a stable system, while a positive value indicates an unstable system. This is only valuable for small-signal analysis, and gives little information about system stability outside the operating point as shown in Section 2.2.3.

The eigenvalue analysis has also been used for algebraic equations, as the modal analysis in [14, 23]. The linearized steady state system power voltage equations are given by,

$$\begin{bmatrix} \Delta P \\ \Delta Q \end{bmatrix} = \begin{bmatrix} J_{P\delta} & J_{PV} \\ J_{Q\delta} & J_{QV} \end{bmatrix} \begin{bmatrix} \Delta V \\ \Delta \delta \end{bmatrix} \tag{2.58}$$

By setting $\Delta P = 0$ the V-Q sensitivity can be examined using the reduced Jacobian

$$J_R = \left[J_{QV} - J_{Q\delta} J_{P\delta}^{-1} J_{PV} \right] \tag{2.59}$$

The left eigenvectors of J_R give an indication of bus participation factors of the different modes given by the eigenvalues. This method could be used to identify the worst direction of load increase. Stability is given by positive eigenvalues, while negative eigenvalues indicate an unstable system. The eigenvalue also gives an indication of distance to maximum loadability, but this is not a good indicator because of the nonlinearity of the power flow equations. The difference in sign from the traditional small-signal stability should be noticed.

2.4.4 Dynamic simulations

Although most of the work done within the field of voltage collapse has been studied assuming steady state models, the phenomenon is dynamic, all system dynamic must be examined. A thorough investigation of the voltage stability problem would involve full nonlinear simulations. However, this requires a lot of CPU time due to the large time span of voltage collapse scenarios and also the large difference in time constants of the dynamics involved. The different phases of voltage instability need to modeled and analyzed separately.

Transient voltage stability can be modeled and analyzed by traditional simulation programs, while special programs must be used when examining long-term voltage dynamics. In [22] a time domain simulation tool is proposed combining Full Time Scale (FTS) in the short-term period following a contingency and Quasi Steady-State (QSS) approximation for the long-term phase. A criterion is devised to automatically switch from FTS to QSS simulation as soon as sufficient damping of short-term dynamics is reached. In QSS the

short-term dynamics are supposed to be infinitely fast so that the corresponding differential equations can be replaced by their equilibrium form, the long-term dynamics are still modeled by differential equations.

Chapter 3

Voltage Instability Predictor

Much effort has been put into research of the phenomenon of voltage collapse*, and many approaches have been explored. Both dynamic and steady-state behavior have been studied thoroughly, though very few protection and control schemes have been implemented. This chapter gives a description of a smart relay called "VIP" [18, 29–32], which uses local area measurements to predict distance to voltage collapse. The methods described are based on the published articles*

3.1 Background

The VIP method is based on the assumption that voltage instability is closely related to maximum loadability of a transmission network [28], thus the Thevenin impedance is equal to the apparent load impedance at the PoC. Figure 3.1 shows a load bus and the rest of the system treated as a Thevenin equivalent.

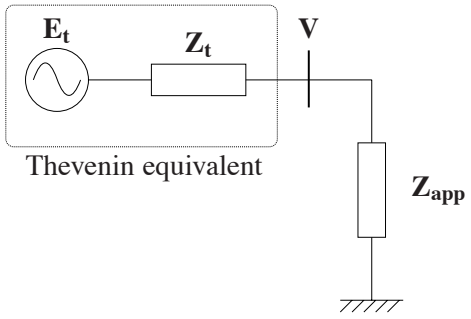

Figure 3.1: Local bus and the rest of the system treated as a Thevenin equivalent

The load delivered to the local bus can be expressed as given in Equation (3.1).

$$\mathbf{S} = \mathbf{V} \cdot \mathbf{I}^* = \mathbf{V} \left(\frac{\mathbf{E} - \mathbf{V}}{\mathbf{Z}_{thev}} \right)^* = \frac{EV}{Z_{thev}} e^{j(\delta_V - \delta_E + \theta_{thev})} - \frac{V^2}{Z_{thev}} e^{j\theta_{thev}} \tag{3.1}$$

Equation (3.1) is an equation of complex variables, which can be represented by two equations of real variables.

$$P = \frac{EV}{Z_{thev}} \cos(\delta_V - \delta_E + \theta_{thev}) - \frac{V^2}{Z_{thev}} \cos\theta_{thev} \tag{3.2}$$

$$Q = \frac{EV}{Z_{thev}} \sin(\delta_V - \delta_E + \theta_{thev}) - \frac{V^2}{Z_{thev}} \sin\theta_{thev} \tag{3.3}$$

Equations (3.2) and (3.3) can be combined as

$$\begin{aligned} \left(\frac{EV}{Z_{thev}} \right)^2 &= \left(P + \frac{V^2}{Z_{thev}} \cos\theta_{thev} \right)^2 + \left(Q + \frac{V^2}{Z_{thev}} \sin\theta_{thev} \right)^2 \\ &= (P^2 + Q^2) + 2\frac{V^2}{Z_{thev}} (P\cos\theta_{thev} + Q\sin\theta_{thev}) + \left(\frac{V^2}{Z_{thev}} \right)^2 \end{aligned} \tag{3.4}$$

If we express Equation (3.4) by polynomials of V^2 we get a second-degree equation

$$(V^2)^2 + (V^2) \cdot (2 \cdot Z_{thev} \cdot (P\cos\theta_{thev} + Q\sin\theta_{thev}) - E^2) + Z_{thev}^2 S^2 = 0 \tag{3.5}$$

which can be solved as

$$V^2 = \frac{E^2 - 2 \cdot Z_{thev} \cdot (P\cos\theta_{thev} + Q\sin\theta_{thev}) \pm \sqrt{(\cdot)}}{2} \tag{3.6}$$

where

$$(\cdot) = (E^2 - 2 \cdot Z_{thev} \cdot (P\cos\theta_{thev} + Q\sin\theta_{thev}))^2 - 4Z_{thev}^2 S^2 \tag{3.7}$$

On the tip of the nose curve the discriminant in Equation (3.5), given by Equation (3.7), is equal to zero. Solving this, and substitute it into Equation (3.6), we get

$$V^2 = Z_{thev} S \tag{3.8}$$

which can be expressed as

$$Z_{thev} = \frac{V^2}{S} = Z_{app} \tag{3.9}$$

We have a steady-state maximum power transfer when the apparent load impedance is equal to the Thevenin impedance in absolute value.

It is noted that no assumption has been made about the characteristic of the load. The apparent impedance $\mathbf{Z}_{app}$ is merely the ratio between the voltage and current phasors measured at the bus. Relation in Equation (3.9), holding true regardless of the load characteristic, separates the impedance plane into two regions as shown in Figure 3.2. As the load varies, $\mathbf{Z}_{app}$ traces a path in the plane, and voltage instability occurs in the steady-state sense, when $\mathbf{Z}_{app}$ crosses the Thevenin circle.

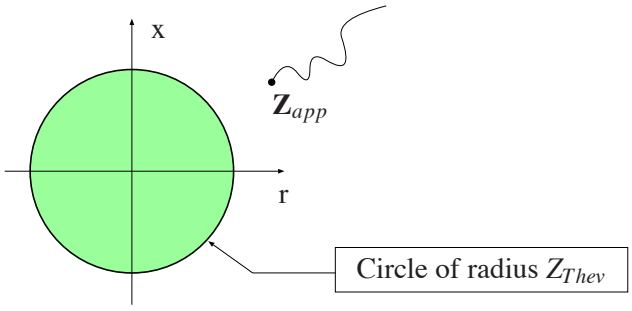

Figure 3.2: Maximum power transfer is reached (voltage instability) when the apparent impedance of the load bus hits the Thevenin circle

Tracking closeness to voltage instability, therefore, becomes tracking the distance of the present-time $\mathbf{Z}_{app}$ to the Thevenin circle. This circle is by no means a fixed object because it represents the rest of the system as one entity, including a large number of components, any of which can change at a given time.

3.2 Tracking the Thevenin equivalent

Tracking the Thevenin equivalent is essential for the detection of voltage collapse. There are many methods to track the Thevenin parameters. The Kalman filter was used by [10] in the problem of out-of-step protection (R_{Thev} was assumed zero). The tracking is based on Equation (3.10).

$$\mathbf{E_t} = \mathbf{V} + \mathbf{Z_t} \cdot \mathbf{I} \tag{3.10}$$

3.2.1 Cartesian coordinates

Denote $\mathbf{E_t} = E_r + jE_i$, $\mathbf{V} = V_r + jV_i$ and $\mathbf{I} = I_r + jI_i$. Equation (3.10) is rewritten as:

$$\begin{bmatrix} 1 & 0 & -I_r & I_i \\ 0 & 1 & -I_i & -I_r \end{bmatrix} \times \begin{bmatrix} E_r \\ E_i \\ R_t \\ X_t \end{bmatrix} = \begin{bmatrix} V_r \\ V_i \end{bmatrix} \tag{3.11}$$

where the subscripts r and i indicate the real and the imaginary part of phasors. Note that **V** and **I** are directly available from the measurements at the local bus. The unknowns are R_{Thev}, X_{Thev}, E_r and E_i. In Equation (3.11) there are two equations, and four unknowns, so clearly, measurements taken at two or more different times are required to solve for the unknowns. In the real environment, measurements are not precise and the Thevenin parameters drift due to the system's changing conditions. To suppress oscillations, a larger data window needs to be used. The estimation therefore attempts to minimize the error in a least-square sense.

3.2.2 Least squares method

Equation (3.11) can be written as

$$y(t_j) = \phi(t_j)\theta \tag{3.12}$$

where

$$y(t_j) = \begin{bmatrix} V_r(t_j) & V_i(t_j) \end{bmatrix}^T \tag{3.13}$$

and

$$\phi(t_j) = \begin{bmatrix} 1 & 0 & -I_r(t_j) & I_i(t_j) \\ 0 & 1 & -I_i(t_j) & -I_r(t_j) \end{bmatrix} \tag{3.14}$$

with $t_j = jT_{sl}, j \in \mathbb{N}$, T_{sl} being the sampling period, and the unknown parameter vector θ can be characterized from the Thevenin equivalent circuit.

$$\theta = \begin{bmatrix} E_r & E_i & R_t & X_t \end{bmatrix}^T \tag{3.15}$$

To obtain the estimate of $\hat{\theta}$ of the unknown parameter matrix θ, using N couples of voltage and current phasor estimations, the following least squares model can be adopted:

$$\min_{\hat{\theta}} \quad J(\hat{\theta}) \tag{3.16}$$

where

$$J(\hat{\theta}) = \varepsilon^T \varepsilon \tag{3.17}$$

with

$$\varepsilon = Y - \Phi\hat{\theta} \tag{3.18}$$

$$Y = \begin{bmatrix} y^T(t_1) \cdots y^T(t_n) \end{bmatrix}^T \tag{3.19}$$

$$\Phi = \begin{bmatrix} \phi^T(t_1) \cdots \phi^T(t_n) \end{bmatrix}^T \tag{3.20}$$

Differentiating J with respect to θ

$$\frac{dJ}{d\theta} = -2\Phi^T Y + 2\Phi^T \Phi\hat{\theta} = 0 \tag{3.21}$$

The parameters given by $\hat{\Theta}$ can now be found by the least squares method as given in Equation (3.22).

$$\hat{\Theta} = (\Phi^T \Phi)^{-1}\Phi^T Y \tag{3.22}$$

The Thevenin voltage and impedance, the unknowns, are assumed to be constant within the window where the measurements are taken. It is important here to note that changes in measurements of current have to occur during the sampling interval, see Section 3.4. The method involves inversion of the matrix $(\Phi^T \Phi)$, which consists of the measurements of current, and with badly scaled matrix Φ the algorithm will be subjected to numerical problems. These problems can either be overcome by increasing the number of measurements, n, or by the cumulative sum method described in Section 3.2.4, which guarantees such changes. Adding too many measurements can result in an erroneous estimate as the assumption of a constant Thevenin equivalent might fail.

A similar approach to this method has been proposed in [13], using a rewriting of Equation (3.11) and a constrained least square method, which is computationally slightly faster than the method presented here.

3.2.3 Delta method

Using two successive measurements at times t_1 and t_2:

$$\begin{array}{rcl} \mathbf{E_2} &=& \mathbf{V_2} + \mathbf{Z_2}\cdot\mathbf{I_2} \\ \mathbf{E_1} &=& \mathbf{V_1} + \mathbf{Z_1}\cdot\mathbf{I_1} \end{array} \tag{3.23}$$

Assuming the Thevenin equivalent is constant ($\mathbf{E_2} = \mathbf{E_1}$ and $\mathbf{Z_2} = \mathbf{Z_1}$), and using $\Delta\mathbf{F_2} = \mathbf{F_2} - \mathbf{F_1}$, the two equations in (3.23) can be reduced to:

$$\mathbf{Z_2} = -\frac{\Delta\mathbf{V_2}}{\Delta\mathbf{I_2}} \tag{3.24}$$

which is the Thevenin equivalent at time t_2. At time t_1 there are not enough measurements to make an estimation of the equivalent. If a larger window is to be considered, the number of equations in (3.23) is increased with n set of measurements.

$$\begin{array}{rcl} \mathbf{E_n} &=& \mathbf{V_2} + \mathbf{Z_n}\cdot\mathbf{I_2} \\ &\vdots& \\ \mathbf{E_2} &=& \mathbf{V_2} + \mathbf{Z_2}\cdot\mathbf{I_2} \\ \mathbf{E_1} &=& \mathbf{V_1} + \mathbf{Z_1}\cdot\mathbf{I_1} \end{array} \tag{3.25}$$

This can be simplified to Equation (3.26) with the assumption that the Thevenin equivalent is constant.

$$\begin{bmatrix} \Delta\mathbf{I_n} \\ \vdots \\ \Delta\mathbf{I_3} \\ \Delta\mathbf{I_2} \end{bmatrix} \cdot \tilde{\mathbf{Z}}_n = - \begin{bmatrix} \Delta\mathbf{V_n} \\ \vdots \\ \Delta\mathbf{V_3} \\ \Delta\mathbf{V_2} \end{bmatrix} \tag{3.26}$$

The Thevenin equivalent can then be solved, using a least square method:

$$\tilde{\mathbf{Z}}_n = -\frac{\sum_{j=2}^{n} \Delta\mathbf{I}_\mathbf{j}^* \cdot \Delta\mathbf{V_j}}{\sum_{j=2}^{n} |\Delta\mathbf{I_j}|^2} \tag{3.27}$$

As for the method in Section 3.2.2, it is vital that there are changes in the current vector for this method to produce a result. With zero change in current the denominator is equal to zero, which gives an infinite value of the estimated Thevenin impedance. Also here this can be solved by increasing the number of measurements, n, or by the method in Section 3.2.4. As mentioned earlier, care must be taken when increasing the number of measurements, n.

3.2.4 Cumulative sum filter[26]

The magnitude of $\Delta\mathbf{V}_k = \mathbf{V}_k - \mathbf{V}_{k-1}$ and $\Delta\mathbf{I}_k = \mathbf{I}_k - \mathbf{I}_{k-1}$ depends on changes in the load, generation and topology. If the system changes slowly and Δt (time window) between the measurements are very small, it may result in a very small magnitude or even zero values for $\Delta\mathbf{V}$ and $\Delta\mathbf{I}$. It is therefore interesting to expand the time window between each time $|\mathbf{Z}_{Thev}|$ is calculated in order to increase the magnitude of $\Delta\mathbf{V}$ and $\Delta\mathbf{I}$. One obvious way is to include more time steps e.g. $\Delta\mathbf{V} = \mathbf{V}_k - \mathbf{V}_{k-5}$ and $\Delta\mathbf{I} = \mathbf{I}_k - \mathbf{I}_{k-5}$. Cumulative sum filtering is another way to change the time window and smoothen the result. $|\Delta\mathbf{I}|$ is the most critical value. Small disturbances and noise can bring $|\Delta\mathbf{I}|$ close to zero and makes the tracking of $|\mathbf{Z}_{Thev}|$ very difficult. One of the advantages by using the cumulative sum filter is that it divides $|\Delta\mathbf{I}|$ into equal quantities greater than zero.

The first step is to take the cumulative sum of $|\Delta\mathbf{V}|$ and $|\Delta\mathbf{I}|$, and define two new vectors, Equations (3.28) and (3.29).

$$A = \begin{bmatrix} |\Delta V|_2 & \sum_{n=2}^{3} |\Delta V|_n & \cdots & \sum_{n=2}^{k} |\Delta V|_n \end{bmatrix} \tag{3.28}$$

$$B = \begin{bmatrix} |\Delta I|_2 & \sum_{n=2}^{3} |\Delta I|_n & \cdots & \sum_{n=2}^{k} |\Delta I|_n \end{bmatrix} \tag{3.29}$$

Dividing the difference of the two subsequent elements of A and B, gives the same result as in Equation (3.24), but with absolute values.

$$|Z_n| = \frac{A(n) - A(n-1)}{B(n) - B(n-1)} = \frac{|\Delta V|_n}{|\Delta I|_n} \tag{3.30}$$

Figure 3.3 displays the value of A versus the value of B. The idea is to divide the x-axis,

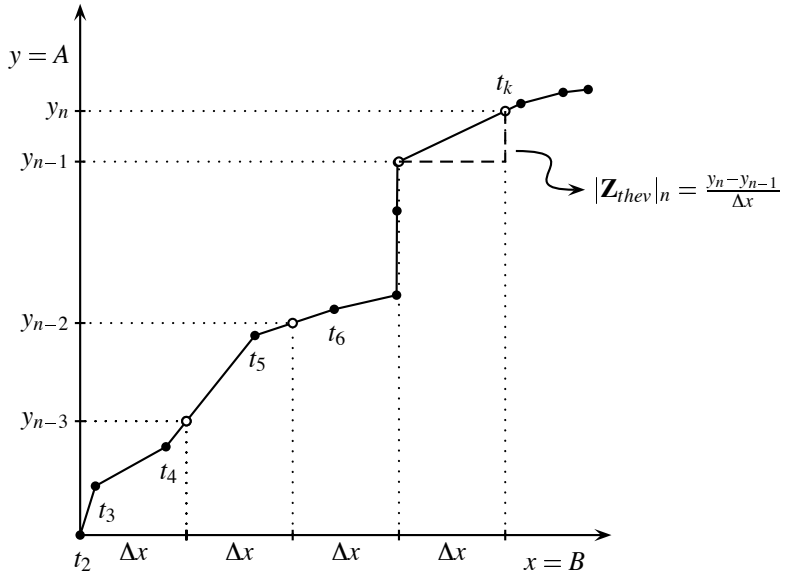

Figure 3.3: Mapping the cumulative sums of $|\Delta \mathbf{V}|$ to the cumulative sums of $|\Delta \mathbf{I}|$

which represents $|\Delta \mathbf{I}|$ into fixed quantities of Δx, and map the y-axis, which represents $|\Delta \mathbf{V}|$ to these quantities by use of interpolation. Δx is given by:

$$\Delta x = \frac{\sum_{i=2}^{k} |\Delta \mathbf{I}|_i}{\text{number of steps}} \tag{3.31}$$

The number of steps is chosen based on the level of noise in the VIP plot, without any filtering. The method keeps track of the measurements from t_k, present time when the last measurement is taken, back to the time t_1. Finding the Thevenin equivalent can now be done as

$$|\mathbf{Z}_{thev}|_k = \frac{y_k - y_{k-1}}{\Delta x} \tag{3.32}$$

Equation (3.32) is in principle the same as Equation (3.24), but with adjusted values due to the mapping of the y-axis.

The time vector t has to be mapped to the new fixed quantity vector Δx in the same manner as for the vector A. This method of interpolating from a data of small ΔI to a set of fixed value Δx can be applied to all the other methods described in Sections 3.2.2 and 3.2.3. By mapping the measured values to the new time vector, the methods will overcome the problem ΔI being close zero.

3.2.5 Polar coordinates

A similar equation to that in Equation (3.11) can be found in polar coordinates, in which case Ohm's law is given by Equation (3.33).

$$\begin{aligned} E\cos\delta_E &= U\cos\delta_U + IZ\cos(\delta_I+\delta_Z) \\ E\sin\delta_E &= U\sin\delta_U + IZ\sin(\delta_I+\delta_Z) \end{aligned} \tag{3.33}$$

Finding the time derivative of these equations

$$\begin{aligned} 0 &= -U\sin(\delta_U)\dot{\delta}_U + \cos(\delta_U)\dot{U} - IZ\sin(\delta_I+\delta_Z)\dot{\delta}_I + Z\cos(\delta_I+\delta_Z)\dot{I} \\ 0 &= \;\; U\cos(\delta_U)\dot{\delta}_U + \sin(\delta_U)\dot{U} + IZ\cos(\delta_I+\delta_Z)\dot{\delta}_I + Z\sin(\delta_I+\delta_Z)\dot{I} \end{aligned} \tag{3.34}$$

Solving for Z and δ_Z we get

$$Z = \sqrt{\frac{(U\dot{\delta}_U)^2+\dot{U}^2}{(I\dot{\delta}_I)^2+\dot{I}^2}} \tag{3.35}$$

and

$$\delta_Z = -\delta_I + \tan^{-1}\left(\frac{(IU\dot{\delta}_I\dot{\delta}_U + \dot{I}\dot{U})\sin\delta_U - (I\dot{U}\dot{\delta}_I - U\dot{I}\dot{\delta}_U)\cos\delta_U}{(IU\dot{\delta}_I\dot{\delta}_U + \dot{I}\dot{U})\cos\delta_U + (I\dot{U}\dot{\delta}_I - U\dot{I}\dot{\delta}_U)\sin\delta_U}\right) \tag{3.36}$$

Using the approximation

$$\frac{df}{dt} \approx \frac{\Delta f}{\Delta t} \tag{3.37}$$

Equation (3.35) can be expressed as

$$Z = \sqrt{\frac{(U\Delta\delta_U)^2+\Delta U^2}{(I\Delta\delta_I)^2+\Delta I^2}} \tag{3.38}$$

which can be used to track the Thevenin equivalent of the system, using the local measurement **U** and **I**. This method is not explored any further in this dissertation.

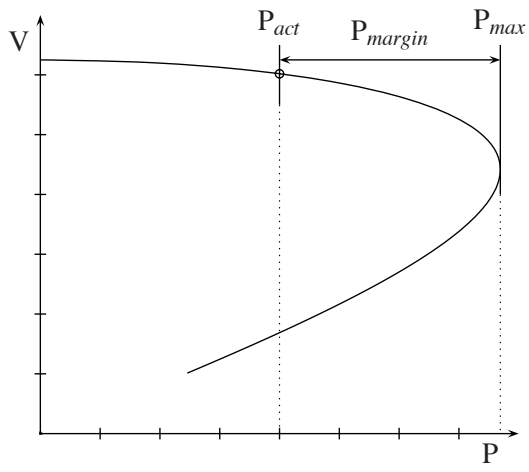

Figure 3.4: Power margin

3.3 Power margin

Traditional voltage stability analysis uses the "*tip of the nose curve*", see Figure 3.4, as the critical point or point of collapse. Thus, finding the *power margin* for a given state can be found as the difference between present state and the maximum load flow.

The load flow equations for the system in Figure 3.1, are given in Equations (3.2) and (3.3), and yield two solutions of the voltage given by the upper and lower parts of the nose curve. At the critical point the two solutions coalesce to one solution, which can be found by setting the discriminant in Equation (3.5) to zero. The expression $(\cdot)$ is given by Equation (3.7).

$$(\cdot) = (E^2 - 2(Pr + Px\tan\phi))^2 - 4P^2(r^2 + x^2)(1 + \tan^2\phi) = 0 \tag{3.39}$$

In Equation (3.39), it is assumed that there is a constant power factor $Q = P\tan\phi$. Moving the negative part to the left-hand side and taking the square root of both sides, the maximum load power can found as given in Equation (3.40).

$$P_{max} = \frac{E^2}{2(r_t + x_t\tan\phi \pm \sqrt{(r_t^2 + x_t^2)(1 + \tan^2\phi)})} \tag{3.40}$$

where

$$\mathbf{Z}_t = Z_t e^{i\theta_t} = r_t + ix_t \tag{3.41}$$

is the estimated Thevenin impedance. $P_{margin} = P_{max} - P_{act}$ in Equation (3.40) is the power margin for a given Thevenin equivalent calculated using the VIP algorithm. The maximum

apparent power can be found as given in Equation (3.42).

$$\begin{aligned} S_{max} &= |P_{max} + iQ_{max}| = P_{max}|(1 + i\tan\phi)| = P_{max}\sqrt{1+\tan^2\phi} \\ &= \frac{E^2\sqrt{1+\tan^2\phi}}{2(r_t + x_t\tan\phi \pm \sqrt{(r_t^2 + x_t^2)(1+\tan^2\phi)})} \end{aligned} \tag{3.42}$$

In the specific case where $P = 0$ the critical apparent load power can be found as

$$S_{max} = Q_{max} = E^2\frac{x_t \pm \sqrt{r_t^2 + x_t^2}}{-2r_t^2} \tag{3.43}$$

Assuming a positive reactive load the negative sign of the plus minus sign should be used. If the real part of the Thevenin impedance is negligible, $r_t \approx 0$, maximum apparent power transfer is

$$S_{max} = Q_{max} = \frac{E^2}{4x_t} \tag{3.44}$$

3.4 Data window estimation: problems and requirements

Including in a particular data window at least two successive sets of measurements in the VIP algorithm, will solve the problem of not having enough measurements to estimate the unknown variables. However, there are additional requirements to make the estimation feasible and avoid erroneous conclusions:

1. There must be a significant change in load impedance in the data window between the two sets of measurements.
2. The estimation algorithm can accept "small" changes in the "*true*" Thevenin equivalent within a particular data window. If a sudden large change occurs then estimation of the Thevenin impedance is postponed until the next data window.

These requirements are explained below. The first requirement can easily be detected by the difference between load measurements

$$\Delta\mathbf{Z_{load,i}} = \frac{\mathbf{U_i}}{\mathbf{I_i}} - \frac{\mathbf{U_{i-1}}}{\mathbf{I_{i-1}}} \tag{3.45}$$

The latter can only be detected by looking at the error in the estimation when the assumption of constant Thevenin equivalent does not hold. Equation (3.23) can be written as:

$$\begin{bmatrix} \mathbf{E_{i-1}} \\ \mathbf{E_i} \end{bmatrix} = \begin{bmatrix} \mathbf{V_{i-1}} \\ \mathbf{V_i} \end{bmatrix} + \mathbf{Z_i}\cdot\begin{bmatrix} \mathbf{I_{i-1}} \\ \mathbf{I_i} \end{bmatrix} + \begin{bmatrix} (\mathbf{Z_{i-1}} - \mathbf{Z_i})\cdot\mathbf{I_{i-1}} \\ 0 \end{bmatrix} \tag{3.46}$$

which leads to

$$\Delta \mathbf{E_i} = \Delta \mathbf{V_i} + \mathbf{Z_i} \cdot \Delta \mathbf{I_i} + \Delta \mathbf{Z_i} \cdot \mathbf{I_{i-1}} \tag{3.47}$$

Solving for $\mathbf{Z_i}$

$$\mathbf{Z_i} = \underbrace{-\frac{\Delta \mathbf{V_i}}{\Delta \mathbf{I_i}}}_{\tilde{\mathbf{Z}}_\mathbf{i}} + \underbrace{\frac{\Delta \mathbf{E_i} - \Delta \mathbf{Z_i} \cdot \mathbf{I_{i-1}}}{\Delta \mathbf{I_i}}}_{-\varepsilon_\mathbf{i}} \tag{3.48}$$

$\tilde{\mathbf{Z}}_\mathbf{i}$ is the estimate , while $\mathbf{Z_i}$ is the "real" Thevenin equivalent. $\varepsilon_\mathbf{i}$ is the error in our estimation if the *true* equivalent is not constant from measurement *(i-1)* to *i*.

$$\tilde{\mathbf{Z}}_\mathbf{i} = \mathbf{Z_i} - \frac{\Delta \mathbf{E_i} - \Delta \mathbf{Z_i} \cdot \mathbf{I_{i-1}}}{\Delta \mathbf{I_i}} \tag{3.49}$$

From Equation (3.49), it is obvious that small changes in load current might lead to a large error in the estimated impedance, and those estimates should therefore be discarded. This could be the case where there is a significant change in load, but at same time there is a similar change in both Thevenin impedance and voltage, as can be seen from Equation (3.54). Now let:

$$\mathbf{E_i} = \frac{1}{\mathbf{n_e}} \mathbf{E_{i-1}} \tag{3.50}$$

$$\mathbf{Z_i} = \frac{1}{\mathbf{n_z}} \mathbf{Z_{i-1}} \tag{3.51}$$

$$\mathbf{Z_{l,i}} = \frac{1}{\mathbf{n_l}} \mathbf{Z_{l,i-1}} \tag{3.52}$$

where $\mathbf{Z_{l,i}}$ is the load impedance measured at time *i*. The current is given by Equation (3.53).

$$\mathbf{I_i} = \frac{\mathbf{E_i}}{\mathbf{Z_i} + \mathbf{Z_{l,i}}} \tag{3.53}$$

Using Equations (3.50-3.53) the estimated impedance can generally (for any time instant *i*) be expressed as:

$$\tilde{\mathbf{Z}} = \mathbf{Z} - \frac{(\mathbf{1} - \mathbf{n_e})\mathbf{n_l}\mathbf{Z_l} + (\mathbf{n_z} - \mathbf{n_e})\mathbf{Z}}{(\mathbf{1} - \frac{\mathbf{n_e}}{\mathbf{n_l}})\mathbf{n_l}\mathbf{Z_l} + (\mathbf{n_z} - \mathbf{n_e})\mathbf{Z}} \cdot (\mathbf{Z} + \mathbf{Z_l}) \tag{3.54}$$

As discussed early in this chapter there have to be some changes in the measured current and voltage before the VIP algorithm can make any estimation, so one of the variables $\mathbf{n_l}$,$\mathbf{n_e}$ or $\mathbf{n_z}$ is unequal to 1. Consider two cases of change in the system:

1. The change *only* happens in the apparent load, thus $\mathbf{n_l} \neq 1$ and $\mathbf{n}_e = \mathbf{n}_z = 1$.

2. The change is *not* in the load, $\mathbf{n}_l = 1$, or the changes in load impedance are very small (n_l - is close to 1).

In the first case, the algorithm estimates the correct value for the Thevenin equivalent, $\tilde{\mathbf{Z}} = \mathbf{Z}$, as the numerator in the fraction in Equation (3.54) is equal to zero. In the second case, the estimated value of Thevenin impedance is close in absolute value to the negative load impedance, $\tilde{\mathbf{Z}} \approx -\mathbf{Z_l}$, as the fraction in Equation (3.54) is close to 1.

According to Figure 3.2, the VIP will incorrectly assume that the system is either close to or at voltage collapse. Thus, it is important to recognize this wrong estimate, reset the estimation, and wait for the next valid estimate of the Thevenin equivalent.

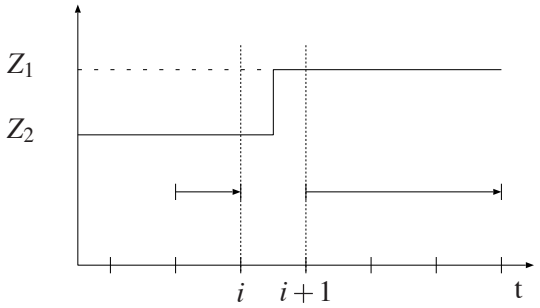

Figure 3.5: Sudden change in Thevenin impedance

In case there is a sudden change in the "true" Thevenin equivalent, in either the voltage or impedance, the VIP has to recognize the change and reset the estimation. Figure 3.5 gives an illustration of this. There is an increase in Thevenin impedance between measurement *i* and *i+1*, so the VIP stops the previous data window at *i* and starts a new window at *i+1*.

Although the filter presented Section 3.2.4 solves some of the problems presented in this section, further work is required to determine what can be considered a valid estimation. This has not been done in this work, instead the effort has been put on "removing" the change in the Thevenin equivalent caused by changes in load on nearby buses, see Chapter 4.

3.5 Reference angle

The voltage $\boldsymbol{V}$ and current $\boldsymbol{I}$ used to estimate the Thevenin equivalent are both complex numbers and are measured using a PMU, see Section 3.8. The PMU uses a reference frequency equal to the nominal power system frequency, $f_n = (50Hz/60Hz)$, so that the

reference angle for the system is given by this frequency. Including a second PMU located on any bus, the reference angle can be chosen as the angle on this new bus.

The VIP method assumes that the angle difference between this reference and the angle at the supplying end, Thevenin equivalent, is constant. In case this does not hold true, the VIP will fail to predict the true Thevenin equivalent, as shown in Section 3.4.

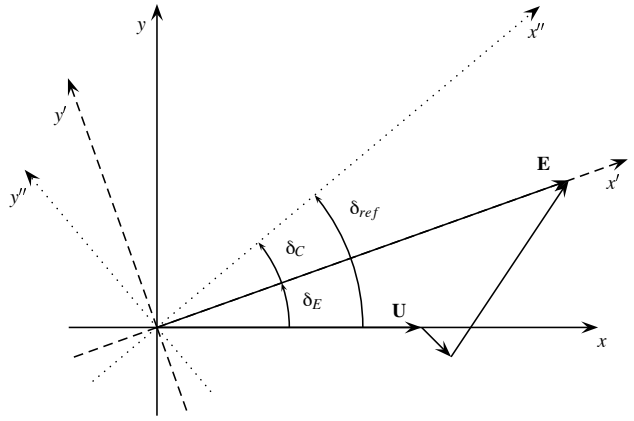

Figure 3.6: Reference angle

The Thevenin equivalent can still be estimated if either the true angle δ_E, or an estimate of this was known. Given an angle with same frequency as the Thevenin equivalent, then

$$\delta_{E_i} - \delta_{ref_i} = \delta_C \tag{3.55}$$

where $\delta_C = const$ for any given measurement i. In Figure 3.6 it is shown how the measurement of **U** is locked to the axis (x,y), when using the VIP bus as a reference. For the VIP to be able to estimate an equivalent it must use the system (x',y'), but since this is not observable an estimate (x'',y'') can be used. An example of an angle estimate could be the angle of a large generator, or a bus in a generator area. By multiplying both sides of Equation (3.10) with this reference angle as shown in Equation (3.56)

$$(Ee^{i\delta_E})e^{-i\delta_{ref}} = (Ve^{i\delta_V} + Ie^{i\delta_I}Ze^{\delta_Z})e^{-i\delta_{ref}} \tag{3.56}$$

the angle variations on the left-hand side have been removed.

$$Ee^{i\delta_C} = Ve^{i\delta'_V} + Ie^{i\delta'_I}Ze^{\delta_Z} \tag{3.57}$$

Here, $\delta'_V = \delta_V - \delta_{ref}$ and $\delta'_I = \delta_I - \delta_{ref}$. Note that no change has been made to the Thevenin impedance. The impedance found in Equation (3.24) can now be written as

$$\mathbf{Z_i} = -\frac{V_i e^{i\delta_{V'_i}} - V_{i-1} e^{i\delta_{V'_{i-1}}}}{I_i e^{i\delta_{I'_i}} - I_{i-1} e^{i\delta_{I'_{i-1}}}} \tag{3.58}$$

This method requires that extra measurements would have to be made, the remote reference frequency cannot be estimated from the measured values **V** and **I** on the bus that the VIP relay is placed.

3.6 Using VIP on an example case

Performance of the VIP algorithm has been tested on the voltage collapse scenario, given by two dynamic factors, presented in Section 2.2.3. Only the stable case for $T_L = 10$ has been considered, as it includes both stable and unstable situations according to the definition of stability used by the VIP. The VIP will be tested both from the high and low voltage sides of the OLTC.

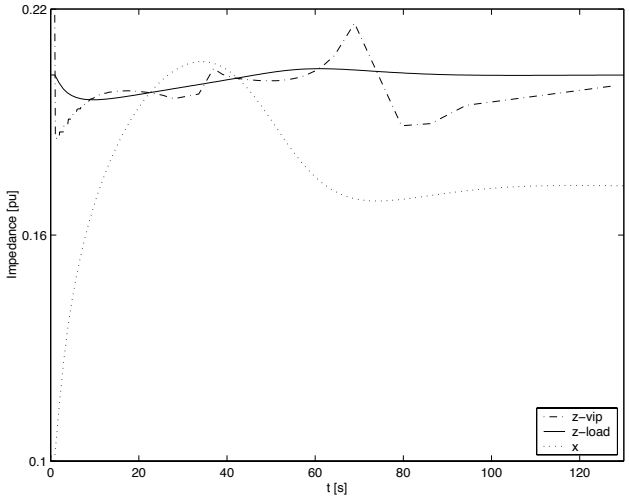

Figure 3.7: VIP on the low voltage side of OLTC

In Figure 3.7 the load resistance, the estimated Thevenin impedance and the line reactance are plotted as solid, dashed and dotted lines respectively. It is clear from the figure that the VIP algorithm is not able to estimate the "true" Thevenin impedance seen from the load bus, given as the dotted line. This is expected as the VIP assumes a constant Thevenin equivalent. The transmission line is not constant, as it has been transformed to

the low voltage side of the OLTC as given in Equation (3.59), remembering that the tap n is not constant.

$$x_{low} = n^2 x_{high} \tag{3.59}$$

By moving the VIP to the high voltage side, as given in Figure 3.8, the VIP succeeds in

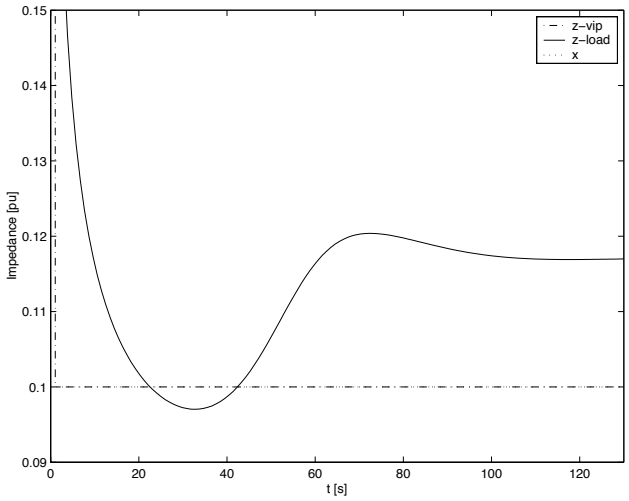

Figure 3.8: VIP on the high voltage side of OLTC

estimating the Thevenin equivalent. As shown in the figure, the VIP algorithm estimates the exact value of line reactance, $x = 0.1 pu$, this is because the Thevenin equivalent seen from the high voltage side is constant.

In both cases: the load impedance transformed to high voltage side and line reactance transformed to low voltage side, the line reactance crosses the load impedance at $t = 22$ seconds and $t = 43$ seconds. According to the steady-state stability criteria this indicates that the system becomes unstable in the period between the two crossings, as the line reactance is higher than the load impedance in absolute value. The fact that the VIP indicates instability, although the system moves to a new stable equilibrium, is caused by the VIP being based on a steady-state criterion. Although the system converges to a new stable equilibrium it is appropriate that a warning should be given before entering the region where $Z_l < Z_{th}$.

The example demonstrates that the limitation of a relay based on steady state facing a dynamic phenomenon. In addition, this example shows that the VIP should be placed on the high voltage side of the OLTCs, in order to avoid problems with a changing tap ($\boldsymbol{n}$).

3.7 Comparison with conventional undervoltage relay

Undervoltage relays provide a simple, cost-effective mitigation of voltage collapse [28]. They "detect" a collapse by comparing the local voltage against a *fixed* threshold. If the voltage drops and stays below the threshold then the usual practice is to shed a block of load. Multiple thresholds are linked to a separate block of load.

It is convenient to map the operation of a conventional undervoltage relay to the impedance plane. Consider a relay with a set-point of 0.95 pu. Let V be the voltage at the local bus and E be the voltage of Thevenin source. One has:

$$\frac{\mathbf{E}}{\mathbf{V}} = \frac{\mathbf{E}/\mathbf{I}}{\mathbf{V}/\mathbf{I}} = \frac{|\mathbf{Z}_{app} + \mathbf{Z}_{Thev}|}{|\mathbf{Z}_{Thev}|} \tag{3.60}$$

For illustration, let us assume that the Thevenin voltage is 1.05 pu. Then the undervoltage relay operates when

$$\frac{|\mathbf{Z}_{app} + \mathbf{Z}_{Thev}|}{|\mathbf{Z}_{Thev}|} > \frac{1.05}{.95} = 1.105 \tag{3.61}$$

which represents a circle in the impedance plane. The relative position between such

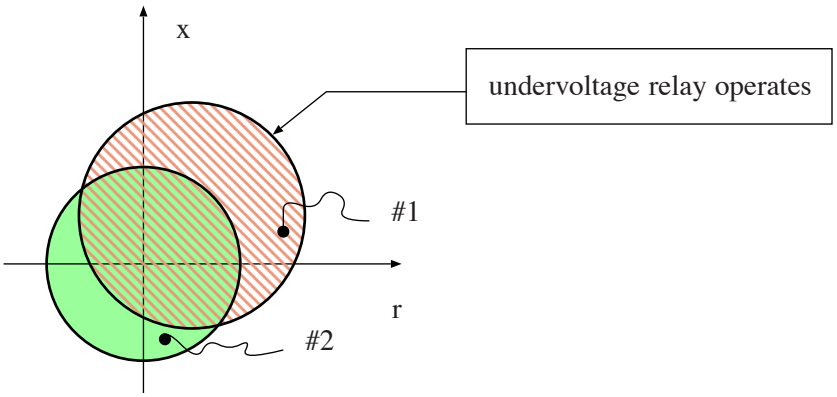

Figure 3.9: Misoperation of undervoltage relay: Premature (Case #1) and failure to operate (Case #2)

a circle and the Thevenin circle is shown in Figure 3.9. Clearly, the two circles do not coincide. Recall that the Thevenin circle represents maximum power transfers. Thus, wherever the two circles do not overlap, this represents misoperation of the conventional undervoltage relay. An impedance trajectory such as #1 is yet to reach maximum power transfer, but is treated by the conventional relay as voltage instability. An impedance

trajectory such as #2 has clearly reached maximum transfer, yet it is not detected by the conventional relay.

3.8 Phasor measurement unit

The VIP presented in this chapter is based on measurements of both voltage and currents on a load bus. Since both angles and absolute values are required to do the estimation, a phasor measurement unit (PMU) must be used. PMUs [8, 24] using synchronization signals from the GPS satellite system have evolved into mature tools and are now being manufactured commercially. Figure 3.10 shows a functional block diagram of a typical PMU. The GPS receiver provides the 1 pulse-per-second (pps) signal, and a time tag,

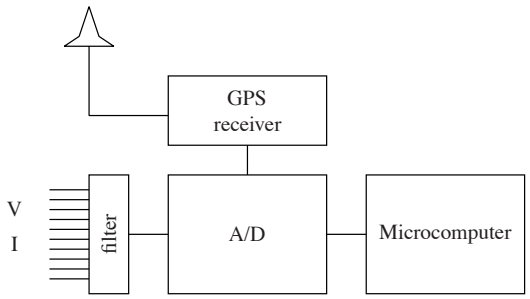

Figure 3.10: Phasor measurement unit

which consists of the year, month, day, hour, minute and second. The time could be the local time, or the Universal Time Coordinate (UTC). The 1-pps signal is usually divided by a phase-locked oscillator into the required number of pulses per second for the sampling of the analog signals. In most systems being used at present, this is 12 times per cycle of the fundamental frequency. The analog signals are derived from the voltage and current transformer secondaries, with appropriate anti-aliasing and surge filtering.

3.8.1 Measurements

Phasor measurements are performed using a Discrete Fourier Transform (DFT). A definition of phasor is given as follows:

Definition 5 (Phasor)
Consider the steady-state wave form of a nominal power frequency signal as shown in Figure 3.11(a). If we start our observation of this wave form at the instant $t = 0$, the steady-state wave form may be represented by a complex number with a magnitude equal to the rms value of the signal and with a phase angle equal to the angle ϕ.

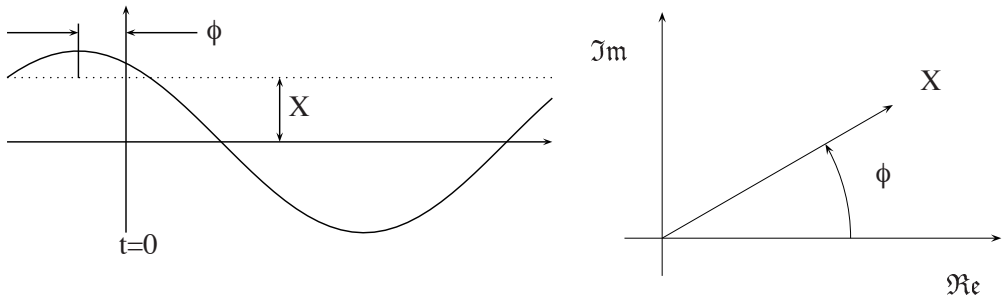

(a) $x(t) = X_m \cos(\omega t + \phi)$ (b) Phasor

Figure 3.11: Phasor representation of a sinusoidal wave form

A sinusoidal quantity as given in Figure 3.11(a) has a phasor representation of

$$X \equiv \frac{X_m}{\sqrt{2}} e^{j\phi} \tag{3.62}$$

Although the concept of a phasor is defined for a pure sinusoid, it can be used in the presence of transient components by stipulating that the phasors represent the fundamental frequency component of a waveform observed over a finite duration (observation window). In case of sampled data x_k, obtained by sampling the signal $x(t)$ at $t = k\tau$, where τ is the sampling interval, the phasor X is given by the forward rotating Fourier coefficient $q\sqrt{2}$, see Appendix C.3.

$$X = \frac{\sqrt{2}}{N} \sum_{k=1}^{N} x_k e^{-i\frac{k2\pi}{N}} = \frac{\sqrt{2}}{N}(X_c - jX_s) \tag{3.63}$$

where

$$X_c = \sum_{k=1}^{N} x_k \cos(k\theta) \quad \text{and} \quad X_s = \sum_{k=1}^{N} x_k \sin(k\theta) \tag{3.64}$$

and N is the total number of samples in one period of the nominal power system frequency. The sampling interval τ corresponds to the sampling angle θ

$$\theta = \frac{2\pi}{N} = 2\pi f_0 \tau \tag{3.65}$$

where f_0 is the nominal power system frequency. Equation (3.63) represents a phasor measurement performed by the DFT of one period data window.

The DFT procedure described above provides the phasor with a very modest amount in terms of computation. By selecting an appropriate sampling interval, the computation

can be made particularly simple. A sampling rate of 12 times the nominal power system frequency (600Hz for a 50Hz power system) has been found to be quite advantageous in many relaying and measurement functions. As time progresses, and a fixed-length data window is used, Equation (3.63) represents a non-recursive DFT calculation. Essentially, calculation during each data window is performed in an identical fashion: Equation (3.63) is repeated in its entirety. This is somewhat wasteful of computing power, and a more efficient algorithm results if a recursive form of Equation (3.63) is used.

Let X^r be the phasor corresponding to the data set x $\{k = r, r+1, \cdots, N+r-1\}$, and let a new data sample be obtained to produce a new data set x $\{k = r+1, r+2, \cdots, N+r\}$. The phasor corresponding to the new data window X^{r+1} is then given by

$$X^{r+1} = X^r + \frac{\sqrt{2}}{N}(x_{N+r} - x_r)e^{-jr\theta} \tag{3.66}$$

The difference between the recursive and non-recursive phasor calculations is illustrated in Figure 3.12. The non-recursive phasor rotates in counter-clockwise direction by an angle θ as the sample time advances, whereas the recursive phasor remains stationary. More importantly, the computations implied in the recursive Equation (3.66) involve only two samples: x_{N+r} and x_r, whereas the non-recursive Equation (3.63) implies computations with N samples. All phasor measurement systems currently in service use the recursive form of phasor calculations. Phasors can be measured for each of the three phases, and the

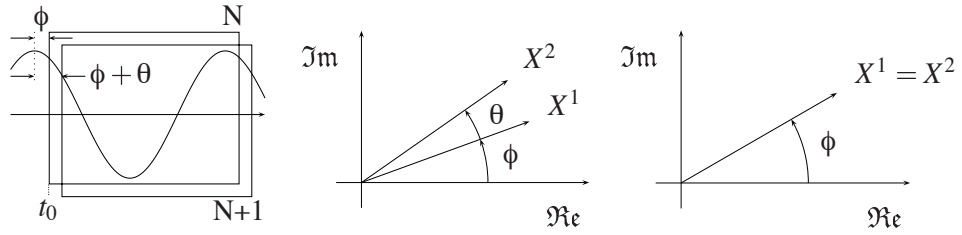

(a) Moving window (b) Non-recursive (c) Recursive

Figure 3.12: Phasors from sampled data

positive, negative and zero components can be calculated according to their definition.

$$\begin{bmatrix} X_0 \\ X_1 \\ X_2 \end{bmatrix} = \frac{1}{3}\begin{bmatrix} 1 & 1 & 1 \\ 1 & \alpha & \alpha^2 \\ 1 & \alpha^2 & \alpha \end{bmatrix}\begin{bmatrix} X_a \\ X_b \\ X_c \end{bmatrix} \tag{3.67}$$

where $\alpha = e^{j\frac{2\pi}{3}}$. X_a,X_b and X_c are the phasors from the three measured phases and X_0,X_1 and X_2 are the zero, positive and negative sequence respectively.

It is essential that the input wave form is being filtered to eliminate the aliasing error in the DFT calculation that has been described. Thus, the signal must not contain frequencies above the Nyquist rate: $N\Omega_0/2$. Often the input signal contains frequencies that are not harmonics of the fundamental frequency. In such cases, the phasor calculation is once again in error. One could treat the extraneous non-harmonic components as a noise signal, and then the computed phasor has an uncertainty associated with it, which can be depicted as shown in Figure 3.13. The circle of uncertainty is inversely proportional to the square

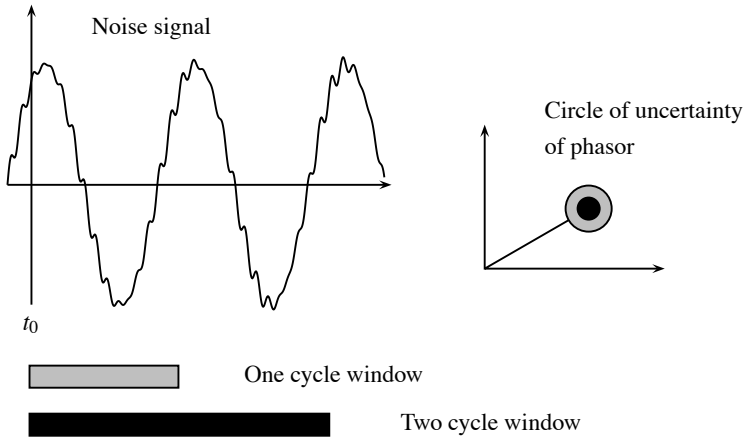

Figure 3.13: Data window and uncertainty in phasor estimation

of the data window. More data used in computing the phasor is beneficial in this regard. It should be noted that the wave form is sampled by the measurement system continuously, and each time a new sample is acquired, a new phasor is obtained with a data window including the latest sample.

3.8.2 Sources of synchronization

Synchronization signals could be distributed over any of the traditional communication media currently in use in power systems. Most communication systems, such as leased lines, microwave, or AM radio broadcasts, place a limit on the achievable accuracy of synchronization, which is too coarse to be of practical use. Fiberoptic links, where available, could be used to provide high precision synchronization signal, if a dedicated fiber is available for this purpose. If a multiplexed fiber channel is used, synchronization errors of the order of 100 μseconds are possible, and are not acceptable for power system measurements. GOES satellite systems have also been used for synchronization purposes, but their performance is not sufficiently accurate.

The chosen technique at present is the Navstar Global Positioning System (GPS) satellite transmissions. This system is designed primarily for navigational purposes, but it furnishes a common-access timing pulse, which is accurate to within 1 μsecond at any location on earth. The system uses transmissions from a constellation of satellites in non-stationary orbits at about 10,000 miles above the earth's surface. For accurate acquisition of the timing pulse, only one of the satellites needs be visible to the antenna. The antenna is small (about the size of a water pitcher), and can be easily mounted on the roof of a substation control house. Experience with the availability and dependability of the GPS satellites transmissions has been exceptionally good.

Accuracy achievable. The basic accuracy of the system while a satellite is in view is ± 0.2 μseconds. These devices presently attain an accuracy of ± 0.5 μseconds, although technical problems with some units can cause excursions up to ± 50 μseconds. The manufacturers are working to overcome these problems and it is believed that the units will provide continuous operation with a maximum time error of $\pm 0.5\mu$seconds.

Signal availability. Reception of the timing signal from one satellite will allow synchronization of the timing signal. There are 24 satellites planned for the complete system, which will give four satellites continuously in view at any location in the world. Locations in deep valleys will limit availability. Presently there is global 24-hour continuous coverage of at least one satellite.

Relative cost and trends The timing systems were priced at $24,000 to $250,000 in 1986. An adequate system for the power industry was in the upper end of the cost range. The manufacturers were made aware of the power industry requirements and design changes were made to the low-end units so they were generally acceptable. With the addition of more satellites, the requirements for Rubidium oscillators to maintain timing accuracy for six hours while satellites were out of view was eliminated and reduced the price further. Competition and increased production have led to the least expensive units that are satisfactory for power industry application to $5,000 - 15,000.

Outputs from these devices. There are two required, and several optional outputs. The first is a precise digital output with 50 nsecond risetime that occurs once per second. The second is an ASCII message transmitted at 9600 baud that identifies the year, month, day, hour, minute and second of the digital output. The output pulse is non-standard between manufacturers of these devices, and the timing edge can be the rising or the falling one, depending on the manufacturer. The ASCII string is unique to each manufacturer and there is no standard as to the preceding of following digital pulse being identified. The manufacturers have been flexible in providing other outputs requested for specialized uses.

It should be borne in mind that it is not necessary to have external sources of synchronization to achieve coherent phasor measurement. At least two methods have been used to implement line differential relaying using alternative synchronization techniques. The first method is based on upon directly measuring the time difference between the sampling instants at different stations, and then converting this delay to a phase angle correction factor. The second method is used extensively in Japan and consists in synchronizing two clocks at the extremities of a line by sending synchronizing signals, and adjusting them locally to compensate for the propagation delays in the synchronizing signals.

Chapter 4

VIP++ method

This chapter introduces a new method denoted by the acronym VIP++, a "smart relay" like the VIP method described in Chapter 3, which uses local area measurements to estimate or track the distance to point of collapse. The distance to the PoC does not only depend on the present state of the system but also on future changes. Therefore, an algorithm that tries to track the system trajectory is based on an assumption or hypothesis about how the system will move. In this chapter a couple of such hypotheses (methods) are illustrated and discussed.

4.1 VIP method and Thevenin equivalent

The VIP++ [39, 40] method is an expansion of the VIP method that attempts to improve the robustness of the estimation of the distance to a voltage collapse. This is done by adding knowledge from the surrounding area, using PMUs to measure the voltages and currents on two or more buses.

A problem with the VIP method described in Chapter 3 is the fact that the Thevenin equivalent seen from any given bus is not observable. There are more unknowns than there are equations, which mean that there is an infinite set of Thevenin equivalents that could all produce the same results as the one that is observed. This is solved by taking measurements at two or more different times, and treating the Thevenin equivalent as a constant.

Problems arise when the Thevenin equivalent is not constant. It has been shown in Section 3.4 that this can cause the VIP to wrongly predict a voltage collapse. To avoid this behavior one has to wait for the next valid estimation. In either way the result is unsatisfactory, and in worst case, the VIP method might be unable to track the system trajectory toward a voltage collapse. Figure 4.1 presents a system that is typical for voltage collapse, with a generator- and load-area separated by long transmission lines. A possible

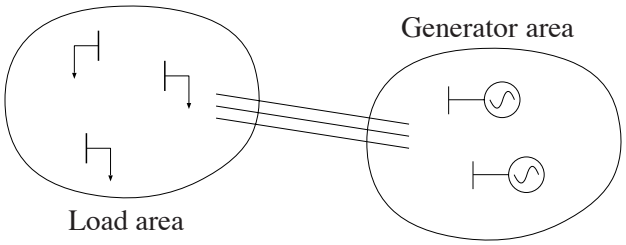

Figure 4.1: Load area supplied through long transmission lines

scenario could be: Loss of a transmission line, generator or SVC component causing a drop in voltage, with the load restoration bringing the system closer to or even into a voltage collapse.

In case of rapid changes in the system, like the removal of a line etc. the VIP method should be able to detect changes in estimation between two consecutive sets of measurements as described in Section 3.4. The problem for the VIP method in this case would be the load restoration. It is important for the VIP method that there is a change in the load, as it would not be able to do the estimation without it. At the same time there are change in loads on nearby buses, which all respond to the previous voltage drop. Seen from the VIP method all of these changes in load on other buses appear as a change in the Thevenin equivalent.

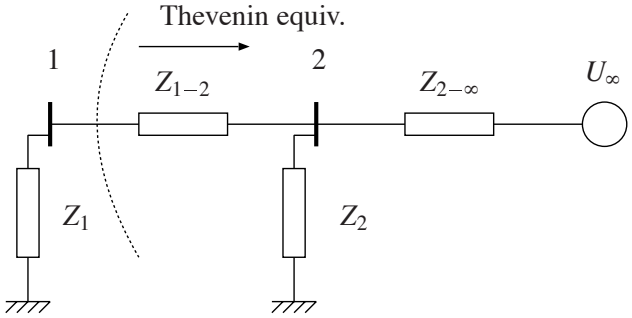

Figure 4.2: Two load buses supplied by an infinite bus behind a transmission line

Consider a system like the one shown in Figure 4.2 where there is a load area consisting of bus no. 1 and no. 2, and the rest of the system is represented by an infinite bus behind an impedance. Both loads, Z_1 and Z_2, respond to the voltage drop by restoring the load to pre-contingency levels. Clearly, the Thevenin equivalent seen from bus no. 1 depends

on how the load at bus no. 2 changes. Table 4.1 shows how two extreme values for the

Table 4.1: Thevenin equivalent given by load at bus no. 2

$\mathbf{Z_2}$	$\mathbf{E}_{Thev}$	$\mathbf{Z}_{Thev}$
0	0	$\mathbf{Z}_{1-2}$
∞	$\mathbf{U}_{\infty}$	$\mathbf{Z}_{1-2} + \mathbf{Z}_{2-\infty}$

load at bus no. 2 affect the Thevenin equivalent seen from bus no. 1. So when impedance at bus no. 2 starts to pick up load, there will be a change in both the Thevenin voltage and impedance seen from bus no. 1. The idea of the VIP++ method is to include the information about changes in load on bus no. 2, so that the distance to voltage collapse seen from bus no. 1 is observable. In this simple illustration, adding an extra measurement on bus no. 2 is the same as moving the dotted line in Figure 4.2 to bus no. 2. Thus, the VIP only has to estimate the Thevenin equivalent, $(U_{\infty}, Z_{2-\infty})$, which in this case is constant.

4.2 Estimating the system

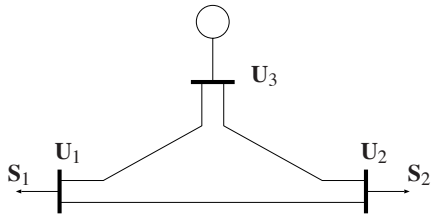

Figure 4.3: Three bus system

Given a three bus system as shown in Figure 4.3, with an infinite bus supplying two load buses, we need to find the distance to voltage collapse on bus no. 1 or no. 2. In this chapter it is assumed that the VIP++ method aims to protect bus no. 1. It is assumed that the VIP fails to estimate a Thevenin equivalent seen from bus no. 1 as well as seen from bus no. 2, due to changes in the other load bus.

The VIP++ measures voltage and current at both load buses, and assumes that the admittance $\mathbf{y}_{12}$ between the two is known. Looking at the two load buses separately, the current coming from the generator bus on both load buses can be used to estimate a Thevenin equivalent for the system in that direction. This is done using the VIP algorithm described in Chapter 3. The current coming from the other load bus over the transmission

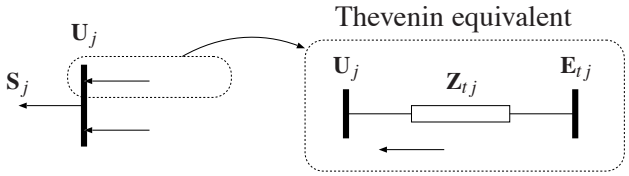

Figure 4.4: Thevenin equivalent of single current

line $\mathbf{y}_{12}$ is kept out of the estimation. This is shown in Figure 4.4, looking at bus no. 1. When this is done for both buses, an equivalent system can be made as shown in Figure 4.5.

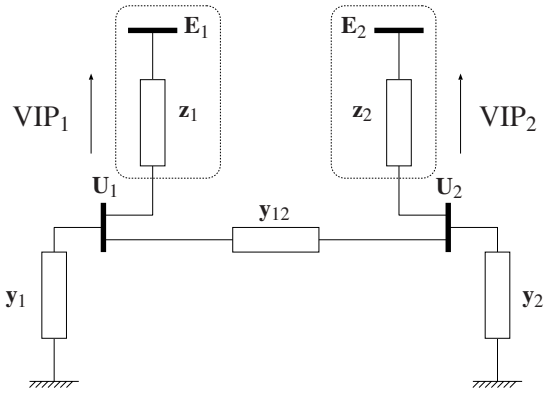

Figure 4.5: VIP using measurements from two buses

$$\begin{bmatrix} (\mathbf{y}_1+\mathbf{z}_1^{-1}+\mathbf{y}_{12}) & -\mathbf{y}_{12} & -\mathbf{z}_1^{-1} & 0 \\ -\mathbf{y}_{12} & (\mathbf{y}_2+\mathbf{z}_2^{-1}+\mathbf{y}_{12}) & 0 & -\mathbf{z}_2^{-1} \\ -\mathbf{z}_1^{-1} & 0 & \mathbf{z}_1^{-1} & 0 \\ 0 & -\mathbf{z}_2^{-1} & 0 & \mathbf{z}_2^{-1} \end{bmatrix} \cdot \begin{bmatrix} \mathbf{U}_1 \\ \mathbf{U}_2 \\ \mathbf{E}_1 \\ \mathbf{E}_2 \end{bmatrix} = \begin{bmatrix} 0 \\ 0 \\ \mathbf{I}_{E_1} \\ \mathbf{I}_{E_2} \end{bmatrix} \tag{4.1}$$

Using the first two rows in the system Equations (4.1), both voltages $\mathbf{U}_1$ and $\mathbf{U}_2$ can be expressed by the Thevenin equivalent, as given in Equation (4.2). Note that the loads $(\mathbf{y}_1, \mathbf{y}_2)$ are included in the admittances matrix, thus there is no nodal current going into these two buses.

$$\begin{aligned} \begin{bmatrix} \mathbf{U}_1 \\ \mathbf{U}_2 \end{bmatrix} &= \begin{bmatrix} (\mathbf{y}_1+\mathbf{z}_1^{-1}+\mathbf{y}_{12}) & -\mathbf{y}_{12} \\ -\mathbf{y}_{12} & (\mathbf{y}_2+\mathbf{z}_2^{-1}+\mathbf{y}_{12}) \end{bmatrix}^{-1} \cdot \begin{bmatrix} \mathbf{E}_1\mathbf{z}_1^{-1} \\ \mathbf{E}_2\mathbf{z}_2^{-1} \end{bmatrix} \\ &= \frac{1}{(\mathbf{y}_1+\mathbf{z}_1^{-1}+\mathbf{y}_{12})(\mathbf{y}_2+\mathbf{z}_2^{-1}+\mathbf{y}_{12})-\mathbf{y}_{12}^2} \begin{bmatrix} (\mathbf{y}_2+\mathbf{z}_2^{-1}+\mathbf{y}_{12})\mathbf{E}_1\mathbf{z}_1^{-1}+\mathbf{y}_{12}\mathbf{E}_2\mathbf{z}_2^{-1} \\ (\mathbf{y}_1+\mathbf{z}_1^{-1}+\mathbf{y}_{12})\mathbf{E}_2\mathbf{z}_2^{-1}+\mathbf{y}_{12}\mathbf{E}_1\mathbf{z}_1^{-1} \end{bmatrix} \end{aligned} \tag{4.2}$$

Both voltages $\mathbf{U}_1$ and $\mathbf{U}_2$ can be expressed as functions of the load admittances $\mathbf{y}_1$ and $\mathbf{y}_2$, as can the apparent load power, $\mathbf{S}_1$ and $\mathbf{S}_1$, delivered to load bus no. 1 and no. 2.

4.3 Distance to the Point of Collapse

Using the model in Figure 4.5, an expression for the apparent power S_1 delivered to load bus no. 1 can be derived. The method assumes that both Thevenin equivalents are constant at the time of estimation, so that S_1 is only a function of the admittances at the two load buses.

$$S_1 = S_1(\mathbf{y}_1, \mathbf{y}_2) = |\mathbf{U}_1(\mathbf{y_1}, \mathbf{y_2})|^2 |\mathbf{y_1}| \tag{4.3}$$

$\mathbf{U}_1(\mathbf{y_1}, \mathbf{y_2})$ is given by Equation (4.2). S_1 in Equation (4.3) is plotted in Figure 4.6 as a

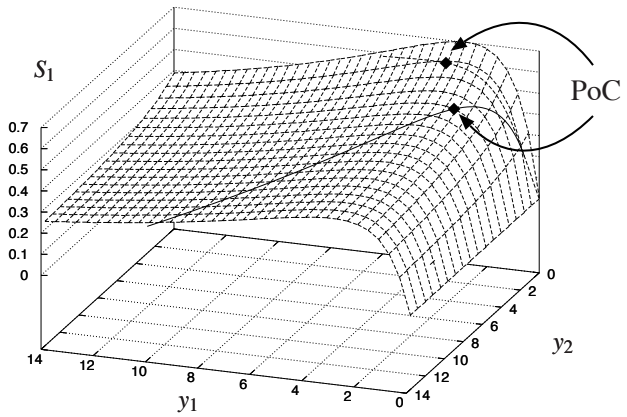

Figure 4.6: Apparent load delivered to bus no. 1

"landscape", and the maximum loading point or the PoC will depend on where the system trajectory "goes over the hill". In the figure, two different trajectories are plotted, the dotted line having a higher increase in the ratio y_2/y_1 than the solid line, which results in a lower maximum loading point, given by the value of $S_{1,max}$. Although the two trajectories start from the same point, where they presumably are equally prone to voltage collapse, they end up passing the PoC at different places. Thus, the distance to voltage collapse does not only depend on the present state, but also on future changes in the system. In online mode, the future of the system is unknown, and an estimate for the system trajectory must be estimated.

4.3.1 Methods

For purposes of illustration we will here consider a system with reactive load only. The resistance of the transmission lines are ignored and the Thevenin voltages are equal to 1.0 pu. Assume that both load admittances are increasing at a steady pace. The power delivered to bus no. 1 will then increase, and at a given time will reach a maximum point before it starts to decrease as shown in Figure 4.6. If both loads are functions of time, the maximum loading point is given by Equation (4.4)

$$\frac{dS_1}{dt} = 0 \tag{4.4}$$

The VIP++ method measures the two loads y_1 and y_2, hence the time derivatives of these variables can be estimated. Using Equation (4.4) and the definition of voltage stability given by Mansour [9], see Section 2.1.1, several strategies to find the distance to voltage collapse can be formulated:

1. Assuming that the load admittance increase $\dot{y}_2/\dot{y}_1$ is constant, the system will move along the gradient in the admittance plane.

2. Shifting the gradient in the y_1 direction.

3. Finding the critical increase in load admittance on a load bus, assuming the rest of the system is constant.

4. Finding a distance to the PoC using time domain simulations, which requires knowledge about load dynamics.

Methods 1 and 2 are explored in this dissertation. While methods 3 and 4 will be used for comparison together with the VIP method.

The VIP++ method can now be summarized as follows:

1. At time step t(i) estimate the Thevenin equivalent (E_{tj}, Z_{tj}) for $j \in \{1, 2, \ldots, N\}$ where $N \geqslant 2$ is the number of measured buses, see Figure 4.4.

2. Using the estimated Thevenin equivalents, a "landscape" is produced as presented in Figure 4.6.

3. Assume that the landscape presented in step number 2 is constant, a distance to voltage collapse, given by a critical admittance $\tilde{y}_1(i)$, can be found using one of the strategies presented above.

4. Go to next time step t(i=i+1) and start over again at number 1.

The critical admittance, $\tilde{y}_1$, is re-calculated every time a new measurement is made. When the measured value of the load admittance at load bus no. 1, y_l is equal to the critical admittance, the system is at the PoC. Since a new landscape is calculated for each time step, it will "float" due to the changes in the Thevenin equivalents.

For both methods presented the PoC_e is used for the estimated point of collapse at the time of the estimation, whereas the PoC_r is the point where the given system trajectory passes the real point of collapse. A new PoC_e has to be calculated for each time a new measurement is made. Here, index m has been used for measured values of admittance/impedances, $\mathbf{y}_{jm}/\mathbf{z}_{jm}$, while critical values calculated by the estimation are denoted by a tilde, $\tilde{y}_1/\tilde{z}_1$.

4.3.2 Test case

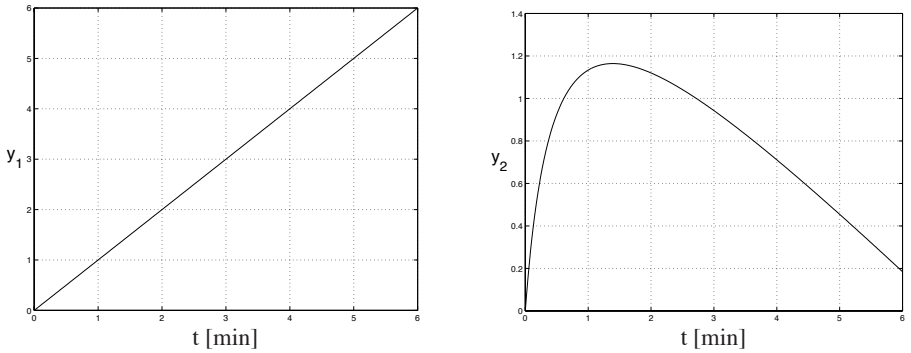

(a) $y_1(t)$ (b) $y_2(t)$

Figure 4.7: Load trajectories

A test simulation has been performed to illustrate how the methods are used to track the distance to the PoC. The two load trajectories $y_1(t)$ and $y_2(t)$ are given in Equation (4.5)

$$\begin{aligned} y_1(t) &= t \\ y_2(t) &= \frac{4t - 0.6t^2}{1 + 2t} \end{aligned} \tag{4.5}$$

and shown in Figure 4.7. In the methods presented in the next sections these variables are "handed" to the algorithm as time progresses, but in a real system they would have to be measured, or calculated from the PMU measurements of voltage and current. Both

load admittances are purely reactive, and the time derivatives can be found as given in Equation (4.6).

$$\begin{aligned}\frac{dy_1}{dt} &= 1 \\ \frac{dy_2}{dt} &= \frac{4 - 1.2t - 1.2t^2}{(1+2t)^2}\end{aligned} \tag{4.6}$$

As for the system trajectory these are assumed to be known to the algorithm, and need to be measured in a real system. This can be done using a filter.

The Thevenin equivalents representing the generators and the transmission system are represented by constant values for illustration purposes. Thus, they will fulfill the requirements of the VIP given in Section 3.4, so the estimation made by the VIP gives the correct value for the equivalents.

The two load trajectories $y_1(t)$ and $y_2(t)$ begin at zero and as they reach the point marked by the open square in the figures, shown in Sections 4.3.3 through 4.3.6, the VIP++ algorithms will try to estimate the distance to PoC. The estimated value at this point is given by the diamond marked PoC_e in the figures. The real system trajectory given by the dotted line is assumed unknown after the open square, but are included in the figures to show how the estimated values differ from the final crossover point, marked PoC_r.

4.3.3 Distance to the PoC along the gradient

An estimated distance to the PoC can be calculated using the assumption that both load admittances keep moving in the same direction as is the case at the moment when the estimation is made.

Simplified system

For the system using the assumption of pure reactive load and ignoring the resistance of the transmission line the load admittances can be written as:

$$\begin{aligned}\tilde{y}_1(\tau) &= y_{1m} + y_{1dm}\tau \\ \tilde{y}_2(\tau) &= y_{2m} + y_{2dm}\tau\end{aligned} \tag{4.7}$$

where

y_{im} measured values of the load admittances

y_{idm} time derivative of the loads at present time

When using this assumption the Equation (4.4) becomes a function of time only.

$$\frac{dS_1}{d\tau} = f(\tau) = 0 \tag{4.8}$$

The solution $\tilde{\tau}$ of Equation (4.8) is the time until the PoC$_e$ is reached. The equation is a polynomial, which can easily be solved numerically. In case of a system as the one given in Figure 4.5 with complex loads and transmission lines, the degree of the polynomial is seven. Substituting the solution $\tilde{\tau}$ into Equation (4.7), a distance to the PoC can be computed

$$d = \tilde{y}_1(\tilde{\tau}) - y_{1m} = y_{1dm}\tilde{\tau} \tag{4.9}$$

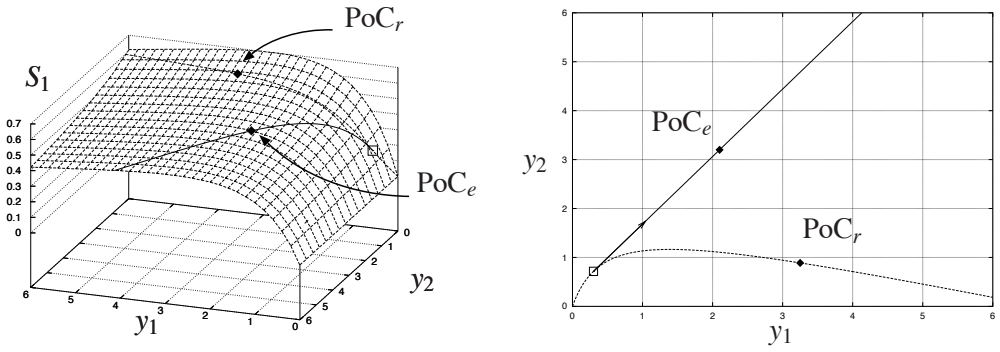

(a) Surface plot of load trajectories

(b) System trajectory in admittance plane

Figure 4.8: Measured and critical values in per unit at time step $t = 0.3$ [min]

The method is illustrated in Figure 4.8, where a system trajectory is plotted as a dotted line in both Figures 4.8(a) and 4.8(b). At the time of estimation, marked by the open square, a new trajectory is computed. An estimated PoC$_e$ can be found using this new trajectory. For each time step, such a new trajectory has to be computed, and when the system reaches the real PoC$_r$, the two will converge. In Figure 4.9(a) the critical admittance, $\tilde{y}_1$, is plotted as a solid line, and the measured value of y_1 as a dotted line. The critical admittance $\tilde{y}_1$ represents the value of y_1 at the estimated point of collapse PoC$_e$ for each time step, and it is re-calculated for every new measurement. Where the two lines meet, just after three seconds, there should be a maximum in the load flow delivered to bus no. 1 according to the method. This is shown in Figure 4.9(b), where the apparent load power delivered to bus no. 1 together with the critical load power PoC$_e$ is plotted as dotted and solid lines respectively. There is a maximum in the load flow where the critical lines cross the measured values in Figures 4.9(a) and 4.9(b).

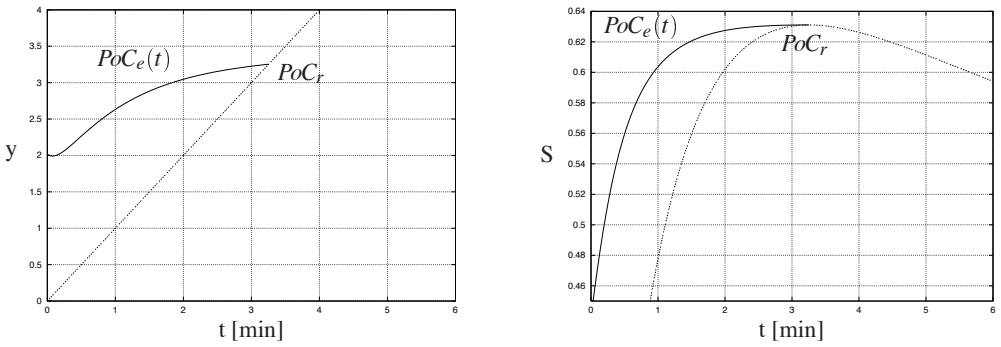

(a) Admittance

(b) Apparent power

Figure 4.9: Measured and critical values in per unit

Complex loads and transmission lines

In the previous section, there is an assumption that both load and transmission lines are purely reactive, while the Thevenin voltage is equal to 1.0 pu. Clearly, this is not the case in a real system where complex values for all the variables must be included. This VIP++ method adds complex values by using the gradient to the real and imaginary parts for loads y_1 and y_2. The estimated system trajectory thus moves in a five-dimensional space as opposed to the three-dimensional space shown in the previous section.

$$\begin{aligned}\tilde{\mathbf{y}}_1(\boldsymbol{\tau}) &= \tilde{g}_1(\boldsymbol{\tau}) + i\tilde{b}_1(\boldsymbol{\tau}) = g_{1m} + g_{1dm}\boldsymbol{\tau} + i(b_{1m} + b_{1dm}\boldsymbol{\tau}) \\ \tilde{\mathbf{y}}_2(\boldsymbol{\tau}) &= \tilde{g}_1(\boldsymbol{\tau}) + i\tilde{b}_1(\boldsymbol{\tau}) = g_{2m} + g_{2dm}\boldsymbol{\tau} + i(b_{2m} + b_{2dm}\boldsymbol{\tau})\end{aligned} \tag{4.10}$$

Substituting U_1 from Equation (4.2) into Equation (4.3)

$$S_1 = \frac{|\mathbf{a}_1 + \mathbf{a}_2\mathbf{y}_2|^2}{|\mathbf{y}_1\mathbf{y}_2 + \mathbf{b}_1\mathbf{y_1} + \mathbf{b}_2\mathbf{y}_2 + \mathbf{b}_3|^2}|\mathbf{y}_1| \tag{4.11}$$

Where $\mathbf{a}_i, \mathbf{b}_j \in \mathbb{C}$ are given by the estimated Thevenin equivalents $(\mathbf{E_1}, \mathbf{z_1})$ and $(\mathbf{E_2}, \mathbf{z_2})$ and the admittance $\mathbf{y}_{12}$ between bus no. 1 and no. 2. By using Equation (4.10), Equation (4.11) can be written as

$$S_1(\tilde{\mathbf{y}}_1, \tilde{\mathbf{y}}_2) = \frac{\sum_{k=0}^{2} c_k\boldsymbol{\tau}^k}{\sum_{r=0}^{4} e_r\boldsymbol{\tau}^r}\sqrt{\sum_{s=0}^{2} d_s\boldsymbol{\tau}^s} \tag{4.12}$$

where the parameters $c_k, e_r, d_s \in \mathbb{R}$ are calculated by the parameters $\mathbf{a}_k$, $\mathbf{b}_k$ and the measured values of the load admittances. The maximum loading point can now be found, as

given by Equation (4.4), by setting the derivative of the load S_1 with respect to the time τ equal to zero.

$$\left.\frac{dS_1}{d\tau}\right|_{\tau=\tilde{\tau}} = 0$$
$$\Downarrow \tag{4.13}$$
$$\sum_{m=0}^{7} s_m \tilde{\tau}^m = 0$$

The parameters s_m are given by the parameters c_k, e_r, d_s, and $\tilde{\tau}$ is the estimated time left until the system passes PoC_e. Solving the Equation (4.13) for the estimated time $\tilde{\tau}$ to the PoC can only be done numerically, and substituting the solution into Equation (4.14) gives the critical load admittance.

$$\tilde{y}_1(\tilde{\tau}) = \sqrt{\tilde{g}_1^2(\tilde{\tau}) + \tilde{b}_1^2(\tilde{\tau})} \tag{4.14}$$

The equivalent estimated maximum apparent load power is given by

$$\tilde{S}_1 = \tilde{S}_1(\tilde{\mathbf{y}}_1(\tilde{\tau}), \tilde{\mathbf{y}}_2(\tilde{\tau})) \tag{4.15}$$

Both the critical admittance in Equation (4.14) and the equivalent apparent load power in Equation (4.15) can be presented as given in Figure 4.9. The presentation in Figure 4.8 cannot be used when complex variables are included.

4.3.4 Shifting the gradient in the y_1 direction

The method named *Shifting the gradient in the y_1 direction* finds the superimposed load at load bus no. 1, which immediately will bring the system to the PoC.

Simplified system

At the time of estimation, given by the open square in Figure 4.10(a) and 4.10(b), the gradient in (y_1,y_2) plane is found. The gradient is shifted in y_1 direction so that the new point will be a maximum point, PoC_e. The estimated distance to PoC_e can be found as the difference $d = \tilde{y}_1 - y_1$, given by the arrow in Figure 4.10(b), where $\tilde{y}_1$ is found by solving Equation (4.4) for the admittance at bus no. 1. This is equivalent to a sudden load increase $d = \tilde{y}_1 - y_1$ coming in addition to the continuous increase along the gradient y_2/y_1.

$$\frac{dS_1}{dt} = f(\tilde{y}_1) = 0 \tag{4.16}$$

As in Section 4.3.3, the critical admittance, $\tilde{y}_1$, and the measured admittance, y_1, have

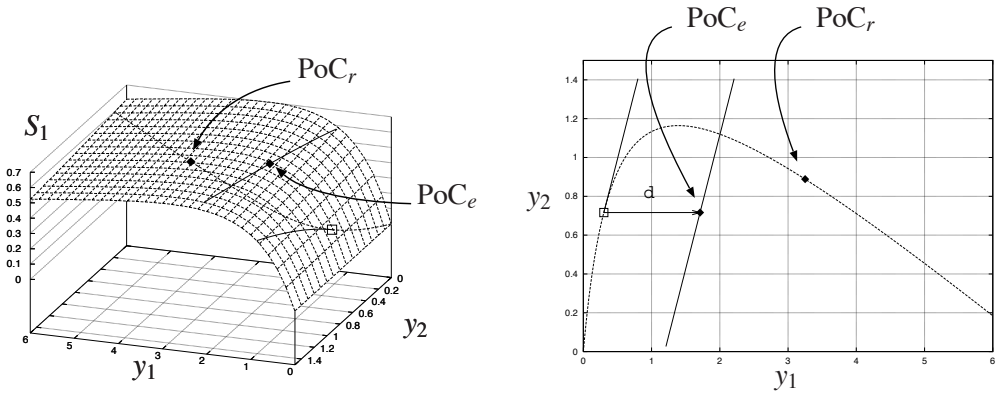

(a) Surface plot of load trajectories

(b) System trajectory in admittance plane

Figure 4.10: Measured and critical values in per unit at time step $t = 0.3$ [min]

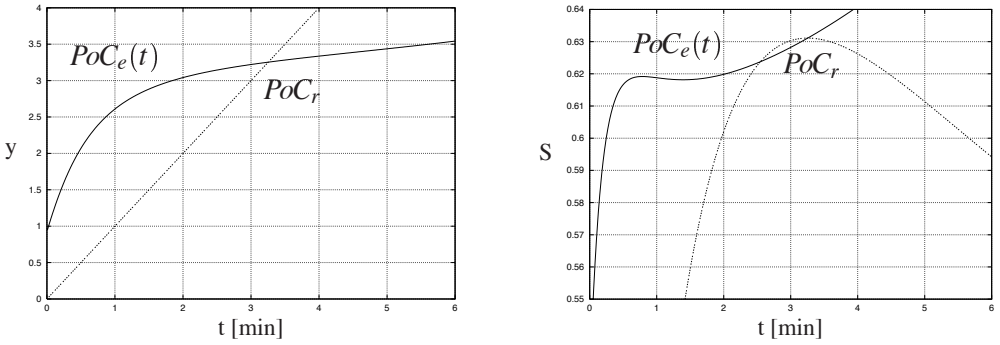

(a) Admittance

(b) Apparent power

Figure 4.11: Measured and critical values in per unit

been plotted in Figure 4.11(a) as solid and dotted lines respectively. There is a difference in the prediction of distance to the PoC$_e$ for the two methods, *Shifting the gradient in the* y_1 *direction* and *Distance to the PoC along the gradient*, but both indicated the same PoC$_r$ as they cross the system trajectory at approximately 3.2 seconds.

Power margin

Using the equivalent estimated maximum apparent load power in this case does not work as shown in Figure 4.11(b), where PoC_e is plotted as dotted lines. Although the critical load flow PoC_e crosses the load flow delivered to load bus no. 1 at PoC_r as expected, it can also cross it at other points than PoC_r. Using the equivalent load flow can thus in special cases cause the VIP++ relay to act when system is still a distance away from the PoC_r.

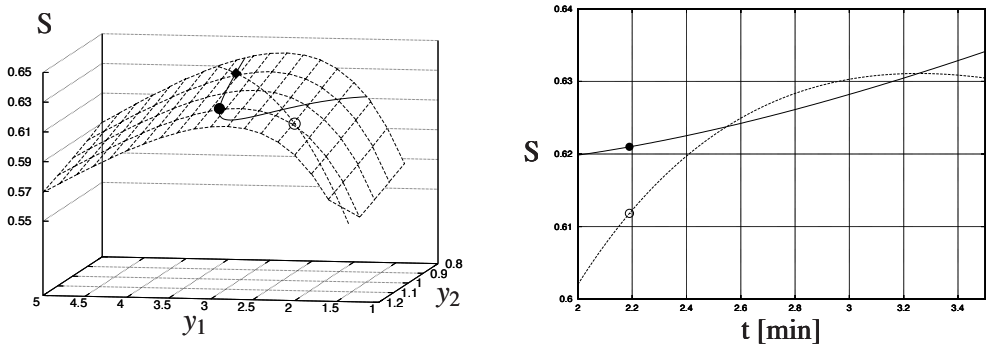

(a) Surface plot

(b) Apparent load power

Figure 4.12: Power margin at t=2.19

The erroneous warning given by the equivalent estimated load power maximum, PoC_e, is illustrated by both Figures 4.12 and 4.13. Here, the system trajectory and the estimated PoC_e are plotted as a dotted and solid line respectively, and the two lines cross prior to the actual PoC_r. In both figures the present state on the system trajectory is given by the open circle, while the estimated maximum, PoC_e, at that given point is given by the solid circle. As in previous figures the final crossing point, PoC_r, is given by a diamond. In Figure 4.12(a) the system trajectory is, in the S-axis, clearly below the estimated critical value. The critical value is at this time estimated to be on the back side of the ridge, which is possible due to the reduction in load admittance $\mathbf{y}_2$, strengthening the system seen from load bus 1. In Figure 4.13(a), it seems like both the estimated critical value PoC_e and the system trajectory is on the back side of the ridge. This is, as stated before, possible due to the reduction in load admittance $\mathbf{y}_2$. The trajectory has not yet crossed the PoC_r, but the estimated value PoC_e is now below the system trajectory value, wrongly indicating that system has passed the PoC. This means that the estimated critical apparent load power should be used with care, as it in special cases such as the *test case* presented in this chapter this will produce wrong results. The *test case* is a constructed case with the purpose of describing the different VIP++ methods, and it is not a realistic voltage collapse

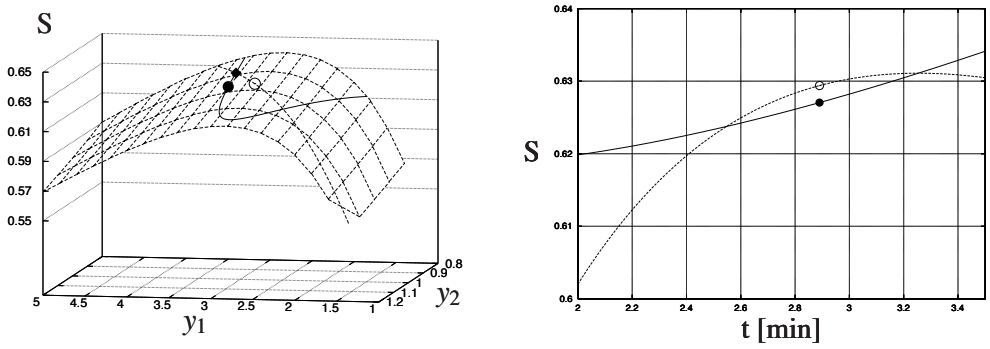

(a) Surface plot

(b) Apparent load power

Figure 4.13: Power margin at t=2.89

scenario. For a general system including both generator and realistic load dynamics, it is more than likely that this phenomenon will not occur. On must also consider that when these phenomenon actually do happen, action might still be appropriate, as the system is very close to the actual PoC_r.

Complex loads and transmission lines

Finding the distance to voltage collapse when complex loads and transmission are considered can be done by using polar coordinates. Setting the time derivative of S in Equation (4.3) to zero,

$$\frac{dS}{dt} = \frac{\partial S}{\partial y_1}\frac{dy_1}{dt} + \frac{\partial S}{\partial \delta_1}\frac{d\delta_1}{dt} + \frac{\partial S}{\partial y_2}\frac{dy_2}{dt} + \frac{\partial S}{\partial \delta_2}\frac{d\delta_2}{dt} = 0 \tag{4.17}$$

the distance to voltage collapse can be found, as shown in Section 4.3, by solving for y_1, denoted $\tilde{y}_1$. This gives a cubic equation

$$s_3\tilde{y}_1^3 + s_2\tilde{y}_1^2 + s_1\tilde{y}_1 + s_0 = 0 \tag{4.18}$$

where the solution of $d = \tilde{y}_1 - y_1$ is the new prediction of distance to voltage collapse. The time derivatives are estimated from the measured loads on each of the two buses. The equivalent estimated maximum apparent load power can now be calculated using the critical admittance $\tilde{y}_1$, the measured angle δ_{1m} and the measured load admittance $\mathbf{y}_{2m}$.

$$\tilde{S}_1 = \tilde{S}_1(\tilde{y}_1 e^{i\delta_{1m}}, \mathbf{y}_{2m}) \tag{4.19}$$

As in the method, *Distance to the PoC along the gradient*, the results from this method using complex variables can be presented as given in Figure 4.11, while the presentation in Figure 4.10 is not possible.

4.3.5 Distance to the PoC when the system is assumed constant

In this method no assumption on future changes are made, neither on load $\mathbf{y}_1$ nor $\mathbf{y}_2$. The estimate of the distance to the PoC is based on the superimposed increase in $\mathbf{y}_1$ that will immediately bring the system to collapse, assuming both loads are constant.

This is the steady-state assumption and as shown in Section 3.1. The critical load impedance can be found as the absolute value of the Thevenin impedance/admittance seen from load bus no. 1.

$$z_t = |\mathbf{z}_{t1}\|(\mathbf{z}_{12}+\mathbf{z}_2\|\mathbf{z}_{t2})| = \frac{|\mathbf{z}_{t1}(\mathbf{z}_{12}(\mathbf{z}_2+\mathbf{z}_{t2})+\mathbf{z}_2\mathbf{z}_{t2})|}{|(\mathbf{z}_{t1}+\mathbf{z}_{12})(\mathbf{z}_2+\mathbf{z}_{t2})+\mathbf{z}_2\mathbf{z}_{t2}|} \tag{4.20}$$

z_t is the critical impedance at load bus no. 1. When the value of z_t crosses the value of the load impedance, the system should be at the PoC according to the method. The equivalent maximum apparent load power can be calculated using a similar to method as for the VIP in Section 3.3, with a constant power factor $\tan\phi$.

$$S_{max} = \frac{E^2\sqrt{1+\tan^2\phi}}{2(r_t + x_t\tan\phi \pm \sqrt{(r_t^2+x_t^2)(1+\tan^2\phi)})} \tag{4.21}$$

Here, the variables r_t and x_t are given the Thevenin impedance, $\mathbf{z}_t = r_t + ix_t$. E is the Thevenin voltage seen from bus no. 1, which can be found as $E = U_1(0, \mathbf{y}_{2m})$ in Equation (4.2).

$$E = \frac{(\mathbf{y}_{2m}+\mathbf{z}_2^{-1}+\mathbf{y}_{12})\mathbf{E}_1\mathbf{z}_1^{-1}+\mathbf{y}_{12}\mathbf{E}_2\mathbf{z}_2^{-1}}{(\mathbf{z}_1^{-1}+\mathbf{y}_{12})(\mathbf{y}_{2m}+\mathbf{z}_2^{-1}+\mathbf{y}_{12})-\mathbf{y}_{12}^2} \tag{4.22}$$

As seen in Figure 4.15 this method will not be able to track the distance to the PoC correctly according to the definition of voltage stability given by Mansour [9]. Both the critical impedance z_{crit} and the equivalent load power cross the real values, just before three seconds, a little before the load power delivered to bus no. 1 reaches its maximum level.

4.3.6 Known load dynamics

In cases where knowledge about the load dynamics at both load buses is known as given in Equation (4.23), the distance to the PoC can be estimated based on this knowledge.

$$\begin{aligned}\frac{dy_1}{dt} &= f_1(y_1, y_2, t)\\ \frac{dy_2}{dt} &= f_2(y_1, y_2, t)\end{aligned} \tag{4.23}$$

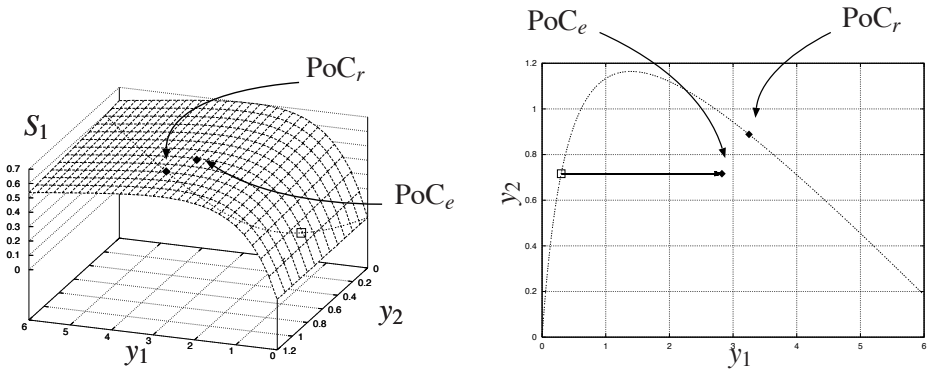

(a) Surface plot of load trajectory (b) System trajectory in admittance plane

Figure 4.14: Measured and critical values in per unit at time step $t = 0.3$ [min]

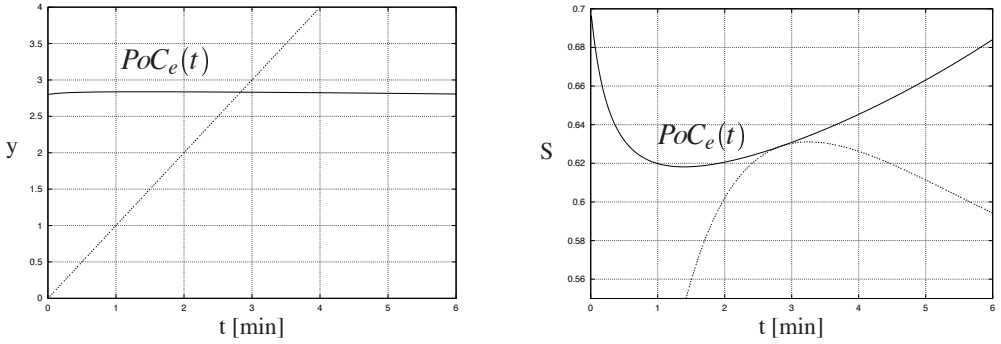

(a) Admittance (b) Apparent power

Figure 4.15: Measured and critical values in per unit

Equations (4.23) can be used together with the estimated system in Figure 4.5, to determine stable and/or unstable equilibrium points. In cases where the differential equations can be solved explicitly the solutions can be used to determine the distance to the PoC "exactly" if no stable equilibrium points exist. Otherwise, numerical simulations have to be performed each time a new measurement is performed.

$$\begin{aligned} y_1 &= y_1(t) \\ y_2 &= y_2(t) \end{aligned} \tag{4.24}$$

Substituting the solution in Equation (4.24) into Equation (4.3) the Equation (4.4) becomes an equation of time only,

$$\frac{dS_1}{dt} = f(t) = 0 \tag{4.25}$$

which can be solved either explicitly or numerically, depending on the complexity of the load dynamics. In this case, both an estimate of time left to voltage collapse and a distance can be found. In case the Thevenin equivalent represents the true system, the estimation made is exact. These methods are not within the scope of this dissertation and are not explored any further.

4.4 Solution of the polynomial

In both methods "Shifting the gradient in the y_l direction" and "Distance to the PoC along the gradient" solving the problem involves solving a polynomial of degree 3 for the first and 7 and higher for the second, which requires a method to choose the correct value.

4.4.1 Shifting the gradient in the y_l direction

In this method, three criteria for choosing the correct value of the polynomial have been established.

1. The solution to the polynomial is the absolute value of the load admittance y_l, thus the solution can neither be negative nor complex, $\tilde{y}_l \in [0, \infty)$.
2. Using the maximum loadability criteria, the measured load admittance has to be less than the critical admittance to be within the stable region. This limits the region for valid solutions of the polynomial to $\tilde{y}_l \in [y_1, \infty)$ or in impedances $\tilde{z}_l \in [0, z_1]$.
3. The method needs to be risk averse, so for all the solution within the allowed region choose the one closest to the measured value.

Any solution to the polynomial outside this definition must be discarded. If none of the solutions to the polynomial is within the allowed region, ignoring the second criteria, the method experiences numerical problems. The second criteria limits the allowed solutions to the stable region, and ignoring this only means finding the distance to the stable region when the system has passed the PoC. This criterion has been ignored for all the simulations in this dissertation. A relay should operate before entering the unstable region.

4.4.2 Distance to the PoC along the gradient

1. The polynomial is the estimated time left until the system reaches the PoC, thus the solution cannot be complex, $\tilde{\tau} \in \mathbb{R}$.

2. Given any positive value of $\tilde{\tau}$ means that there is a maximum going in the present direction, and for negative values of $\tilde{\tau}$ there is a maximum going backwards in the present direction. Thus, the solution is limited to $\tilde{\tau} \in [0, \infty)$. As the value of the solution to the polynomial passes zero, the system reaches the PoC.

3. Of all the positive real values, choose the one closest to zero, as this is the first maximum that the system will cross going in this direction.

The solution of the polynomial chosen by the three criteria presented above is used to calculate the critical admittance, and the estimated PoC_e.

4.5 Comparing VIP++ methods, "Shifting the gradient in the y_1 direction" and "Distance to the PoC along the gradient", with the VIP method

Due to the simplicity of the system and load trajectories, a comparison of VIP++ methods, "Shifting the gradient in the y_1 direction" and "Distance to the PoC along the gradient", with the VIP method, can be done using the simple equation described in Equation (3.24). There is no need to do further filtering of the signals. In Figure 4.16(a), the critical load

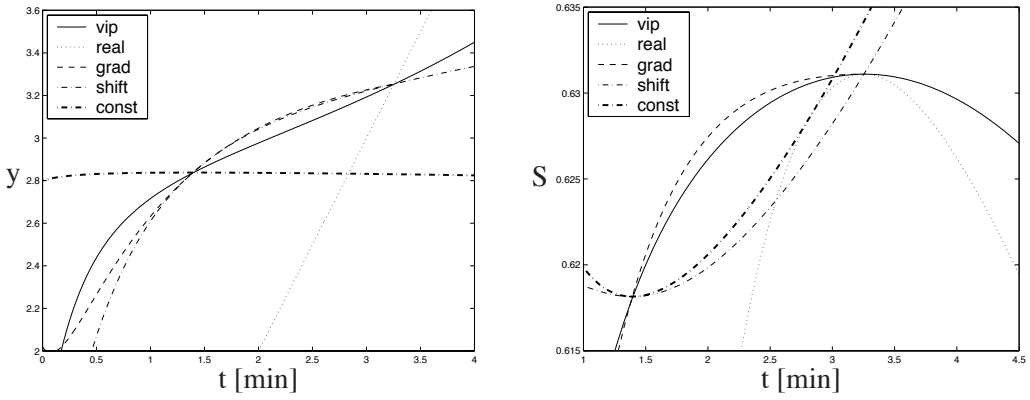

(a) Admittance (b) Apparent Power

Figure 4.16: Comparing critical values from the VIP++ and VIP methods and the system trajectory

admittances are plotted together with real load admittance at load bus no. 1. The legend in the figure is given as follows:

vip The result from the VIP algorithm.

real The load admittances at load bus no. 1.

grad The critical load admittances based on the Distance to the PoC along the gradient method.

shift The critical load admittances based on the Shifting the gradient in the y_1 direction method.

const The critical load admittances based on the "Distance to the PoC when the system is constant" method.

The algorithms "Distance to the PoC along the gradient" and "Shifting the gradient in the y_1 direction" are very close to the result from the VIP algorithm in this test case, and they all intersect the load admittance at the "true" PoC$_r$ as shown in Figure 4.16(a). The method based on the assumption of a constant system crosses the load admittances line earlier than the other methods, as mentioned before, and should not be used. Comparing the results from the equivalent estimated maximum apparent load power, shown in Figure 4.16(b), we get a similar result. The estimated values of the methods "Distance to the PoC along the gradient", "Shifting the gradient in the y_1 direction" and the VIP , cross the system trajectory at the PoC. Both the "Shifting the gradient in the y_1 direction" and the constant system method cross the system trajectory before the PoC, which has been discussed above.

It seems that all the methods, expect for the "const" method, are close throughout the entire test simulation. This is not the general case, the main purpose of test simulation was to illustrate the idea of the different VIP++ methods, not to find the best method to predict distance to the PoC. It is important though to compare the methods to show that they all converge to the same PoC$_r$.

4.6 Generalization to *n* nodes

The VIP++ method can easily be extended to include information from several surrounding buses, as shown in Figure 4.17. Any system might be used as long as the transmission lines between the buses are known, and measurements are made on all the load buses. When estimating Thevenin equivalents along the boundary of the system, an equivalent system can be made. This system includes measured values of apparent loads, estimated Thevenin equivalents, and the known topology. The power delivered to the critical bus can then be expressed as a function of admittances at surrounding load buses.

$$S_1 = S_1(\mathbf{y_1}, \ldots, \mathbf{y_n}) \tag{4.26}$$

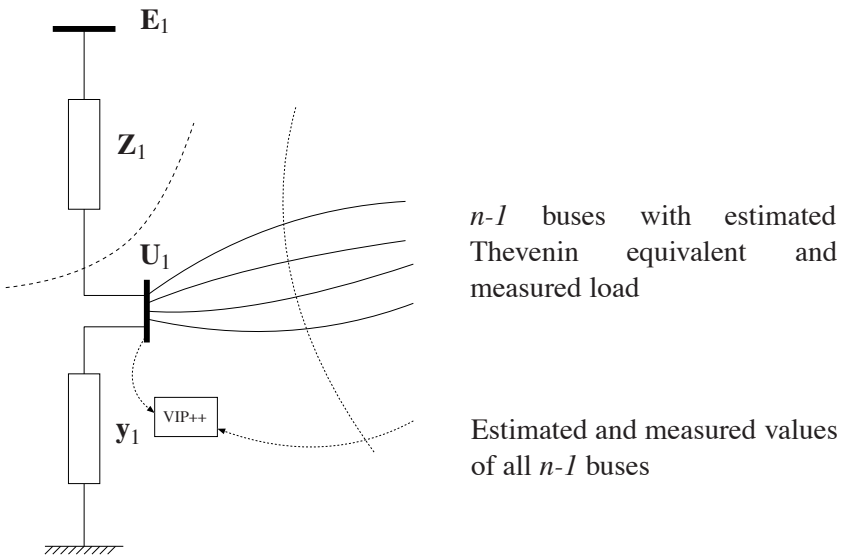

Figure 4.17: n-nodes

4.6.1 Distance to the PoC along the gradient

When using measurements from n buses each of the loads on the measured buses $\mathbf{y_i}$ are assumed to increase according to Equation (4.27).

$$\tilde{\mathbf{y}}_\mathbf{i}(\tau) = \mathbf{y}_{im} + \mathbf{y}_{idm}\tau = g_{im} + g_{idm}\tau + i(b_{im} + b_{idm}\tau) \tag{4.27}$$

where variables with index m and dm are the measured values and the derivatives of the measured values respectively. Substituting Equation (4.27) into Equation (4.26) and solving Equation (4.8) for $\tilde{\tau}$, results in a $4n-1$ polynomial that must be solved.

$$\sum_{i=0}^{4n-1} c_i \tilde{\tau}^i = 0 \tag{4.28}$$

For each new bus that is added to the set of measured buses, the degree of the polynomial is increased by four. For two buses it is seven, and for three buses it is eleven.

4.6.2 Shifting the gradient in the y_1 direction

In the second method described, see Section 4.3.4, setting the time derivative of the apparent load power in Equation (4.26) to zero, we find the maximum load that can be delivered

to the bus:

$$\frac{dS}{dt} = \sum_{j=1}^{n} \left(\frac{\partial S}{\partial y_j} \frac{dy_j}{dt} + \frac{\partial S}{\partial \delta_j} \frac{d\delta_j}{dt} \right) = 0 \tag{4.29}$$

Solving this for y_1, denoted $\tilde{y}_1$, *always* gives a cubic equation, independent of the topology of the surrounding system.

$$s_3 \tilde{y}_1^3 + s_2 \tilde{y}_1^2 + s_1 \tilde{y}_1 + s_0 = 0 \tag{4.30}$$

The complexity of the parameters s_i is increased with growing number of "known" load buses.

4.6.3 Size of the model

There is no general rule deciding on how many extra buses should be included in the VIP++ method. One might consider including the complete network, using measurements from the entire system. This would remove the estimation of Thevenin equivalents completely. Although this might be a theoretical possibility, it is not recommended.

- The VIP++ would lose the advantage of the VIP of being a local device, using only a small amount of measurements.
- The idea of the VIP++, is to include extra information to make the system observable, that is if the assumptions made about the Thevenin equivalents being constant are "true". Adding extra information after this will just add to the complexity of the estimation, and there might not be any new knowledge gained as far as distance to voltage collapse is concerned.
- Distance to the PoC along the gradient
  - The degree of the polynomial that must be solved will increase with growing number of known buses with the order of $4n - 1$.
  - Calculation of the parameters s_j in Equation (4.28) becomes time consuming. For increasing number of known load buses n, the complexity of the algebraic expression for the parameters s_i in the cubic equation increases significantly. The cubic equation can easily be solved when the parameters are calculated.
- Shifting the gradient in y_1 direction
  - The parameters $s_1, \ldots, s_3$ in Equation (4.30) have to be found symbolically for each specific case. For large models, with a high number of known buses, the numerical calculation of these is time consuming.

For systems like the one shown in Figure 4.1, where there is a generator and a load area, VIP++ measurements should only be made in the load area. The only exception to this is the frequency deviation problem mentioned in Section 3.5, where a frequency measurement in the generator area would gain in the estimation of Thevenin equivalents.

Chapter 5

Case Study

In this chapter the VIP and the VIP++ methods have been tested on time domain simulations from a small four bus test system and on a model of the Norwegian grid. Finding the critical impedance after passing the PoC_r has been ignored in all the simulations, using the VIP++ method "Distance to the PoC along the gradient". A case study of the effect of adding extra "known" load buses is also included, using a very simple model.

5.1 Increasing loads

The VIP++ methods, "Distance to the PoC along the gradient" and "Shifting the gradient

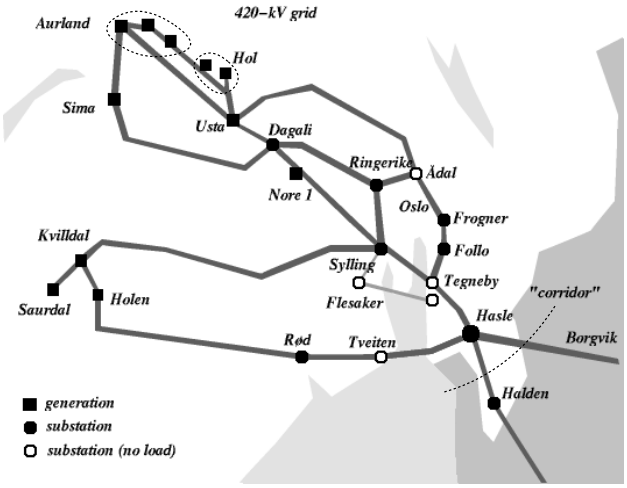

Figure 5.1: Southeastern part of the Norwegian 420 kV grid

in the y_l direction", have been tested on an eight bus model given by the topology of eight of the buses on the Norwegian 420 kV grid shown in Figure 5.1. This has been done to test the effect on the estimated critical admittance when adding extra "known" buses to the estimation.

5.1.1 Model

The test system is presented in Figure 5.2. It is a simplified model where all the trans-

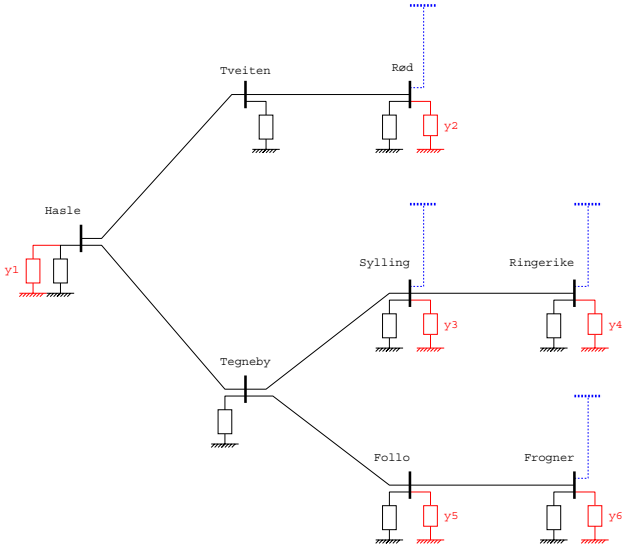

Figure 5.2: Test system

mission lines are given the same value, as are the shunt impedances on each bus. The Thevenin equivalents on each load bus, given by the dotted lines, is a constant voltage of one per unit behind and a constant impedance. On all the load buses there is a constant increase in the load admittance.

Five cases have been tested using the methods "Distance to the PoC along the gradient" and "Shifting the gradient in the y_l direction", denoted by 1 through 5 in Figures 5.4 and 5.5. For each case there is a different set of measurements, the higher case number indicating a higher set of measurements. See Appendix B for further description of the different cases.

5.1.2 Results

In this test case a critical admittance is calculated for the load in Hasle, thus the algorithms are protecting the Hasle "corridor" shown in Figure 5.1. Apparent power delivered Hasle

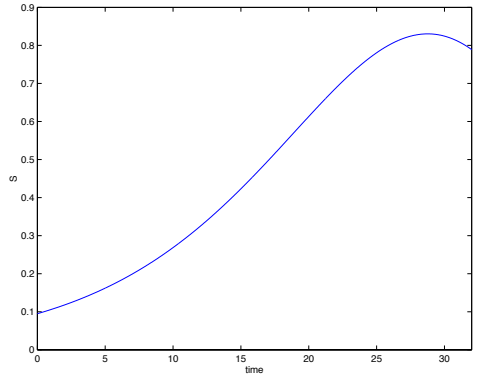

Figure 5.3: Apparent power delivered to Hasle

reaches a maximum at $t \approx 29$ seconds, which is shown in Figure 5.3. The result of estimating critical impedances is presented in Figures 5.4 and 5.5 for both the methods "Distance to the PoC along the gradient" and "Shifting the gradient in the y_l direction". For both methods the estimated value for all the cases crosses the system load trajectory at the point where the apparent load power delivered to Hasle is at its maximum level.

Distance to the PoC along the gradient

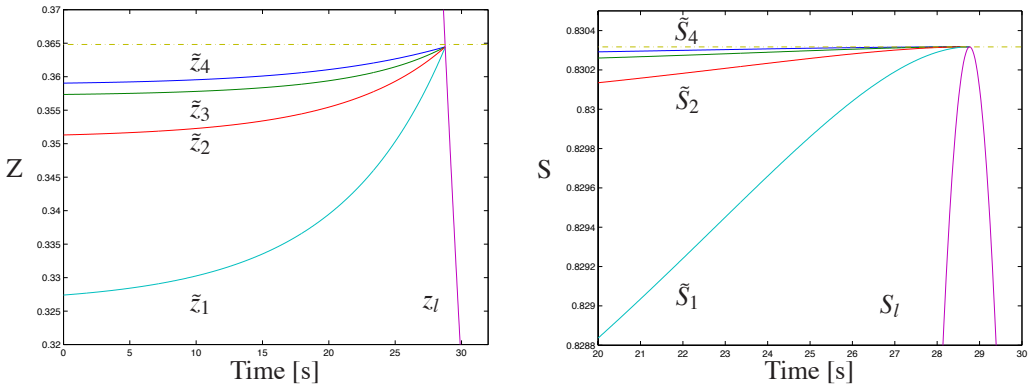

(a) Impedances

(b) Apparent power

Figure 5.4: Measured and estimated critical values in per unit

In Figure 5.4(a) it is shown that when adding an extra "known" bus to the set of mea-

surements, the estimated critical impedance is increased. Going from case 1 to case 2, there is a rather large jump, while the difference between cases 3 and 4 is smaller. Case 5 is not plotted in this figure as it was not possible to make a MATLAB function for this system [1], see Appendix D for details on making MATLAB functions for the methods "Distance to the PoC along the gradient" and "Shifting the gradient in the y_l direction". Since the system complies with the assumptions of the method, when all the load buses are included in the estimation, the estimation should be the horizontal dotted line going through the final crossing point at $t \approx 29$ seconds.

Shifting the gradient in the y_1 direction

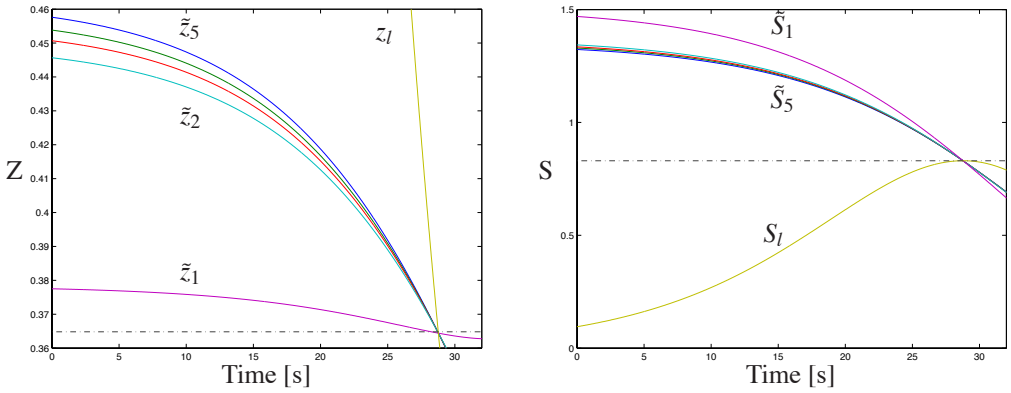

(a) Impedance

(b) Apparent power

Figure 5.5: Measured and estimated critical values in per unit

Also for the "Shifting the gradient in the y_l direction" method there is an increase in the critical load impedance value when extra buses are included, reducing the estimated distance to the PoC. There is a rather large jump between case 1 and case 2, while for the other cases there are small differences.

While the "Distance to the PoC along the gradient" method was below the dotted line, the estimated values for this method are all above. Making any conclusion based on this difference between the two methods, is hard as they are based on two different criteria. The "Shifting the gradient in the y_l direction" method is more risk averse, but when including

[1] Making MATLAB functions for the "Distance to the PoC along the gradient" method using seven "known" buses, required more memory than was available in Maple in order to compute the symbolic equations.

all seven buses in this simple illustration, the "Distance to the PoC along the gradient" method will give the exact critical value.

5.2 Four bus system

Time domain simulations have been performed on the four bus system given in Figure 4.5 using the simulation program SIMPOW. The simulations produce voltage and current values for both load buses, representing a system which the VIP++ in a real case would measure using PMUs. The PMUs in this dissertation are represented by the voltages and currents produced by the simulation. Using the measured values the VIP and both the VIP++ methods, "Distance to the PoC along the gradient" and "Shifting the gradient in the y_1 direction", estimate a distance to voltage collapse for each time step.

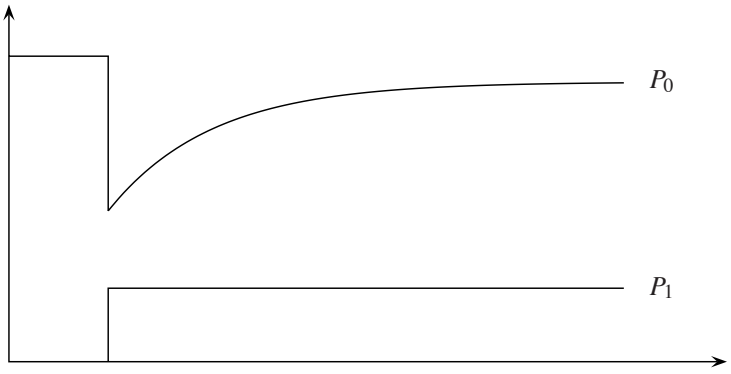

Figure 5.6: Principal figure of load, $P_{tot} = P_1 + P_0$

The generators, E_1 and E_2, are modeled as constant voltages behind reactances where governor and turbine dynamics are included in the generator model. The loads are given by the exponential recovery model described in Section 2.2.2, where the parameters α, β and the time constants are chosen based on values found in [16]. These values vary depending on the time of day and season as well as the type of load. The values used in the simulation are chosen assuming it is daytime during the winter. The system is stressed by adding a constant load, see P_1 in Figure 5.6, at load bus no. 1 and no. 2 at t=1[s], causing a voltage drop. This causes a drop in the original load P_0 followed by an immediate load pickup according to the recovery model. For the stability and robustness of the VIP the generator bus $\mathbf{E}_1$ has been chosen as reference bus. In a real system this could be done by adding a PMU in the generator area.

The apparent load power delivered to bus no. 1 and no. 2 are given in Figure 5.7. Maximum load power is reached at approximately 1000 and 850 seconds for load bus no.

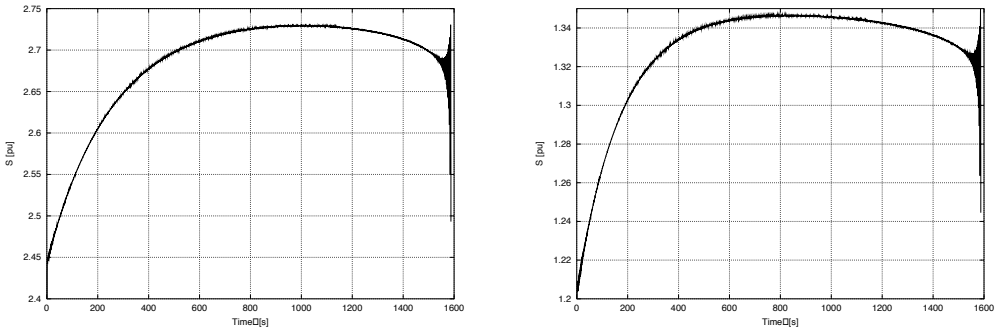

(a) Load bus no. 1

(b) Load bus no. 2

Figure 5.7: Apparent load power

1 and no. 2 respectively, see Figure 5.7(a) and 5.7(b). This shows that voltage collapse is a local problem. The next sections will focus on finding the distance to the PoC seen from load bus no. 1, doing the same on load bus no. 2 would have revealed similar results.

5.2.1 Results from VIP and VIP++ algorithms

For all the methods a combination of the least squares and cumulative sum filter methods described in Sections 3.2.2 and 3.2.4 has been used to estimate the Thevenin equivalents. Using the cumulative sum filter, an interpolated time vector can be found, which is then used to interpolate a current and voltage vector. The interpolated values for current and voltage are then filtered using a constrained least squares method to calculate the Thevenin equivalent. Values based on the measurements of voltage and currents on load bus no. 1, $\mathbf{U}_1$, $\mathbf{y}_1$ and $\mathbf{S}_1$ are plotted as dashed or dotted-dashed lines, while the calculations from the VIP and VIP++ algorithms are plotted as solid lines in Figures 5.9 through 5.13, 5.17 through 5.20 and 5.22 through 5.25.

Figure 5.8 plots the voltage at load bus U_1, with an immediate drop in voltage level with the contingency at $t = 1$ seconds. The voltage continues to decrease as the exponential recovery models start to pickup load in an attempt to reach their steady-state levels, and finally collapses at $t \approx 26$ minutes.

Estimation of $\mathbf{VIP}_1$ and $\mathbf{VIP}_2$

The VIP estimated values of impedance in the direction of the two generator buses, E_1 and E_2, are plotted in Figure 5.9. Estimated values are denoted by a tilde, while the true

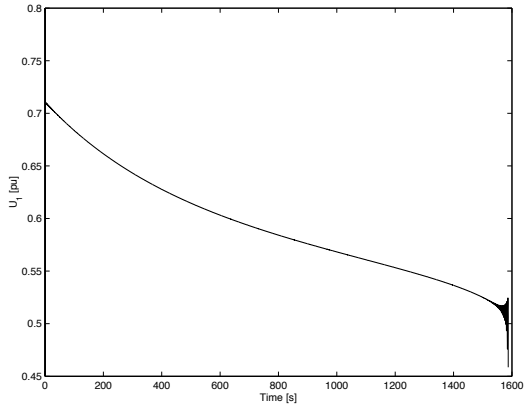

Figure 5.8: Measured voltage U_1 in per unit

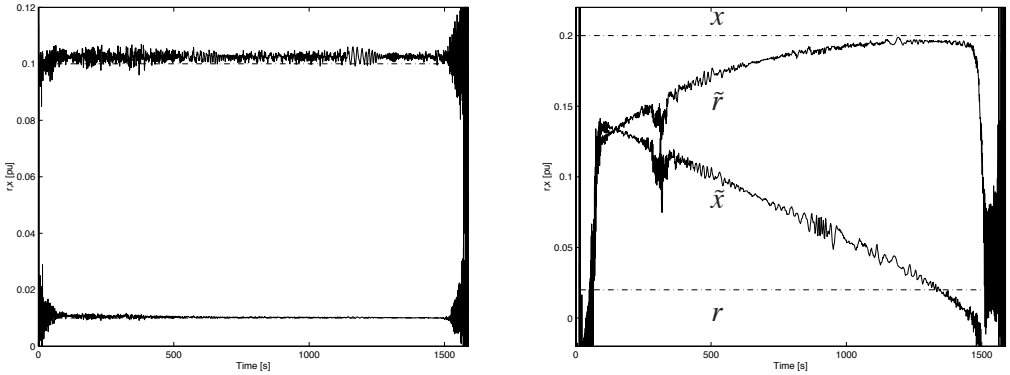

(a) Thevenin impedance in E_1 direction

(b) Thevenin impedance in E_2 direction

Figure 5.9: Results from the VIP algorithm, $n = 10$

impedance values used by the simulation program, given as

$$\begin{aligned} z_1 &= r_1 + ix_1 = 0.01 + i0.1[pu] \\ z_2 &= r_2 + ix_2 = 0.02 + i0.2[pu] \end{aligned} \tag{5.1}$$

are plotted as dotted-dashed lines. In the direction of the first generator bus, Figure 5.9(a), the estimated value of impedance is equal to the true value. This is expected as generator bus no. 1 was chosen as reference bus. Thus, the Thevenin equivalent is constant, which

is a requirement for the VIP algorithm. In Figure 5.9(b) the two estimated values for the impedance in the generator bus no. 2 direction, $\tilde{r}$ and $\tilde{x}$, deviates from the true values, which can be explained by the angle variation in the Thevenin voltage, discussed in Section 3.5. Since generator bus no. 1 has been chosen as the reference bus, and there is an angle variation between the two generator buses, the Thevenin voltage seen from bus no. 2 is not constant. The estimated values can still be used in the VIP++ algorithms as shown in the next sections.

VIP

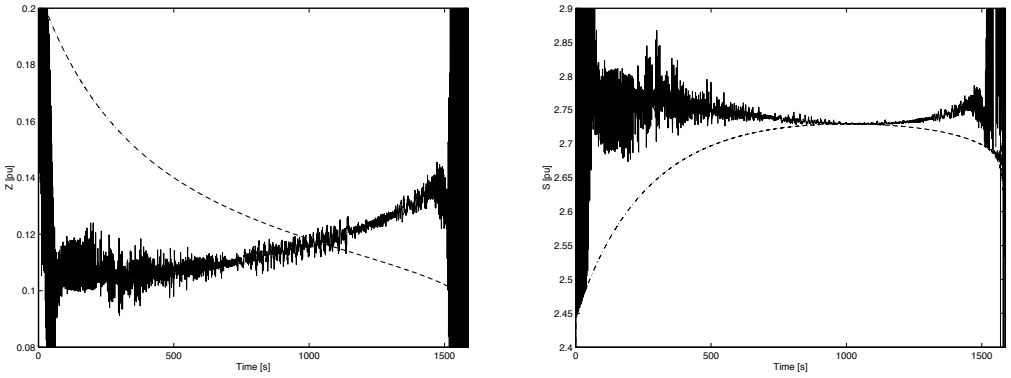

(a) Impedance

(b) Power margin S_{max}

Figure 5.10: Results from the VIP algorithm, $n = 10$

A window size of $n = 10$ has been used to calculate the Thevenin equivalent. Immediately after the voltage drop, caused by added load on both load buses, the fast dynamics of the generators causes the VIP algorithm to fail, giving large oscillations in the estimation of Thevenin equivalents. After $t \approx 1$ minute the fast dynamics of the generators are able to track their equilibrium point almost immediately. At this stage the generator voltages can be considered constant, and any changes in the system are given by the slow dynamics of the load at both load buses. The VIP algorithm is now able to track the Thevenin equivalent with some noise in the output signal, as given in Figure 5.10(a). The noise level can be reduced with a larger window size $n > 10$, as shown in Figure 5.11 where $n = 20$, but then the ability of the VIP to track changes in Thevenin equivalent is reduced.

The apparent load power delivered to load bus no. 1 is plotted as a dotted-dashed line in Figure 5.10(b), and it reaches a maximum point at $t \approx 16$ minutes. At this point the VIP algorithm correctly indicates that the system has crossed the PoC, as the estimated

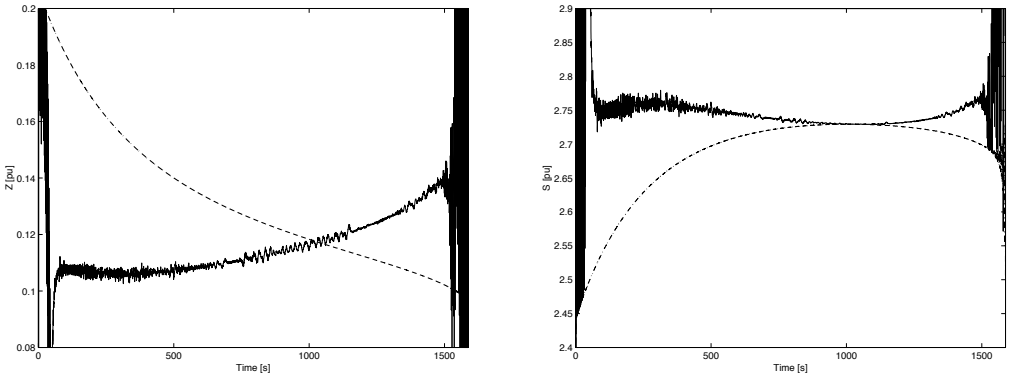

(a) Impedance

(b) Power margin S_{max}

Figure 5.11: Results from the VIP algorithm, $n = 20$

Thevenin impedance crosses the measurements load impedance, and the power margin reaches zero. After this point there is an increase in load admittance while there is a decrease in load power, thus the system is in an unstable state.

Shifting the gradient in the y_1 direction

As for the VIP algorithm in the previous section, estimation of the Thevenin equivalent uses a window size of $n = 10$. Comparison with a larger window has not been made, but would reduce the noise in estimation of Thevenin equivalents, and subsequently in the estimation of critical impedance based on the "Shifting the gradient in the y_1 direction" method. In Figure 5.12(a) the critical impedance $\tilde{z}_1$ is plotted as a solid line, along with the measured value of load impedance z_1. As for the VIP algorithm the two cross each other, as expected, at the point where the apparent load power reaches its maximum level, see Figure 5.12(b), at $t \approx 16$ minutes. The level of noise in the estimated critical value is somewhat reduced compared to the VIP algorithm, see Figure 5.10(a) and 5.12(a).

The equivalent estimated apparent load power maximum PoC_e given in Figure 5.12(b) intersects with the measured apparent load power at the PoC_r, but the distance between the two, representing the load power margin, is very large at an early stage. This indicates that it is a rather poor indicator of voltage stability problems, as warnings should be given at an early stage.

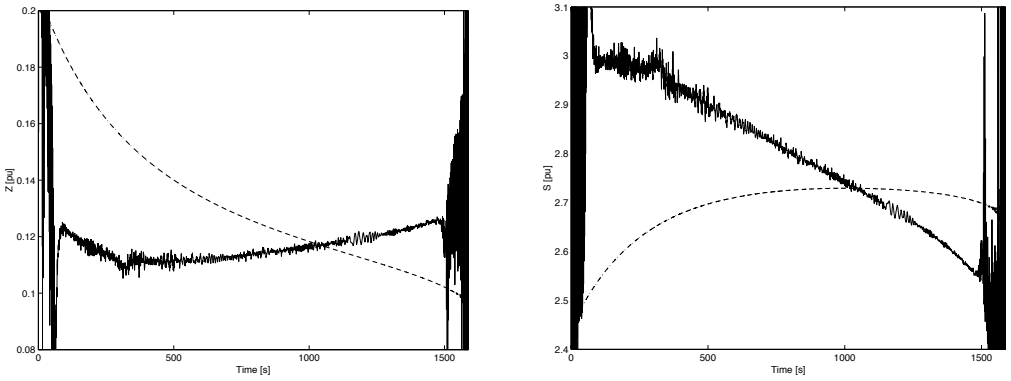

(a) Impedance (b) Power margin

Figure 5.12: Results from the VIP++ algorithm "Shifting the gradient in the y_1 direction"

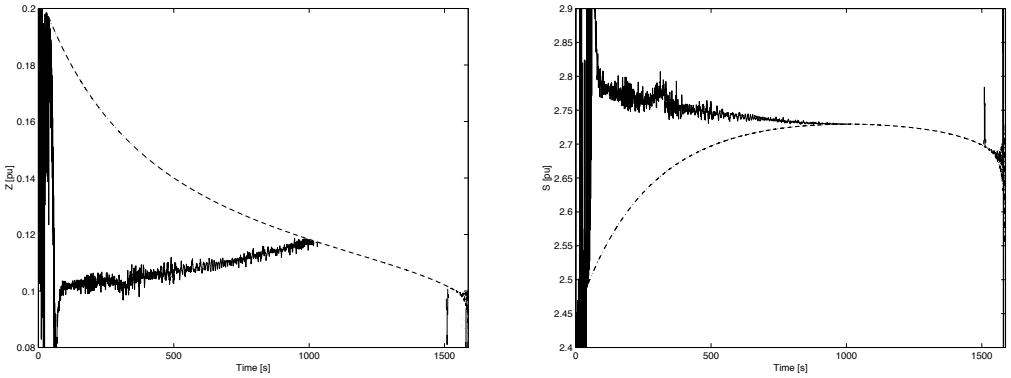

(a) Impedance (b) Power margin

Figure 5.13: Results from the VIP++ algorithm "Distance to the PoC along the gradient"

Distance to the PoC along the gradient

As for the "Shifting the gradient in the y_1 direction" method the critical impedance estimated by this method is less noisy than the one produced by the VIP, see Figure 5.13(a) and 5.10(a). It is a little lower than the "Shifting the gradient in the y_1 direction" method at an early stage, but as seen from Figure 5.13(b) the equivalent load power margin, PoC_e is closer to the final PoC_r throughout the entire simulation. It should be noted that also in

this method a window size of $n = 10$ has been used to estimate the Thevenin equivalents.

5.3 Simulations on the Norwegian grid

Using the SIMPOW program, simulations have been performed on a simplified 313 bus system of the Norwegian grid, which includes both the 420 kV and the 300 kV systems. The Swedish system shown as region 33 in Figure 5.14, has been modeled as two loads

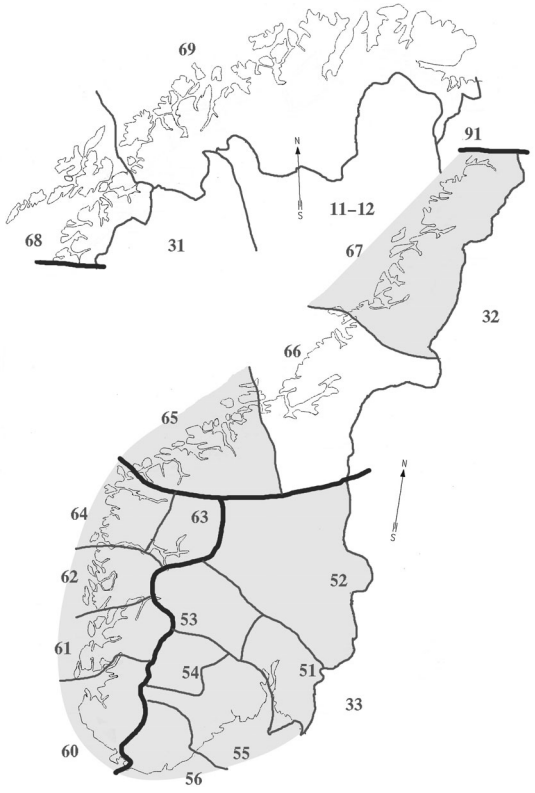

Figure 5.14: Regions in the Norwegian grid

connected at Borgvik and Halden. The Norwegian grid is divided into 16 regions where 13 have been used in the simulations, shown as the gray area in Figure 5.14. The Norwegian grid consists mainly of generation in the western part with long transmission lines to the load center in the east. Thus, the interconnection with Sweden over the "Hasle corridor" shown in Figure 5.1 is considered to be the most critical with respect to voltage stability.

5.3.1 VIP++ model

In order to protect the "Hasle corridor", both VIP and the VIP++ methods have been used to estimate the distance to the PoC seen from the 420 kV bus at Hasle. VIP estimations

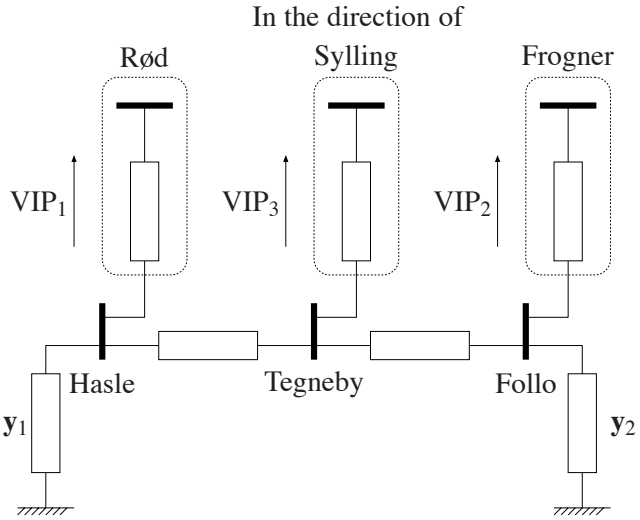

Figure 5.15: VIP++ measurements

are made in three directions, named VIP_1, VIP_2 and VIP_3, in the direction of Rød, Sylling and Frogner. However, as there is a disconnection of the line between Tveiten and Hasle after $t = 10$ seconds, the estimation of a Thevenin equivalent in Rød direction, VIP_1, is irrelevant. The system consists of two known load buses, Hasle and Follo, and although though the system has been expanded compared with the system used when describing the two methods in Chapter 4, the algorithms are still derived using Equation (4.3). See Appendices A and D for further details of the expressions used to find the critical impedances. For the stability and robustness of the VIP a bus in the western generator area has been chosen as reference bus[2]. This will eliminate the problem described in Section 3.5. In a real system this could be done by adding a PMU at this selected bus.

5.3.2 Increasing the load in Hasle

In an attempt to simulate a voltage collapse scenario over the "Hasle-corridor" the Swedish part of the model was replaced by a linearly increasing load at both Borgvik and Halden.

[2]Saurdal is chosen as the reference bus for all the simulations

The rest of the system is modeled with loads as given in Equation (5.2).

$$\begin{aligned} P &= P_0 \left[a_0 + a_1 \left(\frac{V}{V_0} \right) + a_2 \left(\frac{V}{V_0} \right)^2 \right] \\ Q &= Q_0 \left[b_0 + b_1 \left(\frac{V}{V_0} \right) + b_2 \left(\frac{V}{V_0} \right)^2 \right] \end{aligned} \tag{5.2}$$

Here the frequency is neglected, and the load is given by a constant power, current and impedance part. In the simulation the coefficients were given by $a_0 = b_0 = 0$ %, $a_1 = b_1 = 60$ % and $a_2 = b_2 = 40$ %. The system is further stressed by tripping of the line between Hasle and Tveiten at $t = 10$ seconds. This is a subsea transmission line giving reactive support to the Oslo region. A winter load scenario has been used, where the total

Table 5.1: Winter load state 2005

Area	Production		Load absorbed	
	MW	MVAr	MW	MVAr
33	0	0	1489	-84
51	473	1572	4462	1323
52	876	344	1013	208
53	3145	921	209	829
54	2027	350	52	283
55	1013	705	2225	218
56	910	776	1941	574
60	4142	936	1084	968
61	1414	451	1223	583
62	1048	556	1370	413
63	1128	209	769	340
65	1765	809	2580	422
67	3386	729	2668	456
Total	21327	9357	21327	9357

generation and load absorbed for all the regions are given in Table 5.1.

Figure 5.16 plots the voltage at Hasle, with an immediate drop in voltage level with the contingency at $t = 10$ seconds. The voltage continued to decrease as the load increases at both Borgvik and Halden. The simulation was stopped after the system "fell apart" due to angular instability at about $t \approx 43$ minutes.

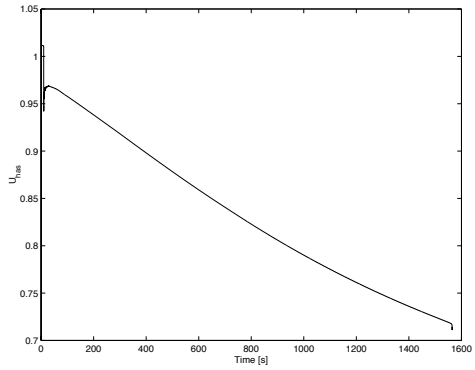

Figure 5.16: Voltage at Hasle

Estimation of VIP_2 and VIP_3

For the VIP++ methods, "Distance to the PoC along the gradient" and "Shifting the gradient in the y_1 direction", estimation of Thevenin equivalents in the direction of both Frogner and Sylling, marked VIP_2 and VIP_3 in Figure 5.15 is needed. It should be noted that the VIP algorithm used here is a simple implementation of the one described in [31]. As seen

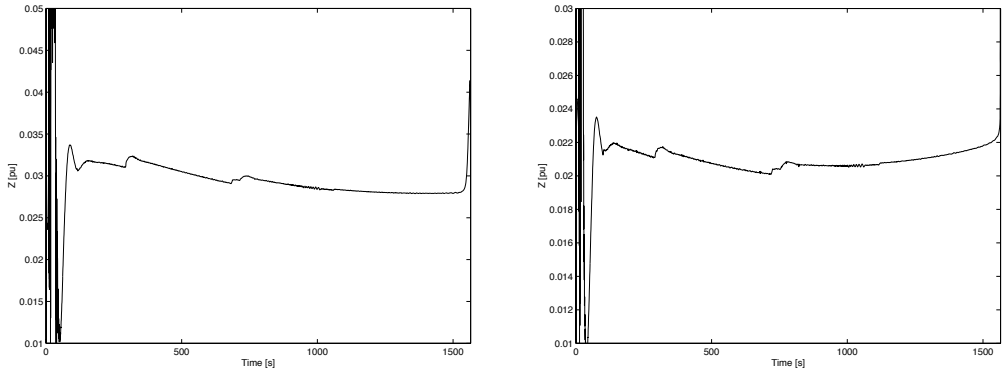

(a) In the direction of Frogner

(b) In the direction of Sylling

Figure 5.17: Thevenin impedance

in Figure 5.17 the VIP algorithm has some problems estimating the Thevenin equivalents in both directions immediately after the line tripping. The VIP estimates a relatively constant value with an increase in the end for the estimation in both directions, Sylling and Frogner. There are some small irregularities which also can be seen in the VIP++ estima-

tion, as it is based on these two Thevenin equivalents.

Shifting the gradient in the y_1 direction

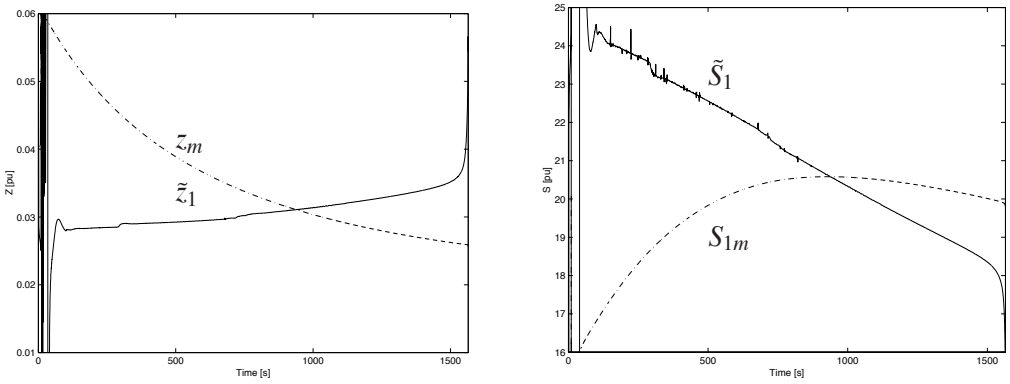

(a) Critical and measured load impedance, $\tilde{z}_1$ and z_{1m}

(b) Power margin

Figure 5.18: Results from the VIP++ algorithm "Shifting the gradient in the y_1 direction"

The oscillations right after the loss of transmission line between Hasle and Tveiten is due to failure of the VIP algorithm to estimate when there are changes in the Thevenin equivalent given by the fast dynamics of the generators. The VIP++ algorithm "Shifting the gradient in the y_1 direction" tracks the system's trajectory towards the PoC, and crosses it at the point where the system load at Hasle is at its maximum level, as expected. This can be seen in both Figures 5.18(a) and 5.18(b) for the critical impedance and the equivalent apparent load power margin respectively.

Distance to the PoC along the gradient

Also this method experiences some oscillation after the loss of the transmission line, for the same reasons as for the "Shifting the gradient in the y_1 direction" method. The two methods are very close both in critical impedance and the equivalent critical apparent load power, though the critical impedance is a little lower at an early stage, with a shaper increase prior to crossing the PoC. At the same time the equivalent apparent load power is closer than the "Shifting the gradient in the y_1 direction" method to the final PoC level throughout the simulation.

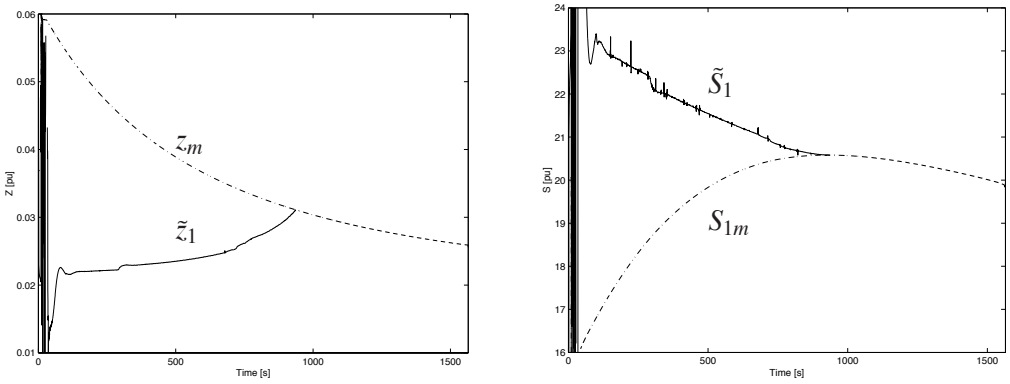

(a) Critical and measured load impedance, $\tilde{z}_1$ and z_{1m}

(b) Power margin

Figure 5.19: Results from the VIP++ algorithm "Distance to the PoC along the gradient"

VIP

In this simulation the estimated Thevenin impedance never crosses the load impedance, as shown in Figure 5.20, indicating that the system never passes the PoC. Looking at the real

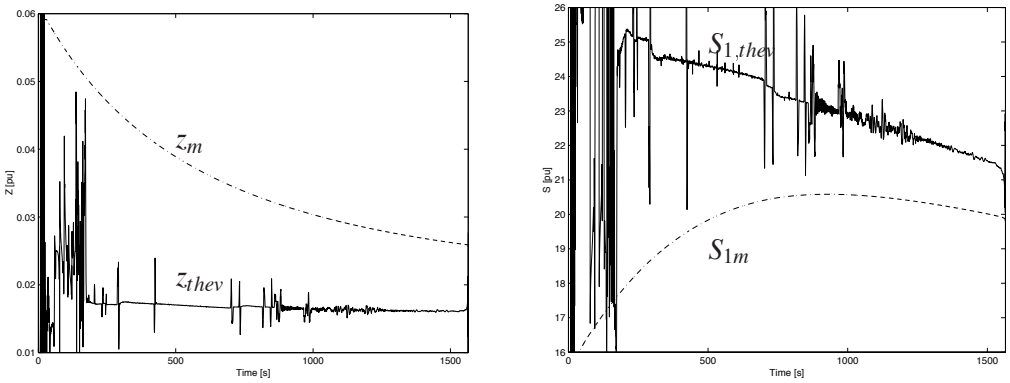

(a) Measured load impedance and Thevenin impedance calculated by VIP

(b) Power margin

Figure 5.20: Results from the VIP algorithm

load power in Figure 5.20(b) it reaches a maximum loading point so that both apparent load

and load impedance after this point is decreasing. According to the definition for voltage stability used to derive the VIP++ methods, the system should then be in an unstable state. The VIP method fails to detect this unstable state in this case.

5.3.3 Contingency using an extra stressed system

In order to provoke a voltage collapse scenario over the Hasle corridor the general load levels of both active and reactive loads, given in Table 5.1, have been increased by 8 %. The

Table 5.2: Winter load state 2005

Area	Production		Load absorbed	
	MW	MVAr	MW	MVAr
33	0	0	1802	-75
51	516	1364	4787	1426
52	954	451	1084	231
53	3418	1373	228	977
54	2102	566	58	328
55	1103	1001	2382	256
56	985	788	2080	613
60	4511	1234	1163	1111
61	1540	510	1311	655
62	1141	608	1467	458
63	1228	238	823	363
65	1922	983	2761	452
67	3687	902	2855	488
Total	23107	10978	23107	10978

new load is given in Table 5.2. The system is further stressed by the removal of all reactive shunt support in the main load center and tripping of the line between Hasle and Tveiten at $t = 10$ seconds. The tripping causes a drop in the original load R_0 followed by a load pickup according to the exponential recovery model for the loads in the Oslo region and on the Hasle corridor. The reactive loads in Halden and Borgvik are given by Equations (2.11) and (2.13) with Q_r set to zero. Since the voltage levels will decrease after the contingency, due to load response, this will result in a further reactive load reduction. This means that the resulting reactive support from Sweden is reduced during the simulation.

Also for this case there is a drop in voltage, see Figure 5.21, due to the contingency at $t = 10$ seconds, but now it is the exponential recovery of loads that further decreases the

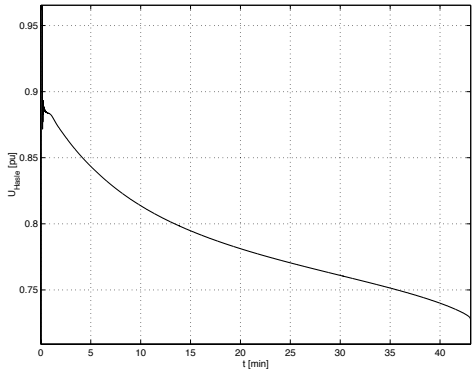

Figure 5.21: Voltage in per unit measured at Hasle

voltage. Note that the time is given in minutes as opposed to seconds, which was the case in the previous section. The simulation was stopped after the system "fell apart" due to angular instability at about $t \approx 43$ minutes.

Estimation of VIP_2 and VIP_3

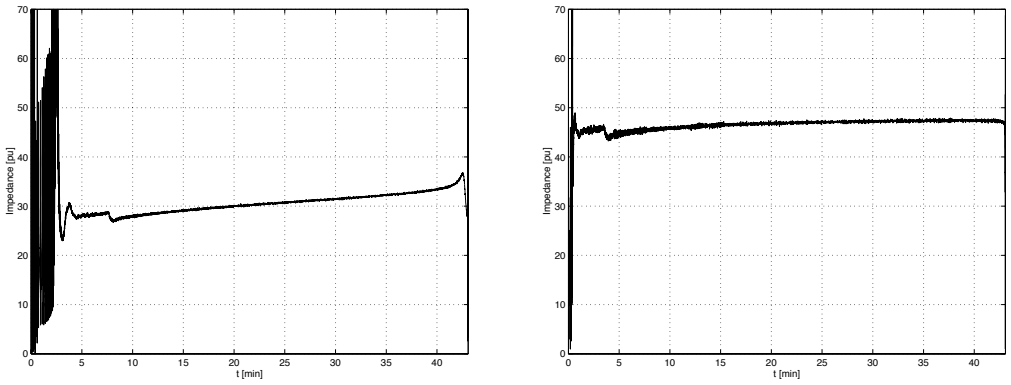

(a) In the direction of Frogner

(b) In the direction of Sylling

Figure 5.22: Thevenin impedances

As seen in Figure 5.22(a) the VIP algorithm has some problems estimating the Thevenin impedances in the Frogner direction for approximately the first 140 seconds after the line

tripped. The estimation of the Thevenin equivalent in the Sylling direction is shown in Figure 5.22(b), experiences similar problems after the contingency, but for a shorter period. These problems can be traced to changes in the Thevenin equivalents due to angular oscillations in the generator areas and changes in load. As the estimation of Thevenin equivalents by the VIP algorithm expect these to be constant, the algorithm fails. The reason why VIP_3 has less problems than VIP_2 is not easily explained as the "true" Thevenin equivalent is hard to obtain for a nonlinear system, but one reason might be that Frogner is in a heavy load area.

Shifting the gradient in the y_1 direction

As for the estimation of VIP presented in the previous section there are some noise in the output signal until $t \approx 150$ seconds, which is expected as the method is based on the estimations of Thevenin equivalents above. Comparing Figures 5.24(a) and 5.23(a) we

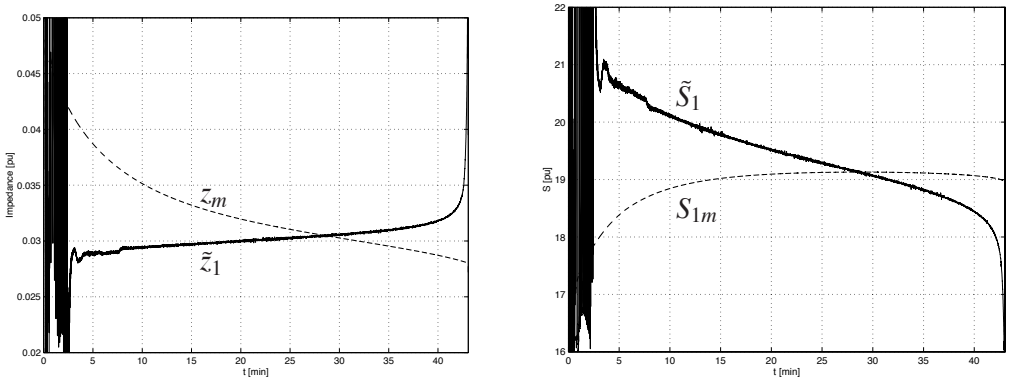

(a) Critical and measured load impedance, $\tilde{z}_1$ and z_{1m}

(b) Power margin

Figure 5.23: Results from the VIP++ algorithm "Shifting the gradient in the y_1 direction"

observe that $\tilde{z}_1$ in Figure 5.23(a) already after $t \approx 5$ minutes comes closer to the value of $z_m \approx 0.03pu$ at the true PoC_r than $\tilde{z}_1$ in Figure 5.24(a). Comparing the critical apparent load power for the two methods the opposite result is shown, "Distance to the PoC along the gradient" being closer to the maximum value $S_1 \approx 19.2pu$ at the PoC_r. They both cross the measured value of load power at the same point at $t \approx 29$ minutes.

Distance to the PoC along the gradient

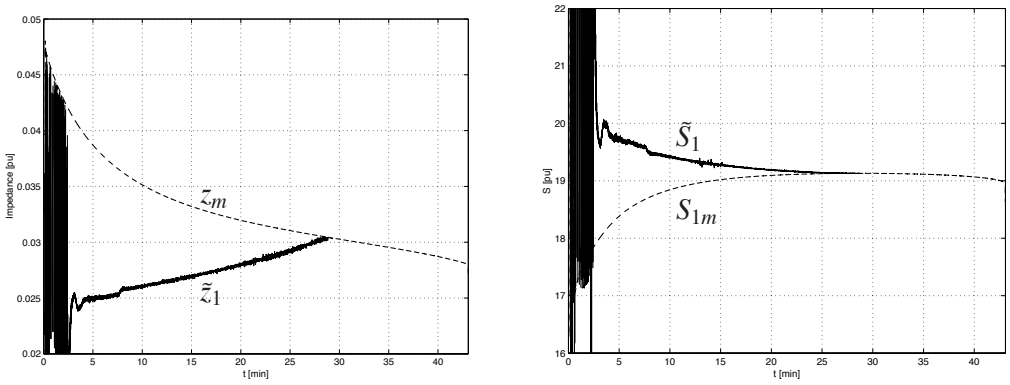

(a) Critical and measured load impedance, $\tilde{z}_1$ and z_{1m}

(b) Power margin

Figure 5.24: Results from the VIP++ algorithm "Distance to the PoC along the gradient"

As with the "Shifting the gradient in the y_1 direction" method, the "Distance to the PoC along the gradient" method also has the same trouble in estimating a critical admittance before $t \approx 150$ seconds, caused by the same reasons. As the voltage drops and the load increases at Hasle the estimated value of a critical load impedance in Figure 5.24(a), $\tilde{z}$, increases slightly until it reaches the measured load impedance, z_m, after $t \approx 29$ minutes. At this point the apparent load power at Hasle shown in Figure 5.24(b) reaches its maximum level, and there is a crossing of the estimated critical apparent load power and measured load power at this point. Since there is increasing load admittance and decreasing load the method, according to the voltage stability definition in [9], correctly indicates a point of collapse.

VIP

For comparison the result from estimating a Thevenin equivalent seen from Hasle using the simple VIP algorithm is shown in Figure 5.25(a), where the Thevenin impedance and the measured load impedance at Hasle are plotted. The simple VIP algorithm results in a more noisy signal than the VIP++ algorithms. The noise is amplified even more when calculating a power margin, based on a constant power factor[3] $\tan\phi$, as shown in Fig-

[3] $\tan\phi = Q/P$

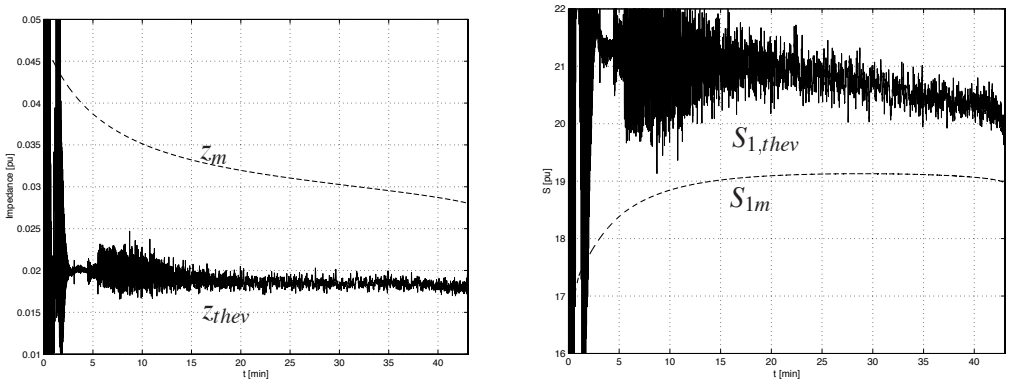

(a) Measured load impedance and Thevenin impedance calculated by VIP

(b) Power margin

Figure 5.25: Results from the VIP algorithm

ure 5.25(b).

A more serious result is the fact that the simple VIP algorithm fails to detect a collapse in this simulation, while the VIP++ methods ”Distance to the PoC along the gradient” and “Shifting the gradient in the y_1 direction” do so, corresponding to the observed voltage reduction in Figure 5.21.

As can be seen from the simulations, the VIP++ method must be considered a long-term voltage instability indicator. The VIP algorithm used is unable to estimate a Thevenin equivalent based on the transients after a contingency such as a line outage, and subsequently the VIP++ methods also fail to estimate a critical value.

Chapter 6

Discussion and Conclusions

A brief discussion of some of the aspects of voltage collapse protection schemes in a highly loaded system is given in this chapter. The chapter includes the main conclusions which can be drawn from this work and some recommendations for further work.

6.1 Objectives

There has been a pressure to operate power systems closer to their security limits. This has partially been the result of the financial consequences following de-regulation and re-regulation of the electricity sector, which started in Norway in 1991. Network companies in Norway are still monopolies and under monopoly control with an income cap regulation set by the regulatory authorities. Another important factor is the increased public and political focus on environmental issues, working against almost any expansion plans. Improved system control and protection, including "smart" power electronic components has also allowed systems to be operated in regions closer to the limit than ever before.

In this situation it is essential to monitor the system and have tools that can predict the distance to the point of collapse (PoC) or predict whether the system will collapse. In such a protection scheme the phasor measurement unit (PMU) is of great importance, as it provides a method for quickly estimation of the system state. When using the measured values for voltage and currents the estimation is faced with a set of linear equations, which can easily be solved. The established methods of using values from SCADA require that nonlinear load flow equations must be solved. This is computationally time consuming, and less suitable for a protection scheme that future systems require.

Much effort has been put into research of the phenomenon *voltage collapse*, and many approaches have been explored. Both dynamic and steady-state behavior have been studied thoroughly, though very few protection and control schemes have been implemented. The majority of methods proposed are based on load flow equations of a full-scale system.

Using PMUs together with sufficient communication systems such an approach is possible for online purposes, though in this dissertation the possibilities of an index based on local area measurements have been explored. Voltage stability can be classified as either a transient or a long-term stability problem, and the index proposed here is based on long-term dynamics. The intention is either to communicate a warning to a system operator, or to automatically counteract a voltage collapse by predetermined actions, when threshold values are violated.

6.2 VIP

The idea of the simple VIP algorithm has been presented in several papers [18, 29–32]. This is a method that uses the maximum loadability of a transmission network as the point of collapse. By estimating a Thevenin impedance and comparing this to the measured load impedance at the bus, the method can track distance to the PoC as this occurs when the two impedances are equal in absolute value.

The VIP algorithm uses a PMU to measure voltage and current, as it requires the real and imaginary parts of both. The problem of the VIP algorithm is that it is based on a system with two equations and four unknowns, thus it is not observable. In order to make it observable the assumption of constant Thevenin equivalent between two set of measurements is made. For the method to be able to perform the estimation, changes have to occur in the voltage and current between two sets of measurements. These changes can be caused by either changes in Thevenin equivalent or in the load impedance. In order to achieve a valid estimation, the changes in load impedance have to be significantly larger than the changes in the Thevenin equivalent. It is shown that when this is not the case the method will estimate a Thevenin impedance of the same size as the measured load impedance, but with a negative sign.

Changes in the Thevenin equivalent can be traced to both angle variation in a remote generator area or to variations in load impedances on nearby buses. One might also include changes such as removal of lines and shunt elements, but these are more or less instantaneous changes which must be handled by the algorithm. The problem of angle variations can be mitigated by the selection of an appropriate reference bus, which can be done by the placement of a second PMU. In order to solve the problem of variations in load on nearby buses, smart filters such as the proposed “Cumulative sum filter” can be used. The “Cumulative sum filter” interpolates the measured data so that the problem of zero current difference between two sets of measurements is removed. The VIP algorithm might also be improved by including more measurements to account for the non-observability. In this dissertation such an approach is explored and is given the acronym VIP++ . The VIP++ method includes additional measurements from the surrounding load buses.

6.3 VIP++

The distance to the PoC does not only depend on the present state of the system but also on future changes. Therefore, an algorithm that tries to track the system trajectory is based on an assumption or hypothesis about how the system will move. Two such hypotheses, called "Distance to the PoC along the gradient" and "Shifting the gradient in the y_1 direction", have been explored in this dissertation. Two additional methods named "Distance to the PoC when the system is assumed constant" and "known load dynamics" are proposed, but it has been shown that the first method fails to identify the true PoC_r, while the second has been considered too extensive for further exploration in the context of the present work.

"Distance to the PoC along the gradient" assumes that loads $\mathbf{y}_1$ and $\mathbf{y}_2$ increase according to a constant gradient. "Shifting the gradient in the y_1 direction" estimates the sudden load increase at bus no. 1 that would immediately bring the system to the PoC at each time step. When the system is far from the PoC the VIP++ method gives an approximate distance to the PoC and indicates that the distance is quite large. As the system trajectory moves closer to the actual PoC the method will become more accurate, and it will be more or less exact at the PoC_r. This is true for both alternatives as verified by the time domain simulations described in the dissertation. It is observed that "Distance to the PoC along the gradient" seems to be more stable when there are oscillations in the load admittances and therefore tends to be more robust.

"Distance to the PoC along the gradient" and "Shifting the gradient in the y_1 direction" can be extended to include more "known" load buses. This extension results in a few more equations to be solved, but that can be handled quite easily. On the other hand, the improvement in robustness and accuracy in the estimation of the PoC by including more measurements is not quite clear. A few tests have shown that the benefit may be marginal, but more thorough investigations are needed. One should also keep in mind that the basic idea is to estimate the PoC based on local measurements, and including too many buses brings us away from this idea.

The VIP as well as the VIP++ algorithm depends on measurements of voltage and current, and as both angle- and absolute values are required, a PMU has been used. For stability and robustness of the VIP algorithm an extra PMU unit can be placed in a remote generator area in order to provide an estimate of the Thevenin voltage angle. The VIP++ method requires additional PMU units placed at nearby buses where additional load admittances are measured. For the Norwegian grid presented here, suitable locations for PMUs would be at Hasle, Follo and Aurland.

The VIP++ method has been tested with promising results on a simple four bus system and on a simplified 313 bus model of the Norwegian grid. As measurements from a real system have not been available, simulations have been performed, including both generator dynamics and load dynamics according to the exponential load recovery model. The results from the simulations have been used as input to the VIP++ algorithms, and it has

been demonstrated that VIP++ is able to track voltage collapse scenarios. Three scenarios have been tested:

1. A sudden load increase on the four bus system.

2. A steady increase in the transmission of load towards Sweden, with a tripping of a "critical" transmission line in the Norwegian grid.

3. Tripping of a "critical" transmission line on a highly stressed Norwegian system, using exponential load recovery models.

6.4 Further work

Currently a field test of the VIP algorithm is being conducted in the Norwegian grid, where a PMU together with a VIP is placed on the 420 kV bus in Hasle, measuring voltage on the bus and the currents going to Borgvik and Halden. The field tests are being conducted in a collaboration between ABB, Statnett and Sintef Energy Research. As a voltage collapse scenario is unlikely to happen in the Norwegian grid, the measurements and estimations of Thevenin equivalents are only being tested in a stable mode, far away from the PoC. Simulations will be performed based on the field test measurements, pushing the system towards the PoC, in order to test the ability of the VIP ability to predict a voltage collapse

In this dissertation the studies of the VIP++ method is only based on simulated cases, with more or less simplified systems. The methods presented should be verified by real system measurements, and by adding PMUs on more buses in the current field test this could be accomplished. A second PMU has been placed in Sima for angular stability studies, but this could not be used by the VIP++ method other than choosing a suitable reference bus. Placing a third PMU in Follo would be sufficient for the VIP++ method to do the estimation.

A fourth method was proposed in the dissertation. This method is based on the assumption that the measured load impedance dynamics are known, or can be predicted. Using a load model as the exponential recovery load, a generic model or a specific dynamic load model, this approach should be explored. If it is possible for the given load model to find an expression for the derivatives based on the measured values, each specific load model would create its own equation like the polynomial presented in this dissertation. More than likely they will not be polynomials, but nonlinear equations which must be solved numerically.

An important issue that remains to be investigated is the criterion for operation of the relay. What is the critical distance to the PoC measured either in terms of "impedance distance" between the load impedance and the estimated VIP++ curve or in terms of "loading distance" between the load and the estimated PoC_e curve? This issue is not addressed here.

Instead, the present work has concentrated on demonstrating a method to generate trajectories based on local measurements that provide useful information about the vulnerability to voltage collapse, and which give the basic information for such a relay.

References

[1] Task Force 38.02.10. Modelling of voltage collapse including dynamic phenomena. Final draft, CIGRE, December 1992.

[2] Task Force 38.02.12. Criteria and countermeasures for voltage collapse. Final draft, CIGRE, December 1994.

[3] V. Ajjarapu and C Christy. The continuation power flow: A tool for steady state voltage stability analysis. *IEEE Trans. Power Systems*, 7(1):416–423, February 1992.

[4] F. L. Alvarado, I. Dobson, and Y. Hu. Computation of closest bifurcations in power systems. *IEEE Trans. Power Systems*, 9(2):918–928, May 1994.

[5] C. A. Cañizares and F. L. Alvarado. Point of collapse and continuation methods for large ac/dc systems. *IEEE Trans. Power Systems*, 8(1):1–8, February 1993.

[6] North American Electric Reliablity Council. Survey of the voltage collapse phenomenon. Technical report, August 1991.

[7] Thierry Van Cutsem. Voltage instability: Phenomena, countermeasures, and analysis methods. *Proceedings of the IEEE*, 88(2):208–227, February 2000.

[8] A. G. Phadke et al. Synchronized sampling and phasor measurements for relaying and control. *IEEE Transactions on Power Delivery*, 9(1):442–452, January 1994.

[9] Charles Concordia et al. *Voltage Stability of Power systems: Concepts, Analytical Tools, and Industry Experience*. IEEE Publication 90TH0358-2-PWR, 1990.

[10] K. Ohtsuka et al. An equivalent of multi-machine power systems and its identification for on-line application to decentralized stabilizers. *IEEE Transactions on Power Systems*, 4(2):687–693, May 1989.

[11] J. Douglas Faires and Richard L. Burden. *Numerical Methods*. PWS Publishing Company, 1993.

[12] A. E. Fitzgerald, Charles Kingsley, Jr., and Stephen D. Umans. *Electric machinery*. McGraw-Hill, Inc., 1992.

[13] Giuseppe Fusco, Arturo Losi, and Mario Russo. Constrained least squares method for parameter tracking of power system steady-state equivalent circuits. *IEEE Transactions on Power Delivery*, 15(3):1073–1080, July 2000.

[14] B. Gao, G. K. Morrison, and P. Kundur. Voltage stability evaluation using modal analysis. *IEEE Trans. Power Systems*, 7(4):1529–1542, November 1992.

[15] David J. Hill. Nonlinear dynamic load models with recovery for voltage stability studies. *IEEE Transactions on Power Systems*, 8(1):166–176, February 1993.

[16] David J. Hill and Daniel Karlsson. Modelling and identification of nonlinear dynamic loads in power systems. *IEEE Transactions on Power Systems*, 9(1):157–166, February 1994.

[17] Arne T. Holen and Leif Warland. Spenningsstabilitet fra dynamisk synsvinkel. Technical report, Sintef Energy Research, Sem Sælandsvei 11, 7465 Trondheim, October 1999.

[18] D.E. Julian, R.P. Schulz, K.T. Vu, W.H. Quaintance, N.B. Matt, and D. Novosel. Quantifying proximity to voltage collapse using the voltage instability predictor (vip). In *Power Engineering Society Summer Meeting, 2000. IEEE*, volume 2, pages 931–936, 2000.

[19] P. Kessel and H. Glavitsch. Estimating the voltage stability of a power system. *IEEE Transactions on Power Delivery*, PWRD-1(3):346–354, July 1986.

[20] Erwin Kreyszig. *Advanced Engineering Mathematics*. John Wiley & Sons, Inc., 7 edition, 1993.

[21] Phraba Kundur. *Power System Stability and Control*. McGraw-Hill, Inc., 1994.

[22] L. Loud, P. Rousseaux, D. Lefebvre, and T. Van Cutsem. A time-scale decomposition-based simulation tool for voltage stability analysis. *IEEE Porto PowerTech*, September 2001.

[23] N. D. Hatziargyriou and T. Van Cutsem, editors. Indices predicting voltage collapse including dynamic phenomena. Technical Report TF 38-02-11, CIGRE, 1994.

[24] A. G. Phadke. Synchronized phasor measurements in power systems. *IEEE Computer Applications in Power*, 6(2):10–15, April 1993.

[25] Sami Repo. *On-line Voltage Stability Assessment of Power System - An approach of Black-box Modelling*. Doctoral dissertation, Tampere University of Technology, 2001.

[26] Kjetil Boyzen Rostoft. Voltage instability predictor: tools and test methods. Master's thesis, Norwegian University of Science and Technology, December 2000.

[27] S. Sechu and M.B. Reed. *Linear Graphs and Electrical Networks*. Addison – Wesley, 1961.

[28] Carson W. Taylor. *Power System Voltage Stability*. The EPRI Power System Engineering Series. McGraw-Hill, Inc., 1994.

[29] K. Vu, M.M. Begovic, and D. Novosel. Grids get smart protection and control. *IEEE Computer Applications in Power*, 10(4):40–44, Oct. 1997.

[30] K. Vu, M.M. Begovic, D. Novosel, and M.M. Saha. Use of local measurements to estimate voltage-stability margin. *Power Industry Computer Applications*, pages 318–323, 1997.

[31] K. Vu, M.M. Begovic, D. Novosel, and M.M. Saha. Use of local measurements to estimate voltage-stability margin. *IEEE Transactions on Power Systems*, 14(3):1029–1034, August 1999.

[32] Khoi Vu, Danny Julian, Jan Ove Gjerde, Navin Bhatt, Beverly Laios, and Richard Schulz. Voltage instability predictor (vip) and its applications. In *PSCC 1999 - 13th Power Systems Computation Conference*, volume 1, pages 308–313, June 1999.

[33] Khoi T. Vu and Chen-Ching Liu. Analysis of tap-changer dynamics and construction of voltage stability regions. *IEEE. Transactions on Circuits and Systems*, 36(4):575–590, April 1989.

[34] Khoi T. Vu and Chen-Ching Liu. Dynamic mechanisms of voltage collapse. *Systems & Control Letters*, 15(4):329–338, November 1990.

[35] Khoi T. Vu and Chen-Ching Liu. Shrinking stability regions and voltage collapse in power systems. *IEEE Transactions on Circuits and Systems I: Fundamental Theory and Applications*, 39(4):271–289, April 1992.

[36] K. Walve. Modelling of power system components at severe disturbances. In *Proceedings of the 31st Session. Paris, France*, volume 2. CIGRE. Paris, France, August/September 1986.

[37] Geir Warland. *Flexible transfer limits in an open power market. Congestion versus risk of interruption.* Doctoral dissertation, Norwegian University of Science and Technology, 1999.

[38] Leif Warland. Dynamic aspects of voltage collapse. Master's thesis, Norwegian University of Science and Technology, February 1997.

[39] Leif Warland and Arne T. Holen. A voltage instability predictor using local area measurements (VIP++). *IEEE Porto PowerTech*, 2:123–128, September 2001.

[40] Leif Warland and Arne T. Holen. Estimation of distance to voltage collapse: Testing an algorithm based on local measurements. *Submitted to: PSCC 14th Power Systems Computation Conference*, June 2002.

[41] W. Xu, Y. Mansour, and P.G Harington. Planning methodologies for voltage stability limited power systems. *International Journal on Electric Power & Energy Systems*, 15(4):221–228, 1993.

Appendix A

VIP++

This appendix presents the calculation of the parameters used by the methods "Distance to the PoC along the gradient" and "Shifting the gradient in the y_1 direction" for the case of two known load buses. There is also a presentation of the general case with n *known buses. For the "Distance to the PoC along the gradient" method the size of the polynomial is calculated, while for the "Shifting the gradient in the y_1 direction" method the general expression for the cubic equation is found.*

A.1 Maximum loading point

Using the system in Figure 4.5 the apparent power delivered to bus no. 1 can found as.

$$S_1 = |\mathbf{U}_1|^2|\mathbf{y}_1| = \frac{|\mathbf{a}_1 + \mathbf{a}_2\mathbf{y}_2|^2}{|\mathbf{y}_1\mathbf{y}_2 + \mathbf{b}_1\mathbf{y_1} + \mathbf{b}_2\mathbf{y}_2 + \mathbf{b}_3|^2}|\mathbf{y}_1| = \frac{|\mathbf{N}(\mathbf{y_2})|^2}{|\mathbf{D}(\mathbf{y1},\mathbf{y2})|^2}|\mathbf{y_1}| \tag{A.1}$$

where

$$\begin{aligned}
\mathbf{a}_1 &= (\mathbf{z_2^{-1}} + \mathbf{y_{12}})\mathbf{E_1}\mathbf{z_1^{-1}} + \mathbf{y_{12}}\mathbf{E_2}\mathbf{z_2^{-1}} \\
\mathbf{a}_2 &= \mathbf{E_1}\mathbf{z_1^{-1}} \\
\mathbf{b}_1 &= \mathbf{z_2^{-1}} + \mathbf{y_{12}} \\
\mathbf{b}_2 &= \mathbf{z_1^{-1}} + \mathbf{y_{12}} \\
\mathbf{b}_3 &= \mathbf{z_1^{-1}}\mathbf{z_2^{-1}} + \mathbf{y_{12}}(\mathbf{z_1^{-1}} + \mathbf{z_2^{-1}})
\end{aligned} \tag{A.2}$$

As the two next sections are based on Equation (A.1), any system which satisfies this equation will be able to use the results presented. The maximum loading point is given by

setting the time derivative of load to zero.

$$\frac{dS_1}{dt} = 0 \tag{A.3}$$

A.2 Distance to the PoC along the gradient

Assuming that both loads move along the gradient,

$$\begin{aligned}\tilde{\mathbf{y}}_\mathbf{1}(\tau) &= \mathbf{y}_{1m} + \mathbf{y}_{1dm}\tau = g_{1m} + g_{1dm}\tau + i(b_{1m} + b_{1dm}\tau) \\ \tilde{\mathbf{y}}_\mathbf{2}(\tau) &= \mathbf{y}_{2m} + \mathbf{y}_{2dm}\tau = g_{2m} + g_{2dm}\tau + i(b_{2m} + b_{2dm}\tau)\end{aligned} \tag{A.4}$$

Where $\mathbf{y}_{jm}$ and $\mathbf{y}_{jdm}$ is the measured and derivative value of the load admittance at bus j respectively. The numerator in Equation (A.1) is given by

$$\begin{aligned}|\mathbf{N}(\mathbf{y_2})|^2 &= \mathbf{N}(\mathbf{y_2})\mathbf{N}(\mathbf{y_2})^* = (\mathbf{a_1} + \mathbf{a_2 y_{2m}} + \mathbf{a_2 y_{2dm}}\tau)(\mathbf{a_1} + \mathbf{a_2 y_{2m}} + \mathbf{a_2 y_{2dm}}\tau)^* \\ &= c_0 + c_1\tau + c_2\tau^2\end{aligned} \tag{A.5}$$

where

$$\begin{aligned}c_0 &= |\mathbf{a}_1 + \mathbf{a}_2\mathbf{y}_{2m}|^2 \\ c_1 &= 2Re\{(\mathbf{a}_1 + \mathbf{a}_2\mathbf{y}_{2m})(\mathbf{a}_2\mathbf{y}_{2dm})^*\} \\ c_2 &= |\mathbf{a_2 y}_{2dm}|^2\end{aligned}$$

The absolute value of the load admittance $\tilde{\mathbf{y}}_1$ is given by

$$\begin{aligned}|\tilde{\mathbf{y}}_\mathbf{1}| &= \sqrt{\tilde{\mathbf{y}}_\mathbf{1}\tilde{\mathbf{y}}_\mathbf{1}^*} = \sqrt{(\mathbf{y_{1m}} + \mathbf{y_{1dm}}\tau)(\mathbf{y_{1m}} + \mathbf{y_{1dm}}\tau)^*} \\ &= \sqrt{d_0 + d_1\tau + d_2\tau^2}\end{aligned} \tag{A.6}$$

where

$$\begin{aligned}d_0 &= y_{1m}^2 = |\mathbf{y}_{1m}|^2 \\ d_1 &= 2Re\{\mathbf{y_{1m}}\mathbf{y_{1dm}}^*\} \\ d_2 &= y_{1dm}^2 = |\mathbf{y}_{1dm}|^2\end{aligned}$$

The denominator is given by.

$$\begin{aligned}|\mathbf{D}(\mathbf{y_1}, \mathbf{y_2})|^2 &= (\mathbf{D}(\mathbf{y_1}, \mathbf{y_2}))(\mathbf{D}(\mathbf{y_1}, \mathbf{y_2}))^* \\ &= e_0 + e_1\tau + e_2\tau^2 + e_3\tau^3 + e_4\tau^4\end{aligned} \tag{A.7}$$

where

$$
\begin{aligned}
e_0 &= |\mathbf{y_{1m}y_{2m}} + \mathbf{b_1y_{1m}} + \mathbf{b_2y_{2m}} + \mathbf{b_3}|^2 \\
e_1 &= 2Re\{(\mathbf{y_{1m}y_{2dm}} + \mathbf{y_{2m}y_{1dm}} + \mathbf{b_1y_{1dm}} + \mathbf{b_2y_{2dm}})^* \\
&\quad (\mathbf{y_{1m}y_{2m}} + \mathbf{b_1y_{1m}} + \mathbf{b_2y_{2m}} + \mathbf{b_3})\} \\
e_2 &= |\mathbf{y_{1m}y_{2dm}} + \mathbf{y_{2m}y_{1dm}} + \mathbf{b_1y_{1dm}} + \mathbf{b_2y_{2dm}}|^2 + \\
&\quad 2Re\{(\mathbf{y_{1dm}y_{2dm}})^*(\mathbf{y_{1m}y_{2m}} + \mathbf{b_1y_{1m}} + \mathbf{b_2y_{2m}} + \mathbf{b_3})\} \\
e_3 &= 2Re\{(\mathbf{y_{1dm}y_{2dm}})^*(\mathbf{y_{1m}y_{2dm}} + \mathbf{y_{2m}y_{1dm}} + \mathbf{b_1y_{1dm}} + \mathbf{b_2y_{2dm}})\} \\
e_4 &= |\mathbf{y_{1dm}y_{2dm}}|^2
\end{aligned}
$$

Equation (A.1) can now be written as

$$
S_1 = \frac{c_0 + c_1\tau + c_2\tau^2}{e_0 + e_1\tau + e_2\tau^2 + e_3\tau^3 + e_4\tau^4}\sqrt{d_0 + d_1\tau + d_2\tau^2} \tag{A.8}
$$

Solving Equation (A.3)

$$
\begin{aligned}
\left.\frac{dS_1}{d\tau}\right|_{\tau=\tilde{\tau}} &= \frac{(c_1 + 2c_2\tilde{\tau})(e_0 + e_1\tilde{\tau} + e_2\tilde{\tau}^2 + e_3\tilde{\tau}^3 + e_4\tilde{\tau}^4)}{(e_0 + e_1\tilde{\tau} + e_2\tilde{\tau}^2 + e_3\tilde{\tau}^3 + e_4\tilde{\tau}^4)^2}\sqrt{d_0 + d_1\tilde{\tau} + d_2\tilde{\tau}^2} \\
&\quad - \frac{(c_0 + c_1\tilde{\tau} + c_2\tilde{\tau}^2)(e_1 + 2e_2\tilde{\tau} + 3e_3\tilde{\tau}^2 + 4e_4\tilde{\tau}^3)}{(e_0 + e_1\tilde{\tau} + e_2\tilde{\tau}^2 + e_3\tilde{\tau}^3 + e_4\tilde{\tau}^4)^2}\sqrt{d_0 + d_1\tilde{\tau} + d_2\tilde{\tau}^2} \\
&\quad - \frac{(c_0 + c_1\tilde{\tau} + c_2\tilde{\tau}^2)}{(e_0 + e_1\tilde{\tau} + e_2\tilde{\tau}^2 + e_3\tilde{\tau}^3 + e_4\tilde{\tau}^4)}\frac{(d_1 + 2d_2\tilde{\tau})}{2\sqrt{d_0 + d_1\tilde{\tau} + d_2\tilde{\tau}^2}} \\
&= 0
\end{aligned} \tag{A.9}
$$

Multiplying with the common denominator

$$
2(e_0 + e_1\tilde{\tau} + e_2\tilde{\tau}^2 + e_3\tilde{\tau}^3 + e_4\tilde{\tau}^4)^2\sqrt{d_0 + d_1\tilde{\tau} + d_2\tilde{\tau}^2} \neq 0
$$

Equation (A.9) is written as

$$
s_0 + s_1\tilde{\tau} + s_2\tilde{\tau}^2 + s_3\tilde{\tau}^3 + s_4\tilde{\tau}^4 + s_5\tilde{\tau}^5 + s_6\tilde{\tau}^6 + s_7\tilde{\tau}^7 = 0 \tag{A.10}
$$

where

$$
\begin{aligned}
s_0 &= c_0 d_1 e_0 - 2d_0 c_0 e_1 + 2d_0 c_1 e_0 \\
s_1 &= -c_0 d_1 e_1 + 2c_0 d_2 e_0 + 3c_1 d_1 e_0 + 4d_0 c_2 e_0 - 4d_0 c_0 e_2 \\
s_2 &= -3c_0 d_1 e_2 + c_1 d_1 e_1 + 4c_1 d_2 e_0 + 5c_2 d_1 e_0 - 2d_0 c_1 e_2 + 2d_0 c_2 e_1 - 6d_0 c_0 e_3 \\
s_3 &= -5c_0 d_1 e_3 - 2c_0 d_2 e_2 - c_1 d_1 e_2 + 2c_1 d_2 e_1 + 3c_2 d_1 e_1 + 6c_2 d_2 e_0 - 4d_0 c_1 e_3 \\
&\quad - 8d_0 c_0 e_4 \\
s_4 &= -7c_0 d_1 e_4 - 4c_0 d_2 e_3 - 3c_1 d_1 e_3 + c_2 d_1 e_2 + 4c_2 d_2 e_1 - 6d_0 c_1 e_4 - 2d_0 c_2 e_3 \\
s_5 &= -6c_0 d_2 e_4 - 5c_1 d_1 e_4 - 2c_1 d_2 e_3 - c_2 d_1 e_3 + 2c_2 d_2 e_2 - 4d_0 c_2 e_4 \\
s_6 &= -4c_1 d_2 e_4 - 3c_2 d_1 e_4 \\
s_7 &= -2c_2 d_2 e_4
\end{aligned}
$$

A.3 Shifting the gradient in y_1 direction

Finding the distance to the PoC, shifting the gradient in y_1 direction can be done solving Equation (A.11) for the load admittance y_1 marked $\tilde{y}_1$.

$$
\left.\frac{dS_1}{dt}\right|_{y_1=\tilde{y}_1} = \frac{\partial S_1}{\partial y_1}\frac{dy_1}{dt} + \frac{\partial S_1}{\partial y_2}\frac{dy_2}{dt} + \frac{\partial S_1}{\partial \delta_1}\frac{d\delta_1}{dt} + \frac{\partial S_1}{\partial \delta_2}\frac{d\delta_2}{dt} = 0 \tag{A.11}
$$

Equation (A.1) can be written as

$$
\begin{aligned}
S_1 &= \frac{(\mathbf{a}_1 + \mathbf{a}_2\mathbf{y}_2)(\mathbf{a}_1 + \mathbf{a}_2\mathbf{y}_2)^*}{(\mathbf{y}_1\mathbf{y}_2 + \mathbf{b}_1\mathbf{y}_1 + \mathbf{b}_2\mathbf{y}_2 + \mathbf{b}_3)(\mathbf{y}_1\mathbf{y}_2 + \mathbf{b}_1\mathbf{y}_1 + \mathbf{b}_2\mathbf{y}_2 + \mathbf{b}_3)^*} y_1 \\
&= \frac{N(\mathbf{y_2})}{D(\mathbf{y_1}, \mathbf{y_2})} y_1
\end{aligned} \tag{A.12}
$$

where

$$
N(\mathbf{y_2}) = a_1^2 + (a_2 y_2)^2 + 2Re\{\mathbf{a_1^* a_2 y_2}\} \tag{A.13}
$$

and

$$
\begin{aligned}
D(\mathbf{y_1}, \mathbf{y_2}) &= (y_1 y_2)^2 + (b_1 y_1)^2 + (b_2 y_2)^2 + b_3^2 + 2(y_1^2 Re\{\mathbf{y_2 b_1^*}\} + y_2^2 Re\{\mathbf{y_1 b_2^*}\} \\
&\quad + Re\{\mathbf{y_1 y_2 b_3^*}\} + Re\{\mathbf{y_1 y_2^* b_1 b_2^*}\} + Re\{\mathbf{y_1 b_1 b_3^*}\} + Re\{\mathbf{y_2 b_2 b_3^*}\}) \\
&= |\mathbf{y_2 b_2} + \mathbf{b_3}|^2 + 2Re\{e^{i\delta_1}(\mathbf{y_2} + \mathbf{b_1})(\mathbf{y_2 b_2} + \mathbf{b_3})^*\} y_1 + |\mathbf{y_2} + \mathbf{b_1}|^2 y_1^2 \\
&= c_0 + c_1 y_1 + c_2 y_1^2
\end{aligned} \tag{A.14}
$$

The partial derivatives of N and D can be found as

$$N_{y_2} = 2a_2^2 y_2 + 2Re\{\mathbf{a_1^* a_2 y_2}\} \tag{A.15}$$

$$N_{\delta_2} = -2Im\{\mathbf{a_1^* a_2 y_2}\} \tag{A.16}$$

Both partial derivatives N_{y_2} and N_{δ_2} are independent of the absolute value of load admittance y_1.

$$D_{y_1} = 2Re\{e^{i\delta_1}(\mathbf{y_2}+\mathbf{b_1})(\mathbf{y_2 b_2}+\mathbf{b_3})^*\} + 2y_1|\mathbf{y_2}+\mathbf{b_1}|^2 = d_0 + d_1 y_1 \tag{A.17}$$

$$D_{\delta_1} = -2Im\{e^{i\delta_1}(\mathbf{y_2}+\mathbf{b_1})(\mathbf{y_2 b_2}+\mathbf{b_3})^*\} y_1 = e_1 y_1 \tag{A.18}$$

$$\begin{aligned} D_{y_2} =& 2(y_2 b_2^2 + Re\{e^{i\delta_2}\mathbf{b_2 b_3^*}\}) + 2(2y_2 Re\{e^{i\delta_1}\mathbf{b_2^*}\} + \\ & Re\{e^{i\delta_1}(e^{i\delta_2}\mathbf{b_3^*} + e^{-i\delta_2}\mathbf{b_1 b_2^*})\})y_1 + 2(y_2 + Re\{e^{i\delta_2}\mathbf{b_1^*}\})y_1^2 \\ =& f_0 + f_1 y_1 + f_2 y_1^2 \end{aligned} \tag{A.19}$$

$$\begin{aligned} D_{\delta_2} =& -2Im\{\mathbf{y_2 b_2 b_3^*}\} - 2Im\{e^{i\delta_1}\mathbf{y_2}(\mathbf{b_3} + (\mathbf{y_2}+\mathbf{b_1^*})\mathbf{b_2})^*\} y_1 - 2Im\{\mathbf{y_2 b_1^*}\} y_1^2 \\ =& g_0 + g_1 y_1 + g_2 y_1^2 \end{aligned} \tag{A.20}$$

As long as $D = 0$ is not a solution to Equation (A.11) both sides of the equation can be multiplied by D^2. For each of the partial derivative of Equation (A.11) a polynomial of y_1 in the order of maximum 3 can be derived.

$$D^2 \frac{\partial S_1}{\partial y_1} = N(D - y_1 D_{y_1}) = Nc_0 - Nc_2 y_1^2 \tag{A.21}$$

$$D^2 \frac{\partial S_1}{\partial y_2} = y_1(DN_{y_2} - ND_{y_2}) \tag{A.22}$$

$$= (N_{y_2} c_0 - N f_0) y_1 + (N_{y_2} c_1 - N f_1) y_1^2 + (N_{y_2} c_2 - N f_2) y_1^3 \tag{A.23}$$

$$D^2 \frac{\partial S_1}{\partial \delta_1} = -y_1 N D_{\delta_1} = -N e_1 y_1^2 \tag{A.24}$$

$$D^2 \frac{\partial S_1}{\partial \delta_2} = y_1(DN_{\delta_2} - ND_{\delta_2}) \tag{A.25}$$

$$= (N_{\delta_2} c_0 - N g_0) y_1 + (N_{\delta_2} c_1 - N g_1) y_1^2 + (N_{\delta_2} c_2 - N g_2) y_1^3 \tag{A.26}$$

Equation (A.11) can be written as

$$s_0 + s_1 \tilde{y}_1 + s_2 \tilde{y}_1^2 + s_3 \tilde{y}_1^3 = 0 \tag{A.27}$$

where

$$s_0 = Nc_0\frac{dy_1}{dt}$$

$$s_1 = (N_{y_2}c_0 - Nf_0)\frac{dy_2}{dt} + (N_{\delta_2}c_0 - Ng_0)\frac{d\delta_2}{dt}$$

$$s_2 = Nc_2\frac{dy_1}{dt} + (N_{y_2}c_1 - Nf_1)\frac{dy_2}{dt} - Ne_1\frac{d\delta_1}{dt} + (N_{\delta_2}c_1 - Ng_1)\frac{d\delta_2}{dt}$$

$$s_3 = (N_{y_2}c_2 - Nf_2)\frac{dy_2}{dt} + (N_{\delta_2}c_2 - Ng_2)\frac{d\delta_2}{dt}$$

A.4 Generalization to *n* nodes

When measurements are taken of both voltages and currents on n buses connected to each other by straight lines, with no unknown buses in between, the following equation can be made.

$$\begin{bmatrix} \mathbf{U_1} \\ \mathbf{U_2} \\ \vdots \\ \mathbf{U_n} \end{bmatrix} = \begin{bmatrix} (\mathbf{y_1}+\mathbf{M_1}) & & & \\ & (\mathbf{y_2}+\mathbf{M_2}) & & \\ & & \ddots & \\ & & & (\mathbf{y_n}+\mathbf{M_n}) \end{bmatrix}^{-1} \begin{bmatrix} \mathbf{F_1} \\ \mathbf{F_2} \\ \vdots \\ \mathbf{F_n} \end{bmatrix} \tag{A.28}$$

Where $\mathbf{U_i}$ and $\mathbf{y_i}$ are the voltage and load admittances on the measured bus number i. Non-diagonal elements $\mathbf{M_i}$ and $\mathbf{F_i}$ are constants, which are calculated using the values of the transmission lines between the "known" buses. The load admittances, $\mathbf{y_i}$, only appear on the diagonal.

The voltage $\mathbf{U_1}$ can be found as

$$\mathbf{U_1} = \frac{\mathbf{N}(\mathbf{y_2},\ldots,\mathbf{y_n})}{\mathbf{D}(\mathbf{y_1},\ldots,\mathbf{y_n})} \tag{A.29}$$

where

$$\mathbf{N} = \mathbf{a}(1)\prod_{i=2}^{n}\mathbf{y_i} + \sum_{k=0}^{n-2}\left(\sum_{i_1=2}^{n-k}\sum_{i_2=i_1+1}^{n-k+1}\cdots\sum_{i_{k+1}=i_k+1}^{n}\mathbf{a}(i_1,\cdots,i_{k+1})\prod_{i\notin\{1,i_1,\cdots,i_{k+1}\}}\mathbf{y_i}\right) \tag{A.30}$$

and

$$\mathbf{D} = \prod_{i=1}^{n}\mathbf{y_i} + \sum_{k=0}^{n-1}\left(\sum_{i_1=1}^{n-k}\sum_{i_2=i_1+1}^{n-k+1}\cdots\sum_{i_{k+1}=i_k+1}^{n}\mathbf{b}(i_1,\cdots,i_{k+1})\prod_{i\notin\{i_1,\cdots,i_{k+1}\}}\mathbf{y_i}\right) \tag{A.31}$$

The apparent power S_1 delivered to bus no. 1 can now be written as

$$S_1 = |\mathbf{U_1}|^2 |y_1| = \frac{|\mathbf{N}(\mathbf{y_2}, \ldots, \mathbf{y_n})|^2}{|\mathbf{D}(\mathbf{y_1}, \ldots, \mathbf{y_n})|^2} |\mathbf{y_1}| \tag{A.32}$$

A.4.1 Distance to the PoC along the gradient

The assumption is made that all the measured loads moves along the gradient

$$\begin{aligned}
\tilde{\mathbf{y}}_\mathbf{1}(\tau) &= \mathbf{y}_{1m} + \mathbf{y}_{1dm}\tau = g_{1m} + g_{1dm}\tau + i(b_{1m} + b_{1dm}\tau) \\
\tilde{\mathbf{y}}_\mathbf{2}(\tau) &= \mathbf{y}_{2m} + \mathbf{y}_{2dm}\tau = g_{2m} + g_{2dm}\tau + i(b_{2m} + b_{2dm}\tau) \\
&\vdots \\
\tilde{\mathbf{y}}_\mathbf{n}(\tau) &= \mathbf{y}_{nm} + \mathbf{y}_{ndm}\tau = g_{nm} + g_{ndm}\tau + i(b_{nm} + b_{ndm}\tau)
\end{aligned} \tag{A.33}$$

Substituting Equation (A.33) into Equation (A.32) gives the expression in Equation (A.34). The highest order of any multiplicity of $\mathbf{y_i}$ in $\mathbf{D}$ is n and in $\mathbf{N}$ is n-1.

$$S_1 = \frac{\sum_{i=0}^{2(n-1)} c_i \tau^i}{\sum_{j=0}^{2n} e_j \tau^j} \sqrt{d_0 + d_1\tau + d_2\tau^2} \tag{A.34}$$

Finding the derivative of apparent power S_1 with respect to the time τ.

$$\begin{aligned}
\left.\frac{dS_1}{d\tau}\right|_{\tau=\tilde{\tau}} &= \sqrt{d_0 + d_1\tilde{\tau} + d_2\tilde{\tau}^2} \\
&\left(\frac{\left(\sum_{j=0}^{2n} e_j \tilde{\tau}^j\right)\left(\sum_{i=1}^{2(n-1)} i c_i \tilde{\tau}^{i-1}\right) - \left(\sum_{j=1}^{2n} j e_j \tilde{\tau}^{j-1}\right)\left(\sum_{i=0}^{2(n-1)} c_i \tilde{\tau}^i\right)}{\left(\sum_{j=0}^{2n} e_j \tilde{\tau}^j\right)^2} \right) \\
&- \frac{(d_1 + 2d_2\tilde{\tau})}{2\sqrt{d_0 + d_1\tilde{\tau} + d_2\tilde{\tau}^2}} \frac{\left(\sum_{i=0}^{2(n-1)} c_i \tilde{\tau}^i\right)}{\left(\sum_{j=0}^{2n} e_j \tilde{\tau}^j\right)} \\
&= 0
\end{aligned} \tag{A.35}$$

and multiplying by the common denominator

$$2\left(\sum_{j=0}^{2n} e_j\tilde{\tau}^j\right)^2\sqrt{d_0+d_1\tilde{\tau}+d_2\tilde{\tau}^2}\neq 0 \tag{A.36}$$

gives the following equation for the VIP++ to solve.

$$\begin{aligned}(d_0+d_1\tilde{\tau}+d_2\tilde{\tau}^2)\left[\left(\sum_{j=0}^{2n} e_j\tilde{\tau}^j\right)\left(\sum_{i=1}^{2(n-1)} ic_i\tilde{\tau}^{i-1}\right)-\left(\sum_{j=1}^{2n} je_j\tilde{\tau}^{j-1}\right)\left(\sum_{i=0}^{2(n-1)} c_i\tilde{\tau}^i\right)\right]-\\ (d_1+2d_2\tilde{\tau})\left(\sum_{i=0}^{2(n-1)} c_i\tilde{\tau}^i\right)\left(\sum_{i=0}^{2n} e_i\tilde{\tau}^i\right)=0\end{aligned} \tag{A.37}$$

The highest order of $\tilde{\tau}$ is

$$2+2n+2(n-1)-1=4n-1 \tag{A.38}$$

Thus Equation (A.37) can be written as Equation (A.39).

$$\sum_{i=0}^{4n-1} s_i\tilde{\tau}^i=0 \tag{A.39}$$

This is for the general case with n measured buses, but for some special configurations the number might actually be less although measurements on n buses have been made. With two known buses as shown in Section A.2 the VIP++ has to solve an equation of degree seven and with three known buses the degree of the equation has increased to eleven.

A.4.2 Shifting the gradient in y_1 direction

The apparent power delivered to the critical bus can generally be expressed as given in Equation (A.32). Finding the distance to the PoC for the general case can be done by solving Equation (A.40) for load admittance y_1 marked $\tilde{y}_1$.

$$\left.\frac{dS}{dt}\right|_{y_1=\tilde{y}_1}=\sum_{j=1}^{n}\left(\frac{\partial S}{\partial y_j}\frac{dy_j}{dt}+\frac{\partial S}{\partial \delta_j}\frac{d\delta_j}{dt}\right)=0 \tag{A.40}$$

The real and imaginary parts of $\mathbf{D}$ can be written as:

$$\begin{aligned}D_r&=f_r(\delta_1,\mathbf{y_2},\ldots,\mathbf{y_n})y_1+m_r(\mathbf{y_2},\ldots,\mathbf{y_n})\\ D_i&=f_i(\delta_1,\mathbf{y_2},\ldots,\mathbf{y_n})y_1+m_i(\mathbf{y_2},\ldots,\mathbf{y_n})\end{aligned} \tag{A.41}$$

while N is independent of y_1, so that

$$S_1 = \frac{N^2 y_1}{g y_1^2 + h y_1 + f} \tag{A.42}$$

where g,h and f is given by Equation (A.43).

$$|\mathbf{D}|^2 = (f_r^2 + f_i^2) y_1^2 + 2(f_r m_r + f_i m_i) y_1 + (m_r + m_i)^2 = g y_1^2 + h y_1 + g \tag{A.43}$$

The partial derivatives in Equation (4.29) can be found as:

$$\frac{\partial S_1}{\partial y_1} = TN(f - g y_1^2) \tag{A.44}$$

$$\frac{\partial S_1}{\partial y_j} = T\left[\left(2g\frac{\partial N}{\partial y_j} - N\frac{\partial g}{\partial y_j}\right) y_1^3 + \left(2h\frac{\partial N}{\partial y_j} - N\frac{\partial h}{\partial y_j}\right) y_1^2 + \left(2f\frac{\partial N}{\partial y_j} - N\frac{\partial f}{\partial y_j}\right) y_1\right] \tag{A.45}$$

$$\frac{\partial S_1}{\partial \delta_1} = -TN\left[\left(\frac{\partial g}{\partial \delta_1}\right) y_1^3 + \left(\frac{\partial h}{\partial \delta_1}\right) y_1^2\right] \tag{A.46}$$

$$\frac{\partial S_1}{\partial \delta_j} = T\left[\left(2g\frac{\partial N}{\partial \delta_j} - N\frac{\partial g}{\partial \delta_j}\right) y_1^3 + \left(2h\frac{\partial N}{\partial \delta_j} - N\frac{\partial h}{\partial \delta_j}\right) y_1^2 + \left(2f\frac{\partial N}{\partial \delta_j} - N\frac{\partial f}{\partial \delta_j}\right) y_1\right] \tag{A.47}$$

where

$$T = \frac{N}{(g y_1^2 + h y_1 + f)^2}$$

Substituting Equations (A.44–A.47) into Equation (4.29), the parameters $s_0, \ldots, s_3$ in Equation (4.30) can be found as

$$s_0 = Nf\frac{dy_1}{dt}$$

$$s_1 = 2f\sum_{j \notin 1}\left(\frac{\partial N}{\partial y_j}\frac{dy_j}{dt} + \frac{\partial N}{\partial \delta_j}\frac{d\delta_j}{dt}\right) - N\sum_{j \notin 1}\left(\frac{\partial f}{\partial y_j}\frac{dy_j}{dt} + \frac{\partial f}{\partial \delta_j}\frac{d\delta_j}{dt}\right)$$

$$s_2 = 2h\sum_{j \notin 1}\left(\frac{\partial N}{\partial y_j}\frac{dy_j}{dt} + \frac{\partial N}{\partial \delta_j}\frac{d\delta_j}{dt}\right) - N\sum_{j \notin 1}\left(\frac{\partial h}{\partial y_j}\frac{dy_j}{dt} + \frac{\partial h}{\partial \delta_j}\frac{d\delta_j}{dt}\right)$$
$$- N\left(g + \frac{\partial h}{\partial \delta_1}\frac{d\delta_1}{dt}\right)$$

$$s_3 = 2g\sum_{j \notin 1}\left(\frac{\partial N}{\partial y_j}\frac{dy_j}{dt} + \frac{\partial N}{\partial \delta_j}\frac{d\delta_j}{dt}\right) - N\sum_{j \notin 1}\left(\frac{\partial g}{\partial y_j}\frac{dy_j}{dt} + \frac{\partial g}{\partial \delta_j}\frac{d\delta_j}{dt}\right) - N\frac{\partial g}{\partial \delta_1}\frac{d\delta_1}{dt}$$

A.5 Derivative

One of the main problems with the VIP++ method is finding the derivatives. Unless a good estimate for this can be found, the prediction of distance to voltage collapse might be numerically unstable.

The derivative[11] of the function f at x_0 is defined as:

$$f'(x_0) = \lim_{h \to 0} \frac{f(x_0+h) - f(x_0)}{h} \tag{A.48}$$

A first approximation to the derivative is given by the two-point formula in Equation (A.49), which can be used for small values of h.

$$f'(x_0) = \frac{f(x_0+h) - f(x_0)}{h} - \frac{h}{2} f''(\xi) \tag{A.49}$$

ξ lies between x_0 and $x_0 + h$. Figure A.1 gives an illustration of the approximation produced from the formula. A second approximation is given by the *Three-point midpoint*

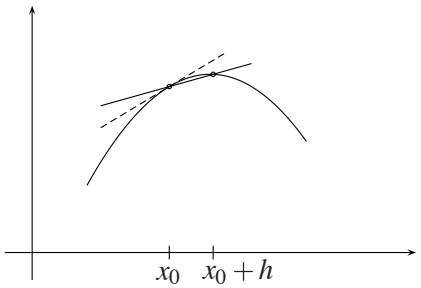

Figure A.1: Two–point formula

formula,

$$f'(x_0) = \frac{f(x_0+h) - f(x_0-h)}{2h} - \frac{h^2}{6} f^{(3)}(\xi) \tag{A.50}$$

which is illustrated in Figure A.2.

To remove high frequency components of the measured signal, a filter as shown in Figure A.3 can be used.

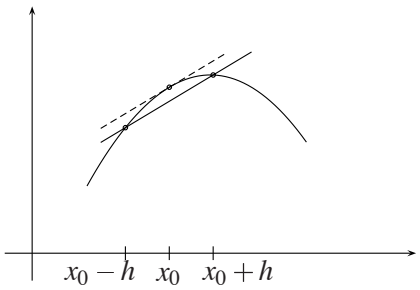

Figure A.2: Three–point formula

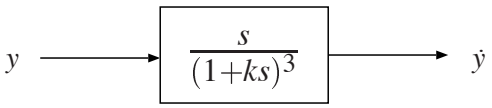

Figure A.3: Third degree filter

Appendix B

Models

This appendix presents the five configuration of the VIP++ methods used in Section 5.1. In all the configurations it is assumed that Hasle is the bus that the VIP++ methods is set to protect.

B.1 Case 1

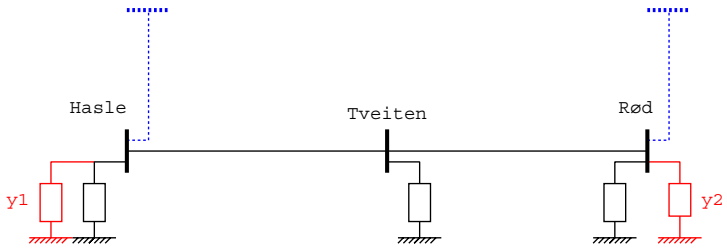

Figure B.1: Configuration of VIP++ with measurements at the Hasle and Rød buses

In the first configuration measurements are only performed on two buses, Hasle and Rød, that is PMUs are only placed on these two buses. There is no need to measure on the bus in between these two, Tveiten, as no load or other transmission line is connected to this bus.

B.2 Case 2

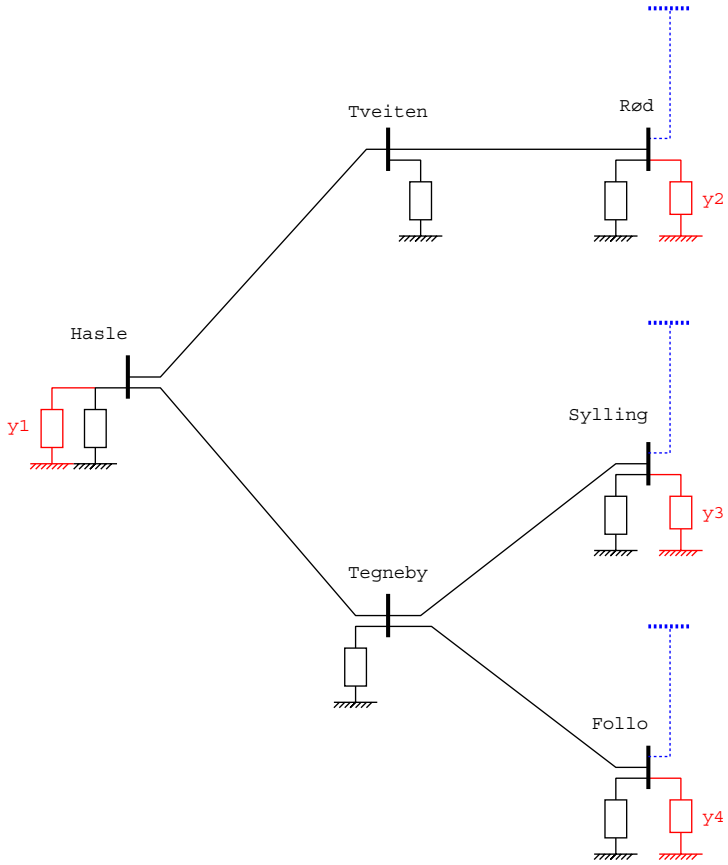

Figure B.2: Configuration of VIP++ with measurements at buses at Hasle, Rød, Follo and Sylling

In this case two more PMUs are on the buses at Follo and Sylling. Also in this case, and in all the following cases, there is a bus in between with no PMU at Tegneby. As for the previous case no measurement is needed in Tegneby as there is no load or other transmission line connected to this bus.

B.3 Case 3

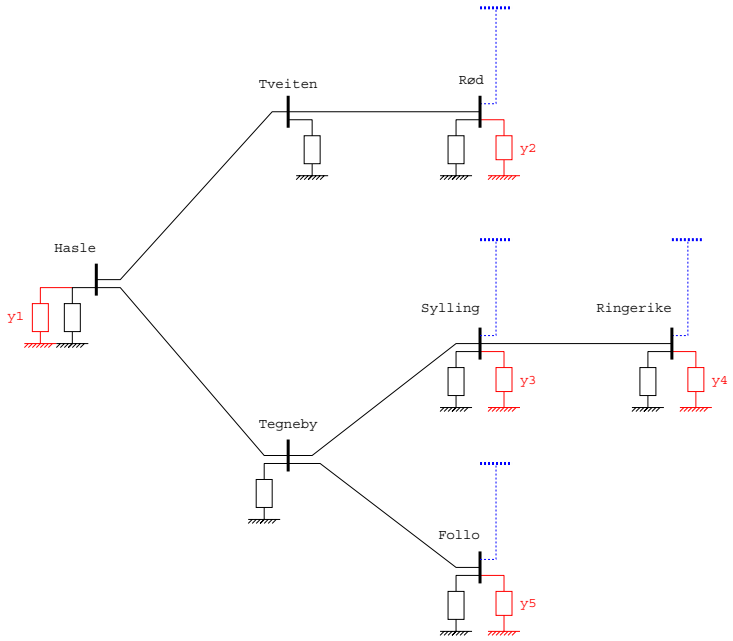

Figure B.3: Configuration of VIP++ with measurements at buses at Hasle, Rød, Follo, Sylling and Ringerike

In this case one more bus, Ringerike, is added to the list of known buses compared to “Case 2”.

B.4 Case 4

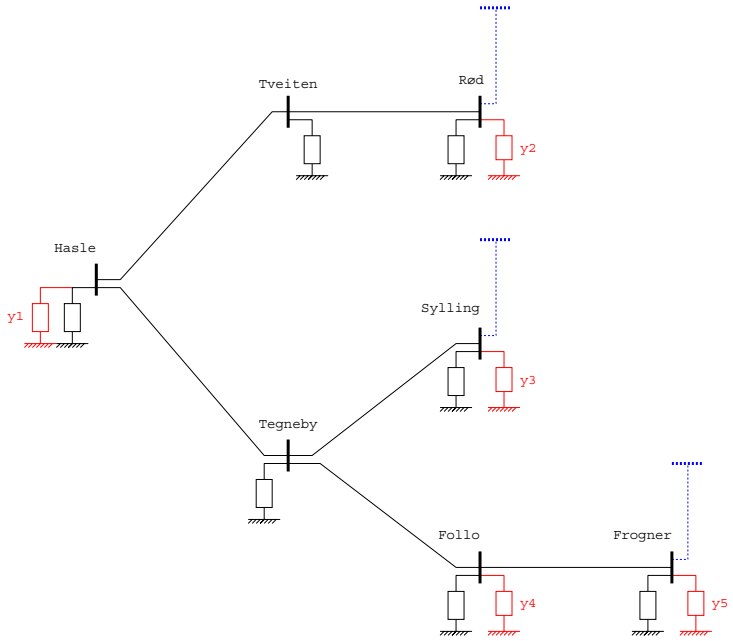

Figure B.4: Configuration of VIP++ with measurements at buses at Hasle, Rød, Follo, Sylling and Frogner

This is a similar configuration to the system in case 3, with an extra measurement at Frogner instead of Ringerike. Note that no estimation of Thevenin equivalent has to be made at Follo, as the only connection there is either in the direction of Frogner or Tegneby, or it is considered the measured load at the bus.

B.5 Case 5

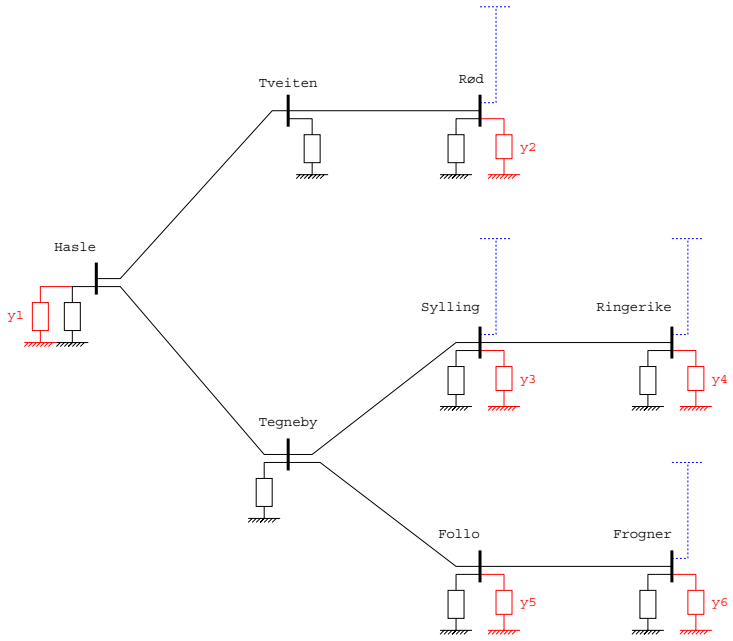

Figure B.5: Configuration of VIP++ with measurements at buses at Hasle, Rød, Follo, Sylling, Ringerike and Frogner

This is the last case, which include all of the “known” buses mentioned in the previous cases.

Appendix C

General Theory and Notations

This appendix presents some general theory and notations used in the dissertation.

C.1 Notations

All complex values are written bold letters, and both vectors and scalar values are written using standard font.

$$\mathbf{z} = x + iy = ze^{i\delta} \quad \text{where} \quad \mathbf{z} \in \mathbb{C} \quad , \quad \{x, y, \delta\} \in \mathbb{R} \quad \text{and} \quad z \in \mathbb{R}^{+} \tag{C.1}$$

The partial derivative of a function can be written in the short form given as:

$$\frac{\partial f}{\partial x} = f_x \tag{C.2}$$

For calculating the values of parallel impedances the following operator $\|$ is used:

$$\mathbf{z}_1 \| \mathbf{z}_2 = \frac{\mathbf{z}_1 \mathbf{z}_2}{\mathbf{z}_1 + \mathbf{z}_2} \tag{C.3}$$

C.2 Functions

The definition of absolute value and angle are given in Equations (C.4) and (C.5).

$$|\mathbf{z}| = \sqrt{\mathbf{z}\mathbf{z}^*} = \sqrt{x^2 + y^2} = z \tag{C.4}$$

$$\angle \mathbf{z} = \arctan \frac{y}{x} = \delta \tag{C.5}$$

The real and imaginary values can be found as

$$Re\{\mathbf{z}\} = x = z\cos\delta \tag{C.6}$$

$$Im\{\mathbf{z}\} = y = z\sin\delta \tag{C.7}$$

and the conjugate

$$\mathbf{z}^* = x - iy = ze^{-i\delta} \tag{C.8}$$

The following relation has been used when calculating the parameters in Appendix A.2.

$$\begin{aligned} 2Re(\mathbf{z_1 z_2^*}) &= 2z_1 z_2 \cos(\delta_1 - \delta_2) = 2z_1 z_2 \frac{\left(e^{i(\delta_1-\delta_2)} + e^{i(-\delta_1+\delta_2)}\right)}{2} \\ &= \mathbf{z}_1\mathbf{z}_2^* + \mathbf{z}_1^*\mathbf{z}_2 \end{aligned} \tag{C.9}$$

C.3 Complex Fourier Series[20]

Using Fourier series any periodic function can be represented by cosines and sinuses, as given by Equation (C.10) and (C.11).

$$f(x) = \sum_{n=-\infty}^{\infty} c_n e^{inx} \tag{C.10}$$

where

$$c_n = \frac{1}{2\pi}\int_0^{2\pi} f(x)e^{-inx}dx \tag{C.11}$$

and $n = 0, \pm 1, \pm 2, \cdots$.

For a sinus waveform like the one given in Figure 3.11(a), the complex Fourier coefficients of $f(t) = \cos(t+\phi)$ is given by c_1 and c_{-1}, where:

$$c_1 = \frac{\cos(\Phi) + i\sin(\Phi)}{2} \quad , \quad c_{-1} = \frac{\cos(\Phi) - i\sin(\Phi)}{2} \tag{C.12}$$

All other coefficients c_n are equal to zero. The discrete Fourier coefficient can be found as:

$$c_n = \frac{1}{2\pi}\sum_{k=1}^{N} f(x_k)e^{-i\frac{k2\pi n}{N}}\frac{2\pi}{N} \tag{C.13}$$

where N is the total number of samples in one period.

Appendix D

Maple Functions

For each specific case, depending on the topology of the system, a function has to be made. This cannot be done manually as the equations for the parameters increases considerably with an increasing number of "known" buses. In order to make functions for estimations with more than two "known" buses, the Maple program has been used. The maple functions presented in this chapter are used to create MATLAB functions, which need some minor changes before they can be used by MATLAB. The output functions for both "Distance to the PoC along the gradient" and "Shifting the gradient in the y_1 direction", called "write_grad.ma" and "write_shift.ma", can easily be changed to fit other computer programs.

D.1 System description

The maple functions are divided into two steps, with one function for each step.

1. Create the numerator and denominator, denoted T and N, of the voltage, U_1, at the bus that the VIP++ is set to protect. The voltage is dependent on the system given by the load admittances, Thevenin equivalents and transmission system, and is the function is the same for the two methods.

2. Calculate the parameters for the polynomial that VIP++ methods must solve. As there are different sets of parameters for the two methods, one function must be made for each method. The calculation of the parameters, a_i and b_j, in the numerator and denominator of the voltage U_1 is the same for both methods, but is repeated in both functions.

With a given topology including Thevenin equivalents, transmission lines and load admittances, three files have to be made, which are all loaded by the maple functions. These three files are:

- The cut-set matrix [27] file “Q.dat”.
- Transmission Lines and Thevenin impedances which are removed from the general system setup given by the file “YYrem.dat”.
- Load impedances on known buses, which are removed from the general setup given by the file “yrem.dat”.

Both the two “removal” files contain a column vector with ones and zeros, where the value one is used to remove a line. The cut-set matrix Q is given as a matrix of size $\#<buses>\times\#<admittances>$, with ones and zeros.

$$Q = \begin{bmatrix} Q_1 & Q_2 & Q_3 & Q_4 \end{bmatrix} \tag{D.1}$$

where

$$Q_1 = Q_3 = \begin{bmatrix} 1 & 0 & \cdots & 0 \\ 0 & 1 & \ddots & \vdots \\ \vdots & \ddots & \ddots & 0 \\ \vdots & & \ddots & 1 \\ \vdots & & & 0 \\ \vdots & & & \vdots \\ 0 & \cdots & \cdots & 0 \end{bmatrix} \tag{D.2}$$

Q_1 and Q_3 represents the “known” buses with both measured load admittances and shunt admittances, respectively.

$$Q_2 = \begin{bmatrix} -1 & 0 & \cdots & 0 \\ 0 & -1 & \ddots & \vdots \\ \vdots & \ddots & \ddots & 0 \\ \vdots & & \ddots & -1 \\ 1 & 0 & \cdots & 0 \\ 0 & 1 & \ddots & \vdots \\ \vdots & \ddots & \ddots & 0 \\ \vdots & & \ddots & 1 \\ \vdots & & & 0 \\ \vdots & & & \vdots \\ 0 & \cdots & \cdots & 0 \end{bmatrix} \tag{D.3}$$

Q_2 represents the estimated Thevenin admittances seen from each of the "known" load buses. Q_4 is given by the transmission lines between the "known" load buses. It can also include buses without any loads. All of the matrixes Q_1 through Q_3 could have been generated by the maple functions themselves, using the two "removal" files to account for any off standard configurations. Since VIP++ methods will only be used on small systems this has not been implemented.

D.2 Loading system

The system is loaded into Maple using the following script called "make_syst.ma": (For the case of seven known load buses)

```
with(linalg);
read "dim.c"

# Description of system

n := 6;    # Number of loads
tot:= 27; # Total number of impedances ( including loads )
nbus:=14; # Number of buses ( including Thevenin buses )
nz:=6;     # Number of Thevenin equivalents

# Load system

Q:= matrix(readdata("/home/leifwar/maple/case/Q.dat",integer,tot))
Yrem :=   readdata("/home/leifwar/maple/case/YYrem.dat",integer,1);
yrem :=   readdata("/home/leifwar/maple/case/yrem.dat",integer,1);

# Make system matrix

yy:=matrix(tot,tot,(i,j)->
    if i=j and i <= n then
        y[i]
    elif i=j and i > n and i <= (n+nz) then
        Yz[i-n]
    elif i=j and i>2*n and i <= tot then
        Ye[i-(n+nz)]
    else 0
 fi);

for i from 1 to n do if Yrem[i] = 1 then Yz[i]:=0 fi;od;

Yk:=multiply(Q,yy,transpose(Q));

if nbus = 2*n then
 Ekm:= submatrix(-Yk,1..n,n+1..2*n);
```

```
 Ykm:= submatrix(Yk,1..n,1..n)
else
 Ekm:= matadd(submatrix(−Yk,1..n,n+1..(n+nz)),
              multiply(submatrix( Yk,1..n,(n+nz)+1..nbus),
                       inverse(submatrix(Yk,(n+nz)+1..nbus,(n+nz)+1..nbus)),
                       submatrix(Yk,(n+nz)+1..nbus,n+1..(n+nz))));
 Ykm:= matadd(submatrix( Yk,1..n,1..n),
              multiply(submatrix(−Yk,1..n,(n+nz)+1..nbus),
                       inverse(submatrix(Yk,(n+nz)+1..nbus,(n+nz)+1..nbus)),
                       submatrix(Yk,(n+nz)+1..nbus,1..n)));
fi;

Ykm_tmp:=matrix(n,n,(i,j)−>
       if Ykm[i,j]=0 then
          0
       elif i=j then
          Ym[i,i]
       elif i>j then
          Y[j,i]
       else
          Y[i,j]
       fi );
Ykm_tmp_det:=det(Ykm_tmp);
Ykm_tmp_inv:=inverse(Ykm_tmp/Ykm_tmp_det);

U:=multiply(Ykm_tmp_inv,Ekm,matrix(nz,1,i−>E[i]));

for i from 1 to n do Ym[i,i]:=Y[i,i]+y[i]; od;

T:=coeffs(expand(U[1,1]),indets(sum(y[k],'k'=2..n)),Tt);
N:=coeffs(expand(Ykm_tmp_det),indets(sum(y[k],'k'=1..n)),Nt);
```

The function “dim.c” is used to calculated the dimensions of a vector.

```
dim:=proc (x) local i,j; j:=0; for i in x do j:=j+1; od; j end: # dim
```

D.3 Distance to the PoC along the gradient

For this method the following script is used to make the function file for MATLAB called “write_grad.ma”:

```
assume(t,real);

for i from 1 to 6 do
   y[i]:=yrm[i]+I*yim[i] + t*(yrd[i]+I*yid[i]);
   assume(yrm[i],real,yim[i],real);
```

```
od;

S1d := sqrt(coeff(y[1],I,0)^2+coeff(y[1],I,1)^2);

# coefficient a[i] og b[i]
for i from 1 to vectdim([T]) do
    a[i]:= ar[i]+I*ai[i];
    assume(ar[i],real,ai[i],real);
od;
for i from 1 to vectdim([N]) do
    b[i]:= br[i]+I*bi[i];
    assume(br[i],real,bi[i],real);
od;

# Numerator (atil) og denominator (apri)
atil := coeff(expand(sum(Tt[k]*a[k],k=1. .vectdim([T]))),I,0)^2+
          coeff(expand(sum(Tt[k]*a[k],k=1. .vectdim([T]))),I,1)^2;
apri := coeff(expand(sum(Nt[k]*b[k],k=1. .vectdim([N]))),I,0)^2+
          coeff(expand(sum(Nt[k]*b[k],k=1. .vectdim([N]))),I,1)^2;

# Start writing to file "vippp_yri.m"
fd:=fopen("vippp_yri.m",WRITE);
fprintf(fd,"function [ s ] = vippp_yri(E,Yz,Ye,y,dy)\n");
fprintf(fd,"%c\n",\293);
fprintf(fd,"%c [ s ] = vippp_yri(E,Yz,Ye,y,dy)\n",\293);
fprintf(fd,"%c\n",\293);

fprintf(fd,"yrm=real(y);\nyim=imag(y);\nyrd=real(dy);\nyid=imag(dy);\n");
for i from 1 to rowdim(Ykm) do
  for j from 1 to rowdim(Ykm) do
     if Ykm[i,j] <> 0 and i<=j and i<>j then
     fprintf(fd,"Y%a%a=%a;\n",i,j,Ykm[i,j]);
     elif Ykm[i,j] <> 0 and i<=j then
     fprintf(fd,"Y%a%a=%a;\n",i,i,Ykm[i,i]-y[i]); fi;
  od;
od;

# a og b
for i from 1 to vectdim([T]) do
  fprintf(fd,"a%a=%a;\nar%a=real(ar%a);ai%a=imag(ai%a);\n",i,collect(T[i],indets(T[i])),i,i,i,i)
od;
for i from 1 to vectdim([N]) do
  fprintf(fd,"b%a=%a;\nbr%a=real(br%a);bi%a=imag(bi%a);\n",i,collect(N[i],indets(N[i])),i,i,i,i)
od;

# c,d og e.
for i from 0 to degree(atil,t ) do
  fprintf(fd,"c%a=%a;\n",i,coeff(atil,t,i));
od;
```

```
for i from 0 to degree(S1d^2,t) do
  fprintf(fd,"d%a=%a;\n",i,coeff(S1d^2,t,i));
od;
for i from 0 to degree(apri,t ) do
  fprintf(fd,"e%a=%a;\n",i,coeff(apri,t,i));
od;

S1 :=sum('c[k]*t^k','k'=0..degree(atil,t))*
                              sqrt(sum('d[k]*t^k','k'=0..degree(S1d^2,t)))/
                              sum('e[k]*t^k','k'=0..degree(apri,t));
eq:=numer(diff(S1,t));

for i from 0 to degree(eq,t) do
  fprintf(fd,"s%a=%a;\n",i,coeff(eq,t,i));
od;
fprintf(fd,"s = [ ");
for i from 0 to degree(expand(eq),t) do fprintf(fd," s%a",i,coeff(eq,t,i)); od;
fprintf(fd," ];\n");
fclose(fd);
```

D.4 Shifting the gradient in the y_1 direction

For this method the following script is used to make the function file for MATLAB called "write_shift.ma":

```
for i from 1 to vectdim([N]) do
  if evalb(Nt[i]=product(y[k],'k'=1..n)) then
     r_indx:=i;
  fi;
od;
if r_indx=1 then
  N:= N[1..vectdim([N])];
  Nt:= Nt[2..vectdim([Nt])];
elif
  r_indx=vectdim([N]) then
  N:= N[1..vectdim([N])-1];
  Nt:= Nt[1..vectdim([Nt])-1];
else
  N:= N[1..r_indx-1],N[r_indx+1..vectdim([N])];
  Nt:= Nt[1..r_indx-1],Nt[r_indx+1..vectdim([Nt])];
fi;
TR:=sum('a[k]*Ti[k]*cos(dla[k]+dTi[k])','k'=1..vectdim([Tt]));
TI:=sum('a[k]*Ti[k]*sin(dla[k]+dTi[k])','k'=1..vectdim([Tt]));
NR:=sum('b[k]*Ni[k]*cos(dlb[k]+dNi[k])','k'=1..vectdim([Nt]));
```

```
NI:=sum('b[k]*Ni[k]*sin(dlb[k]+dNi[k])','k'=1..vectdim([Nt]));
NR:= NR + product(y[k],'k'=1..n)*cos(sum(dl[k],'k'=1..n)) ;
NI:= NI + product(y[k],'k'=1..n)*sin(sum(dl[k],'k'=1..n)) ;
for j from 1 to vectdim([Tt]) do
  dTi[j]:=add(finndelta(indets(Tt[j])[i]),i=1..dim(indets(Tt[j])));
od;
for j from 1 to vectdim([Nt]) do
  dNi[j]:=add(finndelta(indets(Nt[j])[i]),i=1..dim(indets(Nt[j])));
od;
for i from 1 to vectdim([Nt]) do
  Ni[i]:=Nt[i];
od;
for i from 1 to vectdim([Tt]) do
  Ti[i]:=Tt[i];
od;

Gr:=coeff(NR,y[1],0);
Gi:=coeff(NI,y[1],0);
Fr:=coeff(NR,y[1]);
Fi:=coeff(NI,y[1]);

fd:=fopen("vippp.m",WRITE);
fprintf(fd,"function [s0,s1,s2,s3]=vippp(E,Yz,Ye,y,dy,ddl)\n");

for i from 1 to rowdim(Ykm) do
  for j from 1 to rowdim(Ykm) do
     if Ykm[i,j] <> 0 and i<=j and i<>j then
     fprintf(fd,"Y%a%a=%a;\n",i,j,Ykm[i,j]);
     elif Ykm[i,j] <> 0 and i<=j then
     fprintf(fd,"Y%a%a=%a;\n",i,i,Ykm[i,i]-y[i]); fi;
  od;
od;

for i from 1 to vectdim([T]) do
  fprintf(fd,"a%a=%a;\n",i,collect(T[i],indets(T[i])))
od;
for i from 1 to vectdim([N]) do
  fprintf(fd,"b%a=%a;\n",i,collect(N[i],indets(N[i])))
od;

fprintf(fd,"\nT=%a;\n",sum(Tt[k]*a[k],'k'=1..vectdim([T])));
fprintf(fd,"Tr=real(T);\n");
fprintf(fd,"Ti=imag(T);\n");
fprintf(fd,"T=abs(T)^2;\n");

# Her må du finne polar koord

fprintf(fd,"dl    = angle(y);y = abs(y);\n");
```

```
for i from 1 to vectdim([Tt]) do
  fprintf(fd,"\ndla%a = angle(a%a);a%a = abs(a%a);",i,i,i,i);
od;
for i from 1 to vectdim([Nt]) do
  fprintf(fd,"\ndlb%a = angle(b%a);b%a = abs(b%a);",i,i,i,i);
od;

sumdif_r:=0;
sumdif_i:=0;
for i from 2 to n do
 if yrem[i]=0 then
 sumdif_r:=sumdif_r+diff(TR,y[i])*dy[i]+diff(TR,dl[i])*ddl[i];
 sumdif_i:=sumdif_i+diff(TI,y[i])*dy[i]+diff(TI,dl[i])*ddl[i];
 fi;
od;

fprintf(fd,"\nsumdif_r=%a;",
        collect(sumdif_r,indets(cos+sin+sum(a[k],'k'=1..vectim([Tt])))));
fprintf(fd,"\nsumdif_i=%a;",
        collect(sumdif_i,indets(cos+sin+sum(a[k],'k'=1..vectim([Tt])))));
fprintf(fd,"\nsum1 = 2*(Tr*sumdif_r+Ti*sumdif_i)/T;");

sumdif_r:=0;
sumdif_i:=0;
for i from 2 to n do
 if yrem[i]=0 then
 sumdif_r:=sumdif_r+diff(Gr,y[i])*dy[i]+diff(Gr,dl[i])*ddl[i];# sum 2
 sumdif_i:=sumdif_i+diff(Gi,y[i])*dy[i]+diff(Gi,dl[i])*ddl[i];# sum 3
 fi;
od;

fprintf(fd,"\nsum2 = %a;",
        collect(sumdif_r,indets(cos+sin+sum(b[k],'k'=1..vectim([Nt])))));
fprintf(fd,"\nsum3 = %a;",
        collect(sumdif_i,indets(cos+sin+sum(b[k],'k'=1..vectim([Nt])))));

sumdif_r:=0;
sumdif_i:=0;
for i from 1 to n do
 if yrem[i] = 0 then
 sumdif_r:=sumdif_r+diff(Fr,y[i])*dy[i]+diff(Fr,dl[i])*ddl[i];
 sumdif_i:=sumdif_i+diff(Fi,y[i])*dy[i]+diff(Fi,dl[i])*ddl[i];
 fi;
od;

fprintf(fd,"\nsum4 = %a;",
        collect(sumdif_r,indets(cos+sin+sum(b[k],'k'=1..vectim([Nt])))));
fprintf(fd,"\nsum5 = %a;",
        collect(sumdif_i,indets(cos+sin+sum(b[k],'k'=1..vectim([Nt])))));
```

```
fprintf(fd,"\nFr=%a;\nFi=%a;\nGr=%a;\nGi=%a;\n\n",Fr,Fi,Gr,Gi);
fprintf(fd,"F=Fr^2+Fi^2;\nG=Gr^2+Gi^2;\n\n");

fprintf(fd,"\n\ns0=G*dy(:,1);\n");
fprintf(fd,"s1=G*sum1-2*(Gr*sum2+Gi*sum3);\n");
fprintf(fd,"s2=2*(Fr*Gr+Fi*Gi)*sum1-2*(Fr*sum2+Fi*sum3+Gr*sum4+Gi*sum5)-F*dy(:,1);\n");
fprintf(fd,"s3=F*sum1-2*(Fr*sum4+Fi*sum5);\n");

fclose(fd);
```

D.5 MATLAB function

Both maple functions generate a MATLAB function, which is given as:

Distance to the PoC along the gradient: [s] = vippp_yri(E,Yz,Ye,y,dy)

Shifting the gradient in the y_1 direction: [s0 s1 s2 s3] = vippp(E,Yz,Ye,y,dy,ddl)

The first parameters for both functions, *E* to *y*, are identical to both functions and they are given by

E Estimated Thevenin voltages.

Yz Estimated Thevenin admittances.

Ye Transmission lines and shunt impedances, known from network topology.

y measured load admittances at the "known" load buses.

The estimated values of derivatives are handled differently by the two methods as the first uses the Cartesian coordinates and the second uses polar coordinates.

dy Estimated values of the derivatives of load at the "known" buses. It is given as a complex quantity for "Distance to the PoC along the gradient", with both real and imaginary part of the derivative. For method "Shifting the gradient in the y_1 direction" it is given as the derivative of the absolute value of the load admittance. In both cases is given with one column for each load bus.

ddl Estimated value of the derivative of load angles.

Index

Glossary of selected terms with reference to this dissertation

A

American Standard Code for Information Interchange (ASCII) is a code for representing English characters as numbers, with each letter assigned a number from 0 to 127. Most computers use ASCII codes to represent text, which makes it possible to transfer data from one computer to another

The standard ASCII character set uses just 7 bits for each character. There are several larger character sets that use 8 bits, which gives them 128 additional characters. The extra characters are used to represent non-English characters, graphics symbols, and mathematical symbols. Several companies and organizations have proposed extensions for these 128 characters, p. 59.

C

Central Prossessing Unit (CPU) is the brain of the computer. Sometimes referred to simply as the processor or central processor, the CPU is where most calculations take place, p. 37.

D

Discrete Fourier Transform (DFT) The Fourier transform is defined as

$$f(v) = \mathfrak{F}[f(t)] = \int_{-\infty}^{\infty} f(t)e^{-2\pi ivt\,dt}$$

Now consider generalization to the case of a discrete function, $f(t) \to f(t_k)$ by letting $f_k \equiv f(t_k)$, where $t_k \equiv k\Delta$, with $k = 0, \ldots, N-1$. Choose the frequency step such that

$$v_n = \frac{n}{N\Delta}$$

with $n = -N/2, \ldots, 0, \ldots, N/2$. There are $N+1$ values of n, so there is one relationship between the frequency components. Writing this out as

$$\mathfrak{F}[f(t)] = \sum_{k=0}^{N-1} f_k e^{-2\pi i n/(N\Delta)k\Delta}\Delta = \Delta \sum_{k=0}^{N-1} f_k e^{-2\pi i n k/N}$$

and

$$F_n \equiv \sum_{k=0}^{N-1} f_k e^{-2\pi i n k/N}$$

The inverse transform

$$f_k = \frac{1}{N}\sum_{k=0}^{N-1} F_n e^{2\pi i n k/N}$$

, p. 55.

F

Full Time Scale (FTS) is, as opposed to Quasi steady state, simulations performed using all the differential equations, including both short- and long-term dynamics, p. 37.

G

Gate Turn-Off (GTO) Like a thyristor the GTO can be turned on by a short-duration gate current pulse, and once in the on-state, the GTO may stay on without any further gate current. However, unlike the thyristor, the GTO can be turned off by applying a negative gate-cathode voltage, therefore causing a sufficiently large negative gate current to flow, p. 29.

Geostationary Operational Environmental Satellites (GOES) consist of two satellites in geostationary orbit at 75^o West and 135^o West longitude. Their primary mission is hurricane monitoring for the western hemisphere with "time transfer" as a secondary mission, p. 58.

Global Positioning System (GPS) satellite navigational system formed by 24 satellites orbiting the earth and their corresponding receivers on the earth. The satellites orbit the earth at approximately 12,000 miles above the surface and make two complete orbits every 24 hours. The GPS satellites continuously transmit digital radio signals that contain data on the satellites location and the exact time to the earth-bound receivers. The satellites are equipped with atomic clocks that are precise to within a billionth of a second, p. 55.

H

High Voltage Direct Current (HVDC) Electrical plants generate power in the form of *AC* voltages and currents. This power is transmitted to the load centers on three-phase, AC transmission lines. However, under certain circumstances, it becomes desirable to transmit this power over *DC* transmission lines. HVDC links may be broadly classified into the following categories

- Monopolar links
- Bipolar links
- Homopolar links

, p. 7.

M

MATrix LABoratory (MATLAB) is a high-performance language for technical computing. It integrates computation, visualization, and programming in an easy-to-use environment where problems and solutions are expressed in familiar mathematical notation.

MATLAB is an interactive system whose basic data element is an array that does not require dimensioning. This allows you to solve many technical computing problems, especially those with matrix and vector formulations, in a fraction of the time it would take to write a program in a scalar noninteractive language such as C or Fortran, p. 86.

O

On Load Tap Changer (OLTC) In addition to voltage transformation, transformers are often used for control of voltage and reactive power flow. Therefore, practically all transformers used for bulk power transmission and many distribution transformers have taps in one or more windings for changing the turns ratio. From the power system viewpoint, changing the ratio of transformation is required to compensate for variations in system voltages. Two types of tap-changing facilities are provided: off-load tap changing and on-load tap changing, also referred to as Under-load tap changing (ULTC), p. 15.

P

Phasor Measurment Unit (PMU) is a device to measure voltages and currents with angles using DFT. With a GPS as synchroniztion source it is possible to get an

improved stated estimation based on phasor measurements, p. 55.

Point of Collapse (PoC) is, when considering *voltage stability*, and in a steady state viewpoint, the maximum load transfer for a given system. This is in many cases referred to as "*the tip of the nose curve*", p. 4.

Q

Quasi Steady-State (QSS) simulations is performed using only the differential equations for the long-term dynamics. In QSS the short-term dynamics are supposed infinitely fast so that the corresponding differential equations can be replaced by their equilibrium form, p. 37.

R

Root Mean Square (rms) value of a sinusoid is defined as the peak value divided by $\sqrt{2}$. With the following sinusoid:

$$f(t) = a\sin(t)$$

the RMS value is given by:

$$a_{rms} = \frac{a}{\sqrt{2}}$$

, p. 55.

S

SIMulation of POWer systems (SIMPOW) Power system simulation & analysis software by ABB, p. 87.

STATic synchronous CONdenser (STATCON) The combination of GTO and SCV gives the device characteristic resembling a synchronous condenser. For that reason it has been dubbed STATCON [2], p. 29.

Static Var Compensator (SVC) are shunt-connected static generators and/or absorbers whose outputs are varied so as to control specific parameters of the electric power system. The term "static" is used to indicate that SVCs, unlike synchronous compensators, have no moving or rotating main components, p. 10.

Supervisory Control And Data Acquisition (SCADA) is a computer system for gathering and analyzing real time data. SCADA systems are used to monitor and control a plant or equipment in industries such as telecommunications, water

and waste control, energy, oil and gas refining and transportation. A SCADA system gathers information, such as where a leak on a pipeline has occurred, transfers the information back to a central site, alerting the home station that the leak has occurred, carrying out necessary analysis and control, such as determining if the leak is critical, and displaying the information in a logical and organized fashion. SCADA systems can be relatively simple, such as one that monitors environmental conditions of a small office building, or incredibly complex, such as a system that monitors all the activity in a nuclear power plant or the activity of a municipal water system, p. 105.

U

UnderVoltage Load Shedding (UVLS) schemes are used to cater to unplanned or extreme situations. This is analogous to underfrequency load shedding, which has become a common utility practice to cater to extreme situations resulting in generation deficiency and underfrequency. Load shedding provides a low cost means of preventing widespread system collapse, p. 30.

Universal Time Coordinate (UTC) is a time scale that couples Greenwich Mean Time, which is based solely on the Earth's inconsistent rotation rate, with highly accurate atomic time. When atomic time and Earth time approach a one second difference, a leap second is calculated into UTC. UTC was devised on January 1, 1972 and is coordinated in Paris by the International Bureau of Weights and Measures. UTC, like Greenwich Mean Time, is set at 0 degrees longitude on the prime meridian, p. 55.